

Applications of deep reinforcement learning to urban transit network design

Andrew Holliday



School of Computer Science
McGill University
Montréal, Québec, Canada

February 26, 2025

A thesis presented for the degree of Doctor of Philosophy in Computer Science

©2024 Andrew Holliday

Abstract

This thesis concerns the use of reinforcement learning to train neural networks to aid in the design of public transit networks. The Transit Network Design Problem (TNDP) is an optimization problem of considerable practical importance. Given a city with an existing road network and travel demands, the goal is to find a set of transit routes - each of which is a path through the graph - that collectively satisfy all demands, while minimizing a cost function that may depend both on passenger satisfaction and operating costs.

The existing literature on this problem mainly considers metaheuristic optimization algorithms, such as genetic algorithms and ant-colony optimization. By contrast, we begin by taking a reinforcement learning approach, formulating the construction of a set of transit routes as a Markov Decision Process (MDP) and training a neural net policy to act as the agent in this MDP. We then show that, beyond using this policy to plan a transit network directly, it can be combined with existing metaheuristic algorithms, both to initialize the solution and to suggest promising moves at each step of a search through solution space.

We find that such hybrid algorithms, which use a neural policy trained via reinforcement learning as a core component within a classical metaheuristic framework, can plan transit networks that are superior to those planned by either the neural policy or the metaheuristic algorithm. We demonstrate the utility of our approach by using it to redesign the transit network for the city of Laval, Quebec, and show that in simulation, the resulting transit network provides better service at lower cost than the existing transit network.

Abrégé

Cette thèse concerne l'utilisation de l'apprentissage par renforcement pour entraîner des réseaux de neurones afin d'aider à la conception des réseaux de transport en commun. Le problème de conception des réseaux de transport en commun (TNDP) est un problème d'optimisation d'une importance pratique considérable. Étant donné une ville avec un réseau routier existant et des demandes de déplacement, l'objectif est de trouver un ensemble de lignes de transport en commun - chacune étant un chemin à travers le graphe - qui satisfait collectivement toutes les demandes, tout en minimisant une fonction de coût qui peut dépendre à la fois de la satisfaction des passagers et des coûts d'exploitation.

La littérature existante sur ce problème considère principalement des algorithmes issus de la littérature sur l'optimisation par métaheuristiques, tels que les algorithmes génétiques et l'optimisation par colonies de fourmis. En revanche, nous commençons par adopter une approche d'apprentissage par renforcement, en formulant le TNDP comme un processus de décision markovien et en entraînant une politique de réseau de neurones avec une architecture novatrice pour assembler des réseaux de transport en commun. Nous montrons ensuite qu'au-

delà de l'utilisation de cette politique pour planifier directement un réseau de transport en commun, elle peut être combinée avec des algorithmes métaheuristiques existants, à la fois pour l'initialisation et pour suggérer des mouvements prometteurs à chaque étape d'une recherche dans l'espace des solutions.

Nous constatons que de tels algorithmes hybrides, qui utilisent une politique neuronale entraînée via l'apprentissage par renforcement comme composant central dans un cadre métaheuristique classique, peuvent planifier des réseaux de transport en commun supérieurs à ceux planifiés soit par la politique neuronale, soit par l'algorithme métaheuristique. Nous démontrons l'utilité de notre approche en l'utilisant pour redessiner le réseau de transport en commun de la ville de Laval, Québec, et montrons qu'en simulation, le réseau de transport en commun résultant offre un meilleur service à moindre coût que le réseau de transport en commun existant.

Acknowledgements

The journey to the completion of this thesis was long and uncertain, and it would not have been possible without help from many quarters. Credit goes first to my two supervisors, professors Gregory Dudek and Ahmed El-Geneidy. With this thesis, both of them took a chance: Greg in accepting my proposal of a topic well outside of both of our expertise, and Ahmed, in taking me on as a student from far outside his own field of urban planning. I am grateful to both of them for taking a chance on me, and I hope I have convinced them both that it was the right call.

Professor Dudek guided me through the mists and mazes of graduate school and the ups and downs of the publishing cycle. His boundless enthusiasm for his field has been a source of inspiration, as has his talent for bringing people together. Because of Greg I have been privileged to meet many other fine teachers and colleagues who have made this journey not only possible but enjoyable.

The data and contacts in the real world of transit planning that professor El-Geneidy provided were essential to this work. Just as important was his guidance to me as a novice

in his field, and his patience and good humour in delivering that guidance.

My many colleagues at the Mobile Robotics Laboratory over the years gave me plenty of advice and encouragement, as well as the simple pleasure of their company. Our lab is unique, not just in its large number of students, but also in the sense of community and camaraderie among them. Belonging to this group of people has been a great privilege.

Anqi Xu, Florian Shkurti, Jimmy Li, Sandeep Manjanna, Malika Meghjani, and Travis Manderson were senior students in the lab when I was just starting out. Their brilliance and friendliness made the lab a very welcoming place, and they were all inspiring examples of what an academic could be. As a new student, I was fortunate to work with and learn from them on numerous robotics projects and trials out in the field. These trips could be chaotic, but they were always great adventures.

I want to thank professor David Meger for his help and advice, and for being so tolerant of my constant second-guessing. Arnold Kalmbach deserves special thanks for giving me a spare room to live in for a crucial few months, and for being such a good roommate. Nikhil Kakodkar has been a good friend to me from the beginning: a teammate in some challenging classes, a sounding board for research ideas and a link to a broader social world. I owe him thanks not just for his friendship but for the many other friends in Montréal that I've met because of him.

Many other colleagues past and present helped make MRL such a great place to work; this includes Lucas Berry, Wilfred Mason, Wei-Di Chang, Scott Fujimoto and Edward

Smith, Julie Al-Hosh, Jean-Francois Tremblay, Johanna Hansen, Chelsea Taylor, Juan Camilo Gamboa Higuera, Amin Abyaneh, Stanley Wu, Hanna Yurchyk, Khalil Virji, Faraz Lotfi and Farnoosh Faraji, Charlotte Morissette, Mariana Sosa, Karim Koreitem, Xiru Zhu, professor Hsiu-Chin Lin, and doubtless others that I've forgotten. I am grateful to have spent this time with you all.

My parents have been unwavering in their encouragement and support of me throughout my academic journey. Beyond that, they deserve the credit for all of the opportunities they worked so hard to provide for me, all of which brought me to undertake this degree. For that I am endlessly grateful, and I can only hope that I have justified their pride in me.

I also give thanks to the reviewers of all the paper submissions I've made over the past seven years. Their feedback, both favourable and not, has provided valuable lessons and an impetus to improve my craft.

Lastly, I want to thank all of the bus drivers and train operators who've ever helped get me where I've been going. Their work was and is an inspiration; without it, this thesis would never have existed.

Contents

Abstract	i
Abrégé	iii
Acknowledgements	v
1 Introduction	1
1.1 Background	3
1.1.1 Why Transit Matters: Cities, Cars, and Mass Transit	3
1.1.2 Neural Nets for Optimization Problems	7
1.1.3 Optimization of Public Transit	13
1.2 The Transit Network Design Problem	15
1.2.1 Constraints	19
1.2.2 Cost Function	20
1.3 Contribution to original knowledge	23
1.4 Dissertation Structure	24

2	Designing Transit Networks with a Graph Attention Net	27
2.1	Markov Decision Process Formulation	28
2.2	Neural Net Architecture and Training	32
2.3	Policy Architecture	34
2.3.1	Graph Attention Backbone	35
2.3.2	Halting Head	37
2.3.3	Extension Head	38
2.3.4	Features and Net Architecture Details	41
2.4	Training The Policy Net	43
2.4.1	Reward Function	46
2.4.2	Training Data	48
2.4.3	Training Parameters	51
2.5	Experiments	54
2.5.1	Training	54
2.5.2	Evaluation	54
2.5.3	Comparison with State of the Art Methods	65
2.6	Summary	68
3	Neural Nets as Initialization Procedures	69
3.1	Evolutionary Algorithm	71
3.2	Hyper-Heuristic with Great Deluge	74

3.3	Initialization procedures	79
3.3.1	Demand-Maximizing Shortest Paths	79
3.3.2	Validity-Maximizing Shortest Paths followed by Repair	80
3.3.3	Growing Routes based on Diverse Edge Weights	81
3.4	Experiments	85
3.4.1	Initialization Results	85
3.4.2	Metaheuristic Improvement Results	88
3.5	Summary	94
4	Neural Nets as Low-Level Heuristics	96
4.1	Comparison with Baseline Evolutionary Algorithm	98
4.2	Ablation Studies	103
4.2.1	Effect of number of samples	103
4.2.2	Contribution of type-2 mutator	104
4.2.3	Importance of learned heuristics	107
4.3	Comparison with State of the Art Methods	111
4.3.1	Operator-perspective results	115
4.3.2	Transfer Statistics	116
4.4	Summary	118
5	Application to a Realistic Scenario	120

5.1	Representing Laval	122
5.1.1	Street graph	122
5.1.2	Existing transit	123
5.1.3	Demand matrix	125
5.2	Enforcing constraint satisfaction	127
5.3	Results	131
5.3.1	Visual Inspection	134
5.4	Practical takeaways	141
5.5	Summary	144
6	Conclusion	146
6.1	Future Work	147
6.1.1	Learned Heuristics in Other Metaheuristic Algorithms	147
6.1.2	Training Policies Differently, and Training Different Policies	148
6.1.3	Interactions with Mobility-On-Demand	149
6.1.4	Going From Simulation to Reality	149
6.2	Concluding Statement	151

List of Figures

- 1.1 Robert Moses (left [Stieglitz, 1939]) and Charles-Édouard Jeanneret, also known as Le Corbusier (right [van Bilsen, 1964]), two influential figures in the development of automobile-centric cities. 4
- 1.2 Automobile congestion causing travel delays in the city of Toronto, where it is a commonplace occurrence [DeClerq, 2020]. 6
- 1.3 A schematic of the message-passing step of a Graph Neural Net (GNN) layer for one node in a graph. As described in Equation 1.1, node i receives messages \mathbf{h}^j from each neighbouring node and from itself, which are the node's feature transformed by the learned matrix M and scaled by the coefficients α_{ij} . The received messages are summed to form the layer's new embedding of node i . 13

1.4	An example city graph with ten numbered nodes and three routes. Street edges are black, routes are in colour, and two example demands are shown by dashed red lines. The edges of the three routes form a sub-graph of the street graph $(\mathcal{N}, \mathcal{E}_s)$. All nodes are connected by this sub graph, so the three routes form a valid transit network. The demand between nodes 2 and 5, 0 and 6, and 7 and 4 can be satisfied directly by riding on the blue line, while the demand from 3 to 9 requires one transfer: passengers must ride the orange line from node 3 to 8, and then the green line from node 8 to 9.	17
1.5	Overview of thesis research	24
2.1	An in-progress route r with the possible extensions available to it, which form \mathcal{A}_t . The route so far is shown with solid blue lines, while the extensions are dashed lines, with different colours for each extension. The corresponding routes after adding each extension are listed below the graph. Only one extension (to node 1, shown in red) is possible from the route's starting terminal, since all nodes reachable from 1 are already on the route. Five extensions are possible from the other end at this step.	30

2.2	A flowchart of the transit network construction process defined by our Markov Decision Process (MDP). Blue boxes indicate points where the timestep t is incremented and the agent selects an action. Red nodes are the beginning and ending of the process. Green nodes are hard-coded decision points. Orange nodes show updates to the state \mathcal{S} and action space \mathcal{A}	33
2.3	A schematic illustration of the role of each component of the policy net in the network construction process. This loop continues until $ \mathcal{R}_t = S$, that is, we have the desired number of routes.	35
2.4	Mean cost on the validation set, and mean reward during training, achieved by our policy net over five epochs of training. The curves show the mean over ten training runs with different random seeds, and the shaded areas shows one standard deviation over the ten seeds.	55
2.5	The Mandl benchmark city and the four Mumford benchmark cities.	58
2.6	Values of average trip time C_p (on the x-axis) and total route time C_o (on the y-axis), across values of α from 0 at lower-right to 1 at upper-left, in increments of 0.1. Each point is the mean over 10 random seeds for one value of α (excluding those that generated invalid networks), and bars around each point indicate one standard deviation. Lines link pairs of points with consecutive α values. Note that RC-100 is not shown for Mumford1 because none of its generated networks were valid for that city.	60

2.7	Values of average trip time C_p (on the x-axis) and total route time C_o (on the y-axis) of solutions from LC-100 with π_θ , LC-100 with $\pi_{\theta_{\alpha=1}}$, and RC-100, all with $\alpha = 1.0$	62
2.8	Of the ten runs with different random seeds for each benchmark city and α , these heat maps show the number of solutions produced by each algorithm that violated one or more network constraints. LC-100 is not shown, as it produced no constraint violations in any case.	64
3.1	A schematic of which extensions of a route are allowed by the type-2 mutator. Here, the mutator will extend a route from its terminal at node 5 to a neighbouring node. Nodes 1, 2, 3, 4, and 6 are neighbours of node 5, but nodes 1, 3, and 4 are already on the route, so may not be chosen. This leaves nodes 2 and 6 as valid choices, so one of these two will be chosen randomly. .	73
3.2	Results for the initialization methods. Nikolic (2013) is excluded as all of its networks are invalid. Curves for LC-100 and John (2014) show values of average trip time C_p (on the x-axis) and total route time C_o (on the y-axis) across values of α from 0 to 1 in increments of 0.1. Ahmed (2019) does not depend on α , so only one point is shown for it. Each point is the mean over 10 random seeds for one value of α and one method, and bars around each point indicate one standard deviation.	87

-
- 3.3 Results for EA with four different initialization methods. Each curve shows values of average trip time C_p (on the x-axis) and total route time C_o (on the y-axis) across values of α from 0 at lower-right to 1 at upper-left, in increments of 0.1. Each point is the mean over 10 random seeds for one value of α and one method, and bars around each point indicate one standard deviation. Lines link pairs of points for the same method and consecutive α values. 89
- 3.4 A schematic of a hypervolume computed based on five points in two dimensions. The point p , represented by + sign, is chosen to be ϵ greater than the largest magnitude of any point on each dimension. Then, we can define an axis-aligned rectangle for each point x with x at one corner and p at the other. The hypervolume of the set of five points is then the area of the union of these five rectangles, shown as the total shaded area. 90
- 3.5 Hypervolumes achieved by EA with different initializations. 91
- 3.6 Results for HH with three different initialization methods. Each curve shows values of average trip time C_p (on the x-axis) and total route time C_o (on the y-axis) across values of α from 0 at lower-right to 1 at upper-left, in increments of 0.1. Each point is the mean over 10 random seeds for one value of α and one method, and bars around each point indicate one standard deviation. Lines link pairs of points for the same method and consecutive α values. 93
- 3.7 Hypervolumes achieved by HH with different initializations. 94

4.1	Values of average trip time C_p (on the x-axis) and total route time C_o (on the y-axis) achieved by NEA, EA, LC-100, and LC-40k, across values of α from 0 at lower-right to 1 at upper-left, in increments of 0.1. Each point is the mean over 10 random seeds for one value of α , and bars around each point indicate one standard deviation. Lines link pairs of points with consecutive α values.	101
4.2	Hypervolumes achieved by LC-100, LC-Greedy, EA, and NEA.	102
4.3	Values of average trip time C_p (on the x-axis) and total route time C_o (on the y-axis) achieved by all-1 NEA, plotted along with EA and NEA (repeated from Figure 4.1) for comparison.	105
4.4	Hypervolumes achieved by NEA vs NEA with only the type-1 mutator. . . .	106
4.5	Trade-offs between average trip time C_p (on the x-axis) and total route time C_o (on the y-axis) achieved by RC-EA, plotted along with NEA (repeated from Figure 4.1) for comparison.	108
4.6	Hypervolumes achieved by NEA and RC-EA with only the type-1 mutator. . .	109
5.1	A map of the city of Laval, Quebec, taken from Google [2024].	121
5.2	Figure 5.2a shows a map of the Census Dissemination Areas of the city of Laval, with “crossover points” used to remap inter-city demands shown as black circles, and the Montreal Metro Orange Line shown in orange. Figure 5.2b shows the street graph constructed from these dissemination areas.	128

-
- 5.3 The routes of our Société de Transport de Laval (STL) network. Routes that go along a single edge are placed next to each other, so thicker “rainbow” edges show multiple parallel routes. The thick orange line shows the Orange Line subway of the Montreal Metro, with its stations as orange circles, and the black circles show the nodes of the Census Dissemination Areas (CDAs) containing Laval’s three major bus terminals: Le Carrefour, Montmorency, and Cartier. 129
- 5.4 Average trip time C_p versus total route time C_o achieved by LC-100 and NEA at $\alpha = 0.0$ (bottom-right), 0.5 (middle), and 1.0 (top-left), as well as for RC-EA at $\alpha = 1.0$ and the STL network itself (independent of α). Except for STL, each point is a mean value over 10 random seeds, and bars show one standard deviation. 133
- 5.5 The routes of one of NEA’s generated networks at $\alpha = 0.0$. The heavy orange line and its circles represent the orange line metro and its stops, while the black dots represent existing bus terminals. 135
- 5.6 The routes of one of NEA’s generated networks at $\alpha = 0.5$. The heavy orange line and its circles represent the orange line metro and its stops, while the black dots represent existing bus terminals. 136

5.7 The routes of one of NEA’s generated networks at $\alpha = 1.0$. The heavy orange line and its circles represent the orange line metro and its stops, while the black dots represent existing bus terminals. 137

5.8 LC-100 initial networks for the three NEA runs shown in Figures 5.5, 5.6, and 5.7. 142

List of Tables

2.1	Policy net architectural hyper-parameters	44
2.2	Training Hyper-Parameters	52
2.3	Statistics of the five benchmark problems used in our experiments. The area is estimated assuming all vehicles travel at 15 meters per second.	56
2.4	A comparison of our algorithms with a selection of methods from recent literature, in terms of C_p achieved when $\alpha = 1$ and C_o achieved when $\alpha = 0$. Values for LC-100 and LC-Greedy are means over 10 random seeds. Bold values are the best on the environment.	67
4.1	Final cost $C(\mathcal{G}, \mathcal{R})$ achieved baseline experiments for three different α values. Values are averaged over ten random seeds; the \pm value is the standard deviation of $C(\mathcal{G}, \mathcal{R})$ over the seeds.	100

4.2	Passenger-perspective results. C_p is the average passenger trip time. C_o is the total route time. d_i is the percentage of trips satisfied with number of transfers i , while d_{un} is the percentage of trips satisfied with 3 or more transfers. Arrows next to each quantity indicate which of increase or decrease is desirable. Bolded values in C_p , d_0 , and d_{un} columns are the best on that environment.	114
4.3	Operator perspective results. C_p is the average passenger trip time. C_o is the total route time. d_i is the percentage of trips satisfied with number of transfers i , while d_{un} is the percentage of trips satisfied with 3 or more transfers. Arrows next to each quantity indicate which of increase or decrease is desirable. Bolded values in C_o , d_0 and d_{un} columns are the best on that environment.	117
5.1	Statistics and parameters of the Laval scenario	127

-
- 5.2 Performance of networks from LC-100 and NEA at three α values, RC-EA at $\alpha = 1.0$, and the STL network. Bolded values are best for the corresponding α , except where STL performs better than all methods at that α , in which case no values are bolded. C_p is the average passenger trip time. C_o is the total route time. d_i is the percentage of trips satisfied with number of transfers i , while d_{un} is the percentage of trips satisfied with 3 or more transfers. All values are averaged over ten random seeds, with one standard deviation following “ \pm ”, except for those in the STL row. 132
- 5.3 Counts of the number of routes that visit each bus terminal in each network. For NEA, counts are the average over the ten networks computed at that α value. 134

Chapter 1

Introduction

The Transit Network Design Problem (TNDP) is the problem of designing a network of public transit routes - such as metro lines and bus routes - for a city, so as to satisfy some objectives, such as meeting all travel demand and minimizing operating costs. It is an important problem in urban planning, as public transit is essential for overcoming the inefficiencies inherent in car-based urban transportation. Compared with point-to-point car transit, mass transit can significantly reduce traffic congestion, energy consumption, and emissions [Roughgarden and Tardos, 2002, Oh et al., 2020, Rich et al., 2023]. The spatial layout of a transit network can have a major impact on its ability to realize these benefits. One city planner [Shrikant, 2018] gave the city of Seattle, Washington as a good example: it has recently expanded its transit network in a way that takes into account the interactions between routes, and the city's transit ridership has consequently grown. The same planner

gave the city of Denver, Colorado as a bad example, where much transit has been built that did not reach places people want to go. In each case, the spatial layout of the transit routes was the major reason for the transit system's quality, or lack thereof.

The TNDP's importance has arguably grown in recent years, as the COVID-19 pandemic resulted in declines in transit ridership in cities worldwide [Liu et al., 2020]. This has led to a financial crisis for many municipal transit agencies, putting them under pressure to reduce transit operating costs [Kar et al., 2022]. Many agencies thus find themselves having to do more with less. Improving the design of a transit network, such as by changing bus routes, can improve the quality of service an agency can provide while reducing operating costs.

But the TNDP is very challenging problem. It is NP-hard, and has commonalities with the Travelling Salesman problem (TSP) and Vehicle Routing Problem (VRP), but is much more complex than these, due to the need to plan multiple routes that interact non-linearly due to passengers' ability to make transfers between routes. Since real-world cities typically have hundreds or even thousands of possible stop locations, analytical optimization approaches are infeasible. Real-world transit networks are still commonly designed by hand [Durán-Micco and Vansteenwegen, 2022], but there exists a substantial literature on computational approaches to the TNDP.

The most successful approaches to-date have been metaheuristic algorithms, such as evolutionary algorithms, simulated annealing, and ant colony optimization. Most such algorithms work by repeatedly applying one or more low-level heuristics that make a small

random change to a network; over many iterations, the algorithms guide this random walk towards better networks by means of a metaheuristic such as natural selection (as in evolutionary algorithms) or metallic annealing (as in simulated annealing).

By comparison, only little cross-over exists between the literature on this problem and that on neural nets [Guihaire and Hao, 2008, Kepaptsoglou and Karlaftis, 2009, Durán-Micco and Vansteenwegen, 2022]. In this thesis, we address this gap, considering ways in which Graph Neural Nets (GNNs) and reinforcement learning (RL) may be used to address the TNDP, both in isolation and in combination with existing metaheuristic approaches.

1.1 Background

1.1.1 Why Transit Matters: Cities, Cars, and Mass Transit

With the arrival of the Model T in 1908, automobiles became a mass-market product. As more and more city dwellers became automobile owners, various factors conspired to shift the design of cities around the world away from walking and mass transit and towards the automobile as the chief mode of mobility for their residents. In the 1920s, car manufacturers and drivers' associations engaged in concerted efforts to change public perception of what city streets were for (motorists, rather than pedestrians) and to shape safety laws governing the streets to favour motorists: efforts which proved successful [Montgomery, 2013, chapter 4]. Meanwhile, prominent figures in urban planning such as Le Corbusier and Robert Moses

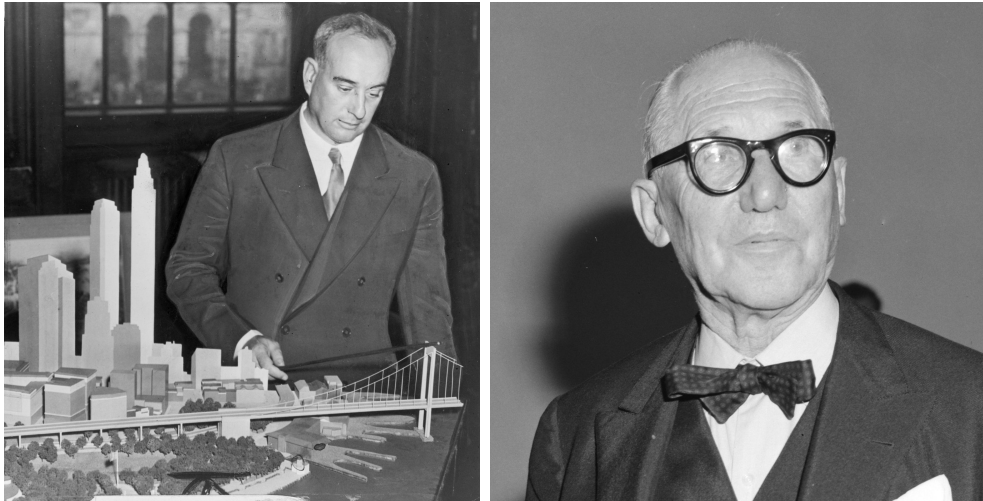


Figure 1.1: Robert Moses (left [Stieglitz, 1939]) and Charles-Édouard Jeanneret, also known as Le Corbusier (right [van Bilsen, 1964]), two influential figures in the development of automobile-centric cities.

(Figure 1.1), who saw the personal automobile as the future of urban transportation, shaped their urban designs around cars and influenced many others to do the same [Caro, 1974, Chapter 25; Le Corbusier, 1929, Chapter 11].

But the middle of the 20th century, the adverse effects of this move towards automobiles were beginning to be seen. Congestion had revealed itself as a major problem, and evidence quickly mounted that, by inducing demand, adding more road capacity worsens congestion rather than relieving it [Caro, 1974, Duranton and Turner, 2011]. The automobile also was key to enabling urban sprawl: the growth of vast low-density residential developments outside of city centres, from which residents commute for work and other purposes. Congestion and sprawl together have led to greatly increased pollution, along with negative effects on social

cohesion and on commuter's well-being [Sandow, 2011, Leyden, 2003, Freeman, 2001].

The early 21st century has seen the advent of ride-hailing services such as Uber and Lyft, as well as major advancements in autonomous driving technology. With these developments, the prospect has arisen of a new auto-mobility in which the commuter will not own a car, but will instead summon an autonomous vehicle (AV) when needed, and then dismiss it to be used by others. It has been suggested that such mobility-as-a-service will reduce congestion and make transportation more efficient [Frank, 2020], and that they may act as a useful supplement to public transit [Madden, 2017].

Unfortunately, the evidence to date suggests the opposite. Schaller Consulting [2018] reports on data from a number of major US cities demonstrating that ride-sharing services such as Uber and Lyft have worsened congestion in major U.S. cities, because they primarily draw users away from non-car transit modes, especially public transit, increasing total vehicle miles driven by as much as 80%. Harb et al. [2018] designed a clever experiment that simulated self-driving personal cars for a sample of real people by giving them free access to human chauffeurs who would drive their cars for them. This experiment showed that freeing car owners from the need to drive induces more demand for car travel - which will tend to exacerbate the problems of congestion.

In fact, even in an ideal world, the benefits to be gained from self-driving cars are limited. A theoretical analysis by Roughgarden and Tardos [2002] compared globally-coordinated routing of cars over a congested road network with "selfish" routing. They demonstrated



Figure 1.2: Automobile congestion causing travel delays in the city of Toronto, where it is a commonplace occurrence [DeClerq, 2020].

that even in idealized theoretical scenarios, coordinated routing could improve on selfish routing by at most a factor of $4/3$ in terms of total transit time for all travellers.

Mass public transit systems, such as rail and bus networks, are far more space-efficient than private automobiles and have far less environmental impact Litman [2012]. A major challenge facing the architects of such systems, however, is persuading travellers in car-centric cities to use public transit. In a study of Los Angeles, Chakrabarti [2017] analyzed factors determining car or bus use by commuters, and found that frequent service, high speed, and reliability were the most important factors in rider's decisions to use public transit. The design of transit networks - the spatial layout of the routes themselves - can have a major impact on passenger's travel times, and so can be instrumental in getting drivers out of their

cars and onto public transit, reducing congestion and pollution and improving the mobility of all citizens.

Applying AV technology to bus systems could help them better provide these qualities by allowing more buses to be operated with less downtime. Critically, they may also reduce cost - according to [Ceder, 2016, chapter 9], driver wages and benefits form the single largest budget item for most transit agencies. A growing number of cities are engaged in pilot projects with autonomous shuttles [Beene, 2018, Plautz, 2018, France-Press, 2021]. Autonomous buses would also be capable of navigating more complex routes, and changing routes more often, than human bus drivers are willing or able to do. This could make feasible more complex but more efficient system designs, which computational network design methods may be better able to provide than human designers.

1.1.2 Neural Nets for Optimization Problems

Combinatorial Optimization (CO) problems are problems in which a solution comprises the arrangement of finite set of elements in some way, so as to accomplish an objective like minimizing the solution's cost or satisfying a set of constraints. A well-known example is the Travelling Salesman problem, in which we are given a set of points in space and we seek the order in which to visit those points that minimizes the overall length of the journey. The points may be visited in any order, so with n points, there are $n!$ possible solutions. The TSP belongs to the class of NP-Hard problems, meaning the fastest known algorithms for

finding the optimal solution take time that grows exponentially with n . Most Combinatorial Optimization (CO) problems of interest share this property, so there has been much research on algorithms that can find good sub-optimal solutions in feasible amounts of time, such as Christophides [1976], Kautz et al. [1992], Applegate et al. [2001] to name only a few.

Artificial neural nets (henceforth, neural nets) are a broad family of models used in machine learning. A neural net composes a sequence of “layers” to map an n -dimensional vector input to an m -dimensional output. The layers together have a set of learnable parameters θ ; by using an appropriate learning algorithm to find values for θ , the neural net can be “trained” to closely approximate arbitrary functions $f : \mathbb{R}^n \rightarrow \mathbb{R}^m$. Such a system is called a “neural net” because the hierarchical arrangement of layers and their internal structure are loosely inspired by the arrangement and function of biological neurons in animal nervous systems. Many different types of neural net have been developed to operate on different types of input, including text, images, and graph-structured data. Neural nets with many layers (typically, more than 3) are often referred to as deep neural nets, and their use in machine learning is referred to as “deep learning”. A comprehensive treatment of these models is presented by Goodfellow et al. [2016].

Reinforcement learning (RL) is a branch of machine learning concerned with training a model, such as a neural net, to interact with an environment so as to maximize the scalar “reward” it receives from that environment over time. RL methods are useful in situations where we want to train a model to take actions that maximize (or equivalently, minimize)

some quantity over time, but do not know in advance what actions can achieve this. This is in contrast with supervised learning, where the desired outputs of the model are known exactly in advance, at least on some partial set of inputs. In most CO problems, it is difficult to find globally optimal solutions but easier to gauge the quality of a given solution. This makes RL a natural fit to CO problems, and as documented by Bengio et al. [2021], there is growing interest in the application of RL with neural nets to CO problems such as the TSP. Most of the work cited in this section uses RL methods to train neural net models.

An important early work in this vein was that of Vinyals et al. [2015], who proposed a deep neural net model called a Pointer Network, and trained it via supervised learning to solve instances of the TSP. Subsequent work, such as that of Dai et al. [2017], Kool et al. [2019], and Sykora et al. [2020], has built on this. These works use similar neural net models with RL to construct CO solutions, and attain impressive performance on the TSP, the VRP, and other CO problems. More recently, Fu et al. [2021] train a model on small TSP instances and present an algorithm that applies the model to much larger instances. Choo et al. [2022] present a hybrid algorithm of Monte Carlo Tree Search and Beam Search that draws better sample solutions for the TSP and Capacitated Vehicle Routing Problem (CVRP) from a neural net policy like that of Kool et al. [2019].

The above approaches all belong to the family of “construction” methods, which solve a CO problem by starting with an “empty” solution and adding to it until it is complete - for example, in the TSP, this would mean constructing a path one node at a time, starting with

an empty path and stopping once the path includes all nodes. The solutions from these neural construction methods come close to the quality of those from specialized algorithms such as Concorde [Applegate et al., 2001], while requiring much less run-time to compute [Kool et al., 2019].

By contrast with construction methods, “improvement” methods start with a complete solution and repeatedly modify it, conducting a search through the solution space for improvements. In the TSP, this might involve starting with a complete path, and swapping pairs of nodes in the path at each step to see if the path is shortened. Improvement methods tend to be more computationally costly than construction methods when generating a solution, but their more exhaustive search of the solution space can yield better results.

Like construction methods, much recent work has considered using deep learning and RL for improvement methods. Deep neural nets have been trained to choose the search moves to be made at each step of an improvement method [Hottung and Tierney, 2019, Chen and Tian, 2019, da Costa et al., 2020, Wu et al., 2021, Ma et al., 2021]. Kim et al. [2021] train one neural net to construct a set of initial solutions, and another to modify and improve them. Mundhenk et al. [2021] train a Recurrent Neural Net (RNN) via RL to construct a population of initial solutions for a genetic algorithm - itself an improvement method - and then use the outputs of the genetic algorithm as data to further train the RNN. And more recently, Ye et al. [2024] train a neural net to provide a heuristic score for choices in CO

problems in the context of an Ant Colony Optimization algorithm. This work has shown impressive performance on the TSP, VRP, and similar CO problems.

We do the same here, applying a method similar to that of Kool et al. [2019] to the TNDP.

Graph Neural Nets

Many classic CO problems like the TSP and VRP lend themselves to being described in terms of a graph. For this reason, most of the above work uses a type of model called a GNN that is designed to operate on graph-structured data [Bruna et al., 2013, Kipf and Welling, 2016, Defferrard et al., 2016, Duvenaud et al., 2015]. Inspired by the success of convolutional neural nets on computer vision tasks, Bruna et al. [2013] proposed a neural graph operator that performed convolution in the spectral domain of the graph. This idea was expanded upon by Kipf and Welling [2016] and Defferrard et al. [2016]. Meanwhile, Duvenaud et al. [2015] proposed a non-spectral graph convolution based only on the spatial neighbourhoods of nodes. Since then, GNNs have been applied in many domains, such as the predicting chemical properties of molecules Duvenaud et al. [2015], Gilmer et al. [2017], analyzing large web graphs Ying et al. [2018], and in combination with RL, designing printed circuit boards Mirhoseini et al. [2021]. An overview of GNNs is provided by Battaglia et al. [2018].

In general, a graph neural net operates on a graph described by an a collection of d_v -

dimensional node features \mathbf{x}_i for each of the n nodes, the set of edges \mathcal{E} , and possibly a collection of d_e -dimensional features E for each edge. Like other neural net architectures, it is composed of a series of layers. Each layer can be thought of as passing “messages” between nodes based on their relationship in the graph, and then having each node form a new embedding by transforming and combining the messages it receives. Many graph neural net layer types can be described by the following equation:

$$\mathbf{h}_{l+1}^i = \sigma \left(\sum_{j \in N(i)} \alpha_{ij} M_l \mathbf{h}_l^j \right) \quad (1.1)$$

Here, \mathbf{h}_l^i is an d_l -dimensional embedding of node i 's descriptor (with $\mathbf{h}_0^i = \mathbf{x}_i$); M_l is a learnable $d_l \times d_{l+1}$ weight matrix; α_{ij} is a weight that indicates how much node j contributes to node i 's embedding; $N(i)$ is a set of nodes which are “connected” in some sense to i ; and σ is a non-linear function such as the sigmoid function or the ReLU function [Fukushima, 1969]. Figure 1.3 provides a schematic illustration of this process.

The choices of $N(i)$ and α_{ij} differentiate GNN architectures from one another. A simple choice is to have $N(i) = \{j | (i, j) \in \mathcal{E}\} \cup \{i\}$, and $\alpha_{ij} = |N(i)|^{-1}$: this means at each layer, each node receives a message from itself and its one-hop neighbours in the graph, and averages these before applying σ to get its new feature. If edge weights e_{ij} are provided, another choice would be to let $\alpha_{ij} = e_{ij}$, so that a node's new feature is a weighted average of its neighbours. $N(i)$ might be expanded to all nodes in the graph, with α_{ij} being a coefficient based on the distance in the graph between i and j . Another choice is that of the Graph Attention

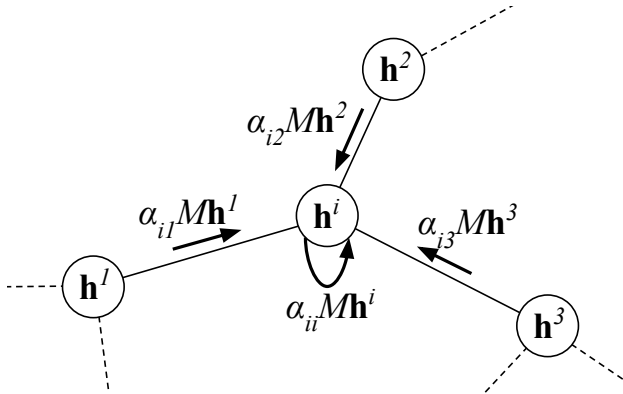


Figure 1.3: A schematic of the message-passing step of a GNN layer for one node in a graph. As described in Equation 1.1, node i receives messages \mathbf{h}^j from each neighbouring node and from itself, which are the node’s feature transformed by the learned matrix M and scaled by the coefficients α_{ij} . The received messages are summed to form the layer’s new embedding of node i .

Network [Veličković et al., 2018, Brody et al., 2021]: here, $N(i) = \{j | (i, j) \in \mathcal{E}\} \cup \{i\}$ as in the one-hop GNN, but α_{ij} is replaced by $\alpha_{ij} = f(\Theta_l, \mathbf{h}_l^i, \mathbf{h}_l^j, \mathbf{e}_{ij})$, a learned function at each layer of node i and j ’s embeddings and of an edge feature \mathbf{e}_{ij} if this is available.

1.1.3 Optimization of Public Transit

As stated above, the TNDP is an NP-hard problem, meaning that it is impractical to find optimal solutions in most cases. While analytical optimization and mathematical programming methods have shown some success on small instances [van Nes, 2003, Guan et al., 2006], they struggle to realistically represent the problem [Guihaire and Hao, 2008, Kepaptsoglou and Karlaftis, 2009]. Metaheuristic approaches, as defined by Sörensen et al. [2018], have thus been more widely used. The most popular of these have been genetic

algorithms, simulated annealing, and ant-colony optimization, along with hybrids of these methods [Guihaire and Hao, 2008, Kepaptsoglou and Karlaftis, 2009, Yang and Jiang, 2020, Durán-Micco and Vansteenwegen, 2022, Hüselmann et al., 2023]. Recent work has shown success on the TNDP with other metaheuristics, such as a sequence-based selection hyper-heuristic [Ahmed et al., 2019], beam search [Islam et al., 2019], and particle swarms [Lin and Tang, 2022].

Many different low-level heuristics have been applied within these metaheuristic algorithms, but most have in common that they select among possible neighbourhood moves uniformly at random. One exception is Hüselmann et al. [2023]. The authors design two heuristics based on a simple model of how each change the heuristic could make would affect the network’s quality. They use this model to adjust the probabilities of different changes being selected. When they use these heuristics in a genetic algorithm along with a set of standard uniformly-random low-level heuristics, they obtain state-of-the-art results. However, their simple model ignores passenger trips involving transfers, and how the user’s preferences may alter the cost function.

While neural nets have often been used for predictive problems in urban mobility [Xiong and Schneider, 1992, Rodrigue, 1997, Chien et al., 2002, Jeong and Rilett, 2004, Çodur and Tortum, 2009, Li et al., 2020] and for other transit optimization problems such as scheduling, passenger flow control, and traffic signal control [Zou et al., 2006, Jiang et al., 2018, Ai et al., 2022, Yan et al., 2023, Wang et al., 2024], they have not often been applied to the TNDP, and

neither has RL. Two recent exceptions are notable here: Darwish et al. [2020] and Yoo et al. [2023]. Both use RL to design routes and a schedule that obtain good results on the Mandl benchmark city [Mandl, 1980], a single small city with just 15 transit stops. Darwish et al. [2020] use a GNN approach inspired by Kool et al. [2019]; in our own work we experimented with a nearly identical approach, but found it did not scale beyond very small instances like Mandl. Meanwhile, Yoo et al. [2023] use tabular RL, an approach which is practical only for small problem sizes. Both of these approaches also require a new model to be trained on each problem instance.

1.2 The Transit Network Design Problem

The planning of transit networks can be divided into three primary sub-problems:

- Transit Network Design Problem (TNDP): establishing the layout of the routes and their stops, given an existing network of roads and candidate stop locations
- Frequency-Setting Problem (FSP): determining the departure frequency on each route
- Timetabling Problem (TP): determining routes and departure times for each vehicle in the system

The three problems can be solved sequentially in isolation, and much work treats them as such [Guihaire and Hao, 2008, Kepaptsoglou and Karlaftis, 2009, Abduljabbar et al., 2019].

In this work, we consider only the TNDP. But we note that their inter-relatedness mean that more optimal solutions may potentially be obtained by optimizing over multiple aspects of the problem at once.

We here use a graph formulation of the TNDP that is common in the literature [Mumford, 2013b]. In this formulation, we are given an augmented graph \mathcal{G} that represents a city:

$$\mathcal{G} = (\mathcal{N}, \mathcal{E}_s, D) \tag{1.2}$$

This augmented graph is comprised of a set \mathcal{N} of n nodes, representing candidate stop locations; a set \mathcal{E}_s of street edges (i, j, τ_{ij}) connecting the nodes, with weights τ_{ij} indicating the time it takes a transit vehicle to drive between the nodes; and an $n \times n$ Origin-Destination (OD) matrix D giving the travel demand (in number of trips) D_{ij} between every pair of nodes $i, j \in \mathcal{N} \times \mathcal{N}$. Each node i has an associated position in 2D space, \mathbf{p}_i . A transit route r is defined as a path through the street graph $\{\mathcal{N}, \mathcal{E}_s\}$: a sequence of nodes $[v_0, v_1, \dots, v_{k-1}, v_k]$ where every pair of consecutive nodes $v_i, v_{j=i+1}$ has a matching edge $((i, j, \tau_{ij}) \in \mathcal{E}_s)$, and where no node is visited more than once in the sequence ($i \neq j \Rightarrow v_i \neq v_j$). A transit network \mathcal{R} is defined as a set of transit routes. The goal in the TNDP is to find a transit network \mathcal{R} that minimizes a cost function $C : \mathcal{G}, \mathcal{R} \rightarrow \mathbb{R}^+$.

We deal with the symmetric TNDP, meaning we assume that $D = D^\top$, $(i, j, \tau_{ij}) \in \mathcal{E}_s$ iff. $(j, i, \tau_{ij}) \in \mathcal{E}_s$, and all routes are traversed both forwards and in reverse by vehicles on them, linking their nodes in both directions. An example city graph with a transit network

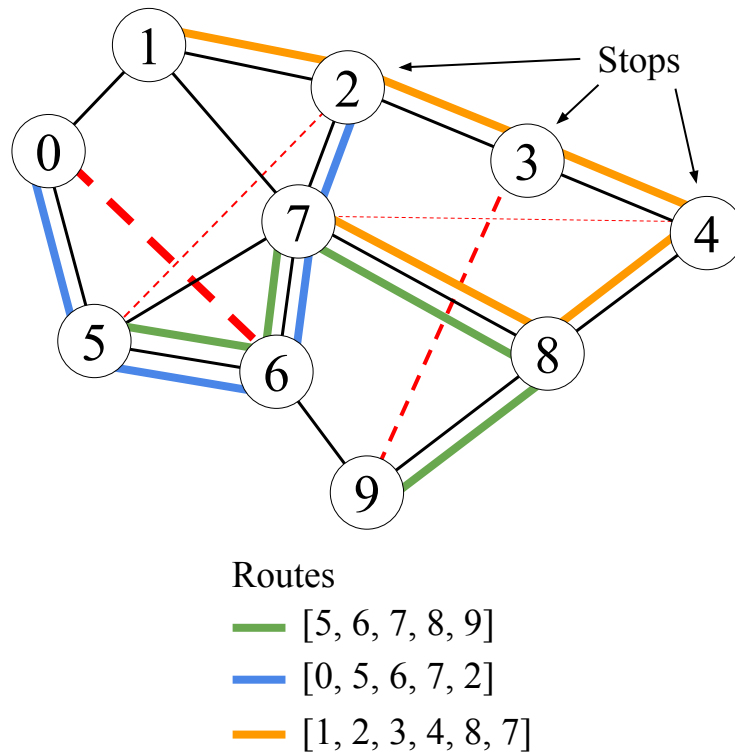


Figure 1.4: An example city graph with ten numbered nodes and three routes. Street edges are black, routes are in colour, and two example demands are shown by dashed red lines. The edges of the three routes form a sub-graph of the street graph $(\mathcal{N}, \mathcal{E}_s)$. All nodes are connected by this sub graph, so the three routes form a valid transit network. The demand between nodes 2 and 5, 0 and 6, and 7 and 4 can be satisfied directly by riding on the blue line, while the demand from 3 to 9 requires one transfer: passengers must ride the orange line from node 3 to 8, and then the green line from node 8 to 9.

is shown in Figure 1.4.

A transit network \mathcal{R} induces a **route graph**, which we denote $\mathcal{G}_{\mathcal{R}}$. The route graph is a graph indicating which trips are possible by transit between stops. An edge between nodes i and j in the route graph means that a passenger can get from i to j by taking only a single transit route, with no transfers needed. The route graph shares the same set of nodes \mathcal{N} as \mathcal{G} , but the edges in its edge set $\mathcal{E}_{\mathcal{R}}$ correspond to direct trips between nodes via transit routes:

$$\mathcal{E}_{\mathcal{R}} = \{(i, j, \tau_{rij}) \mid \exists r \in \mathcal{R}, i \in r \wedge j \in r\} \quad (1.3)$$

For example, a route $r = [0, 1, 3, 4]$ in a city with five nodes induces edges in $\mathcal{G}_{\mathcal{R}}$ between 0 and 1, 0 and 3, 0 and 4, 1 and 3, 1 and 4, and 3 and 4.

Each edge in $\mathcal{E}_{\mathcal{R}}$ also has a weight τ_{rij} , the time of the trip between i and j provided by route r , where r is the route that provides the shortest direct trip between i, j of any route in \mathcal{R} . It may be that $\tau_{rij} > T_{ij}$, as the route r does not necessarily follow the shortest path between i and j .

With $\mathcal{G}_{\mathcal{R}}$ defined, we can then define SR as the collection of shortest paths sr_{ij} between all node pairs i, j over the route graph $\mathcal{G}_{\mathcal{R}}$. $\mathcal{G}_{\mathcal{R}}$ and SR are useful in several ways. Firstly, they let us count $n_{\mathcal{R}ij}^T$, the number of transfers required between two nodes i and j : it is simply two less than the number of nodes along sp_{ij} : $n_{\mathcal{R}ij}^T = |sr_{ij}| - 2$, as long as the shortest path is chosen by breaking ties in favour of paths with fewer nodes (which we do). Secondly,

they let us find the time $\tau_{\mathcal{R}ij}$ for the shortest transit trip between i and j , by summing the edge weights τ_{rij} along sr_{ij} .

We note that in general neither \mathcal{G} nor $\mathcal{G}_{\mathcal{R}}$ are metric graphs: that is, it is not generally true that $\tau_{ij} = \|p_i - p_j\|$ or that $\tau_{rij} = \|p_i - p_j\|$.

1.2.1 Constraints

In this version of the TNDP, a transit network must satisfy the following constraints to be considered valid:

1. Connectedness: $\mathcal{G}_{\mathcal{R}}$ must be connected, providing some path over transit between every pair of nodes $(i, j) \in \mathcal{N}$ for which $D_{ij} > 0$.
2. Number of routes: \mathcal{R} must contain exactly S routes ($|\mathcal{R}| = S$), where S is a parameter set by the user.
3. Number of stops: Every route $r \in \mathcal{R}$ must obey $m_{\min} \leq |r| \leq m_{\max}$, where m_{\min} and m_{\max} are parameters set by the user that limit the number of stops a route may visit.
4. Simple paths: A route $r \in \mathcal{R}$ must be a simple path in \mathcal{G} : that is, it must not contain cycles, and every pair of consecutive nodes in r must have a matching edge in \mathcal{E}_s .

1.2.2 Cost Function

In this work, we assume that the cost function has the following structure. The passenger cost, C_p , is the average passenger trip time over the network. It is computed by assuming that every passenger chooses the shortest path available over the transit network from their origin to their destination, including by transferring between transit routes any number of times by getting off of route A at stop i and then boarding route B which also stops at i . Each transfer extends the time of a trip because the passenger must wait for the vehicle on route B to arrive; also, in reality transfers are viewed as inconvenient by passengers even if waiting times are short, so passengers tend to try to avoid them where possible [Chakrabarti, 2017]. To reflect these factors, we impose a time penalty p_T once for each transfer made on a trip, which will discourage the selection of trips containing transfers when using a shortest-path criterion, and set this time penalty to five minutes (300 seconds). This is common practice for computing C_p for the TNDP [Mumford, 2013b, John et al., 2014, Kılıç and Gök, 2014, Hüsselmann et al., 2023]. C_p is thus computed as:

$$C_p(\mathcal{G}, \mathcal{R}) = \frac{\sum_{i,j} D_{ij}(\tau_{\mathcal{R}ij} + p_T n_{\mathcal{R}ij}^T)}{\sum_{i,j} D_{ij}} \quad (1.4)$$

The operating cost is the total driving time of the routes, or total route time:

$$C_o(\mathcal{G}, \mathcal{R}) = \sum_{r \in \mathcal{R}} \tau_r \quad (1.5)$$

Where τ_r is the time needed to completely traverse a route r in one direction.

To enforce constraints 1 and 3 on \mathcal{R} , we use a third term C_c , itself the sum of three terms:

$$C_c(\mathcal{G}, \mathcal{R}) = F_{un} + F_s + 0.1\delta_v \quad (1.6)$$

Here, F_{un} is the fraction of node pairs (i, j) with $D_{ij} > 0$ for which \mathcal{R} provides no path: a measure of how many possible violations of constraint 1 really occur in \mathcal{R} . F_s is a similar measure for constraint 3, but it is proportional to the actual number of stops more than m_{\max} or less than m_{\min} that each route has. Specifically:

$$F_s = \frac{\sum_{r \in \mathcal{R}} \max(0, m_{\min} - |r|, |r| - m_{\max})}{S * m_{\max}} \quad (1.7)$$

δ_v is a delta function that takes value 0 if $F_{un} = 0$ and $F_s = 0$, and takes value 1 otherwise.

We use fractional measures F_{un} and F_s instead of absolute measures so that C_c will tend to fall in the range $[0, 1]$ regardless of the size of the city graph. This is desirable for reasons relating to the numerical stability of neural net training. However, it has the drawback that if the city graph C has very many nodes (large n), and if \mathcal{R} violates only a few constraints, F_{un} and F_s may become vanishingly small compared to C_o and C_p . This could lead to algorithms ignoring small numbers of constraint violations. To prevent this, we include the term $0.1\delta_v$, which ensures that if any constraints are violated, C_c cannot be less than 0.1,

but it will be 0 if all constraints are respected. This ensures that even one violation will have a significant impact on overall cost $C(\mathcal{G}, \mathcal{R})$, no matter the size of the city graph.

C_c does not penalize violations of constraints 2 and 4, because as we will show in later chapters, the TNDP algorithms we consider in this thesis always respect those constraints by design.

The complete cost function is a weighted sum of the three parts:

$$C(\mathcal{G}, \mathcal{R}) = \alpha w_p C_p(\mathcal{G}, \mathcal{R}) + (1 - \alpha) w_o C_o(\mathcal{G}, \mathcal{R}) + \beta C_c(\mathcal{G}, \mathcal{R}) \quad (1.8)$$

The weight $\alpha \in [0, 1]$ controls the trade-off between passenger and operating costs, while β is the penalty assigned for each constraint violation. In practice, we hold β constant in our experiments. w_p and w_o are re-scaling constants chosen so that $w_p C_p$ and $w_o C_o$ both vary roughly over the range $[0, 1]$ for different \mathcal{G} and \mathcal{R} ; this is done so that α will properly balance the two, and to stabilize training of the GNN policy. The values used are:

$$w_p = (\max_{i,j} T_{ij})^{-1} \quad (1.9)$$

$$w_o = (S \max_{i,j} T_{ij})^{-1} \quad (1.10)$$

1.3 Contribution to original knowledge

In this work, we train neural net models using RL to construct transit networks, and then use these models in combination with existing metaheuristic search algorithms for the TNDP. We show that this technique is competitive with the state of the art on large benchmark cities, and sets a new state of the art on the largest benchmark city in terms of the operating cost of the transit network. Furthermore, we show that our technique can be applied to a very large real-world problem instance and find transit networks that improve on the city’s existing transit. To our knowledge, the work presented in this thesis represents the first successful attempt to use deep reinforcement learning to address the TNDP for cities of realistic size.

As noted by Fan and Mumford [2010], metaheuristic search algorithms depend on three factors for their success:

1. The representation of solutions,
2. The algorithm for constructing the initial solution,
3. The “moves” in solution space chosen at each step of search.

Our neural policies share a standard solution representation (factor 1) with most metaheuristic approaches to this problem. We use our neural policies to augment the second and third factors, showing in each case that this leads to significant improvements in performance over baseline algorithms.

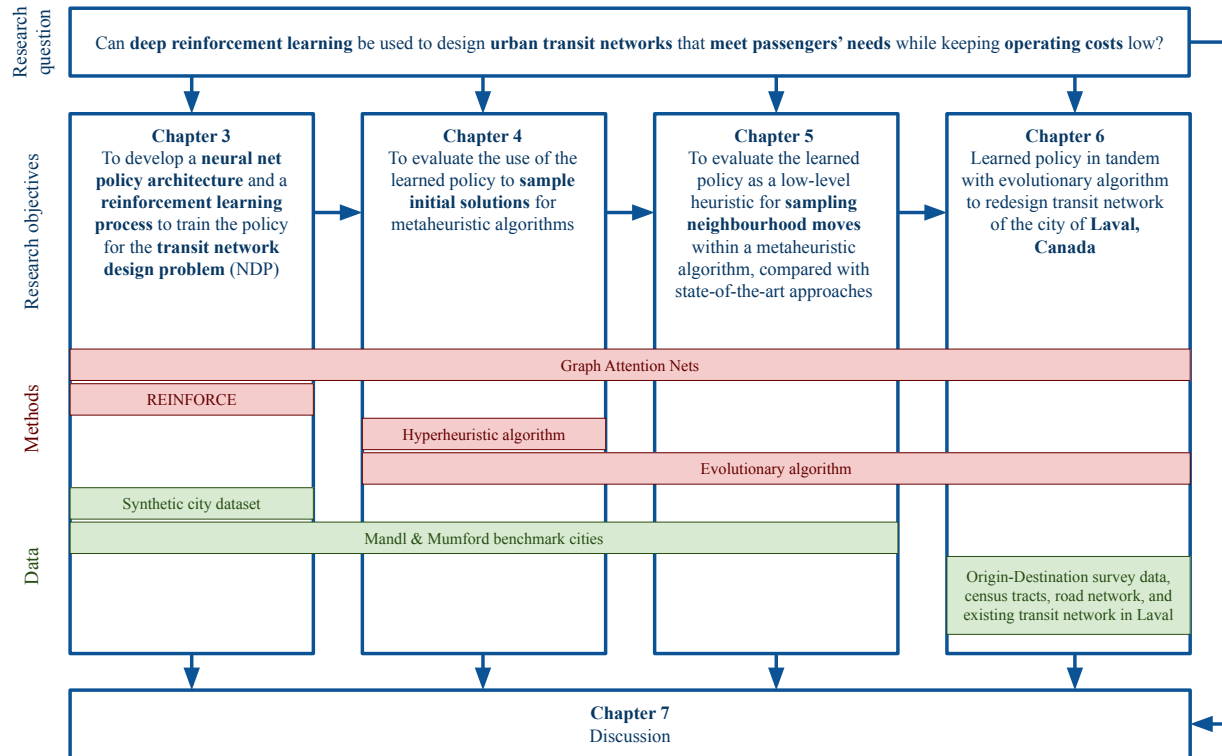


Figure 1.5: Overview of thesis research

1.4 Dissertation Structure

Each chapter of this dissertation concerns one of four research objectives, each of which is based on our central research question: Can deep reinforcement learning be used to design effective urban transit networks? By “effective”, we here mean that they meet passengers’ needs for efficient trips with few transfers, while also meeting the transit agency’s need to keep operating costs affordably low. Figure 1.5 outlines these research objectives, and the data and methods we use to accomplish them.

In Chapter 2, we first formulate a construction approach to the TNDP as a Markov

Decision Process (MDP). Based on this formulation, we propose an architecture for a neural net model to address the TNDP, and an RL algorithm and synthetic dataset to train this model to serve as an effective policy on the MDP. We present the results achieved by this policy on the widely-used Mandl [Mandl, 1980] and Mumford [Mumford, 2013b] benchmark cities.

In Chapter 3, we address the second of Fan and Mumford’s three factors by using the neural policies trained in Chapter 2 to generate the initial transit networks in two existing metaheuristic algorithms for the TNDP. We compare the results with those achieved using the original initialization procedures of those algorithms, again using the Mandl and Mumford benchmark cities as our points of comparison.

In Chapter 4, we consider the use of the same neural policies to select neighbourhood moves within an evolutionary algorithm. This addresses the third of Fan and Mumford’s factors. We compare the results with those of an evolutionary algorithm that does not use a learned policy to select neighbourhood moves, and perform a series of ablation studies to understand the impact of different components of our algorithm. All experiments are again performed on the Mandl and Mumford benchmark cities.

In Chapter 5, we apply Chapter 4’s synthesis of a neural policy and an evolutionary algorithm to a simulated city based on real-world data from the city of Laval, Canada. We perform experiments under three different assumptions about the planner’s preferences, and compare the results to the city’s current real transit network. Finally, we present some

concluding remarks in Chapter 6.

Chapter 2

Designing Transit Networks with a Graph Attention Net

In this chapter, we describe our approach to solving the TNDP using deep reinforcement learning alone. We begin by presenting a formulation of the TNDP as a Markov Decision Process. We then describe the neural net policy architecture that we designed to address this Markov Decision Process, and the reinforcement learning algorithm we used to train this policy. We then evaluate learned policies on a widely-used benchmark, and consider the quality of these results in comparison with metaheuristic improvement methods.

2.1 Markov Decision Process Formulation

A Markov Decision Process (MDP) is a formalism originating with Bellman [1958], and which is commonly used to define problems in reinforcement learning [Sutton and Barto, 2018, Chapter 3]. In an MDP, an **agent** interacts with an **environment** over a series of **timesteps** t , starting at $t = 1$. At each timestep, the environment has **state** $s_t \in \mathcal{S}$, and the agent observes the state and takes some **action** $a_t \in \mathcal{A}_t$, where \mathcal{A}_t is the set of available actions at t . The environment then transitions to a new state $s_{t+1} \in \mathcal{S}$ according to the state transition distribution $P(s_{t+1}|s_t, a_t)$, and the agent receives a numerical **reward** $R_t \in \mathbb{R}$ according to the reward distribution $P(R_t|s_t, a_t, s_{t+1})$. The agent chooses actions according to its **policy** $\pi(a_t|s_t)$, which is a probability distribution over \mathcal{A}_t given the state s_t . In RL, the goal is to learn a policy π that maximizes the return G_t , defined as a time-discounted sum of rewards:

$$G_t = \sum_{t'=t}^{t_{\text{end}}} \gamma^{t'-t} R_{t'} \quad (2.1)$$

Where $\gamma \in [0, 1]$ is a parameter that discounts rewards farther in the future, and t_{end} is the final timestep of the MDP. The sequence of states visited, actions taken, and rewards received from $t = 0$ to t_{end} constitutes one **episode** of the MDP.

We here describe the MDP we use to represent a construction approach to the TNDP. As shown in Equation 2.2, the state s_t is composed of the set of routes \mathcal{R}_t planned so far,

and an incomplete route r_t which is being planned.

$$s_t = (\mathcal{R}_t, r_t) \quad (2.2)$$

The starting state is $s_1 = (\mathcal{R}_1 = \{\}, r_1 = [])$. At a high level, the MDP alternates at every timestep t between two modes: on odd-numbered t , the agent selects an extension to the route r_t that it is currently planning; on even-numbered t , the agent chooses whether or not to stop extending r_t and add it to the set of finished routes.

On odd-numbered timesteps, the available actions are drawn from SP, the set of shortest paths between all pairs of nodes in \mathcal{G} . If $r_t = []$, then:

$$\mathcal{A}_t = \{a \mid a \in \text{SP}, |a| \leq m_{\max}\} \quad (2.3)$$

Otherwise, $\mathcal{A}_t = \text{EX}_{r_t}$, where EX_{r_t} is the set of paths $a \in \text{SP}$ that satisfy all of the following conditions:

- $(i, j, \tau_{ij}) \in \mathcal{E}_s$ (the set of street edges), where i is the first node of a and j is the last node of r_t , or vice-versa
- $|a| \leq m_{\max} - |r_t|$, to respect transit network constraint 3
- a and r_t have no nodes in common, to respect transit network constraint 4

Figure 2.1 shows an example of the extensions available to a partial route. Once a path

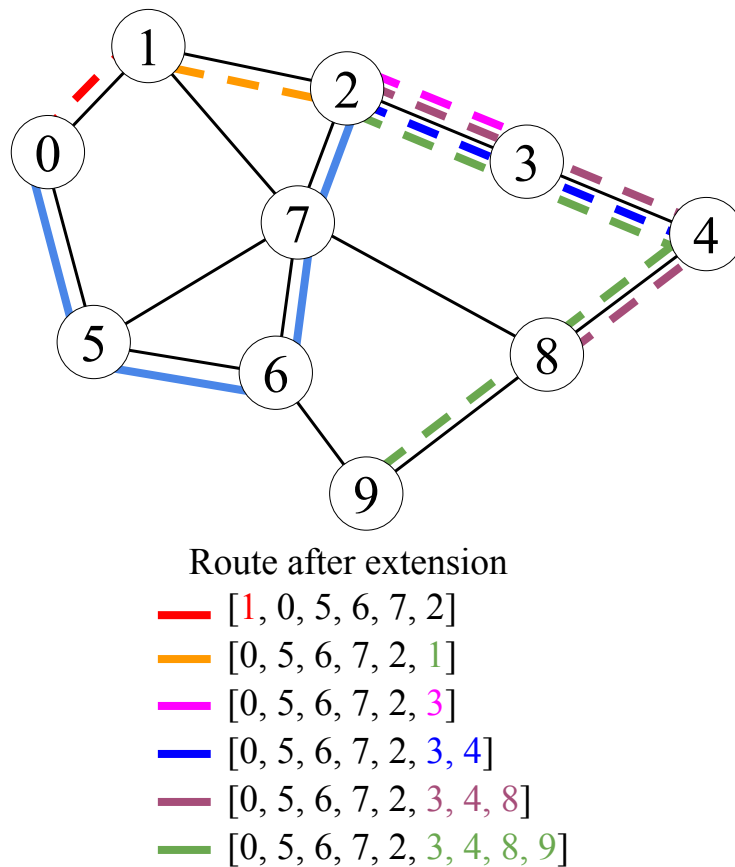


Figure 2.1: An in-progress route r with the possible extensions available to it, which form \mathcal{A}_t . The route so far is shown with solid blue lines, while the extensions are dashed lines, with different colours for each extension. The corresponding routes after adding each extension are listed below the graph. Only one extension (to node 1, shown in red) is possible from the route's starting terminal, since all nodes reachable from 1 are already on the route. Five extensions are possible from the other end at this step.

$a_t \in \mathcal{A}_t$ is chosen, r_{t+1} is formed by appending a_t to the beginning or end of r_t as appropriate.

On even-numbered t , the action space depends on the number of stops in r_t :

$$\mathcal{A}_t = \begin{cases} \{\text{continue}\} & \text{if } |r_t| < m_{\min} \text{ and } |\text{EX}_{r_t}| > 0 \\ \{\text{halt}\} & \text{if } |r_t| = m_{\max} \text{ or } |\text{EX}_{r_t}| = 0 \\ \{\text{continue, halt}\} & \text{otherwise} \end{cases} \quad (2.4)$$

If $a_t = \text{halt}$, r_t is added to \mathcal{R}_t to get \mathcal{R}_{t+1} , and $r_{t+1} = []$ is a new empty route. If $a_t = \text{continue}$, then $\mathcal{R}_{t+1} = \mathcal{R}_t$ and $r_{t+1} = r_t$. Thus, the full state transition distribution is deterministic.

The episode ends when the S -th route is added to \mathcal{R} : that is, if $|\mathcal{R}_{t+1}| = S$, the episode ends at timestep t . This ensures network constraint 2 will be respected. The output transit network is set to $\mathcal{R} = \mathcal{R}_{t+1}$, and the final reward is $R_{t_{\text{end}}} = -C(\mathcal{G}, \mathcal{R})$. At all prior steps, $R_t = 0$.

This MDP formalization imposes some helpful biases on the kinds of transit networks we consider. First, it requires any route connecting i and j to stop at all nodes along some path between i and j , biasing planned routes towards covering more nodes. Second, it biases routes toward directness by forcing them to be composed of shortest paths. While an agent may construct arbitrarily indirect routes by choosing paths with length 2 at every step, this is unlikely because in a realistic street graph, the majority of paths in SP are longer than two nodes. Third, the alternation between deciding to continue or halt a route and deciding

how to extend the route means that the probability of halting does not depend on how many different extensions are available; so a policy learned in environments with fewer extensions should generalize more easily to environments with more, and vice versa.

2.2 Neural Net Architecture and Training

Reinforcement learning algorithms can be broadly categorized into value-learning methods and policy-gradient methods. Value-learning algorithms attempt to estimate the “value”, or time-discounted cumulative return, of states and actions. If the value estimates are accurate, they can be used to define a policy π that simply chooses the action with the highest estimated value at each step. Policy gradient algorithms, on the other hand, view a policy as a probability distribution $\pi(a|s)$ over actions given the current state, and they attempt to learn the policy’s distribution directly. They do this by updating an action’s probability based on the observed results, increasing $\pi(a|s)$ when a leads to higher-than-expected returns, and decreasing $\pi(a|s)$ in the opposite case.

Policy gradient methods produce non-deterministic policies that can be sampled stochastically to produce diverse solutions. This makes them well-suited to CO problems: finding optimal solutions to these is often intractable, so it is useful to be able to sample multiple promising solutions and choose the best of them. This property also makes these policies useful as a source of random “neighbourhood moves” in the space of solutions to a CO, the purpose to which we will put them later in Chapter 4. For these reasons, we chose

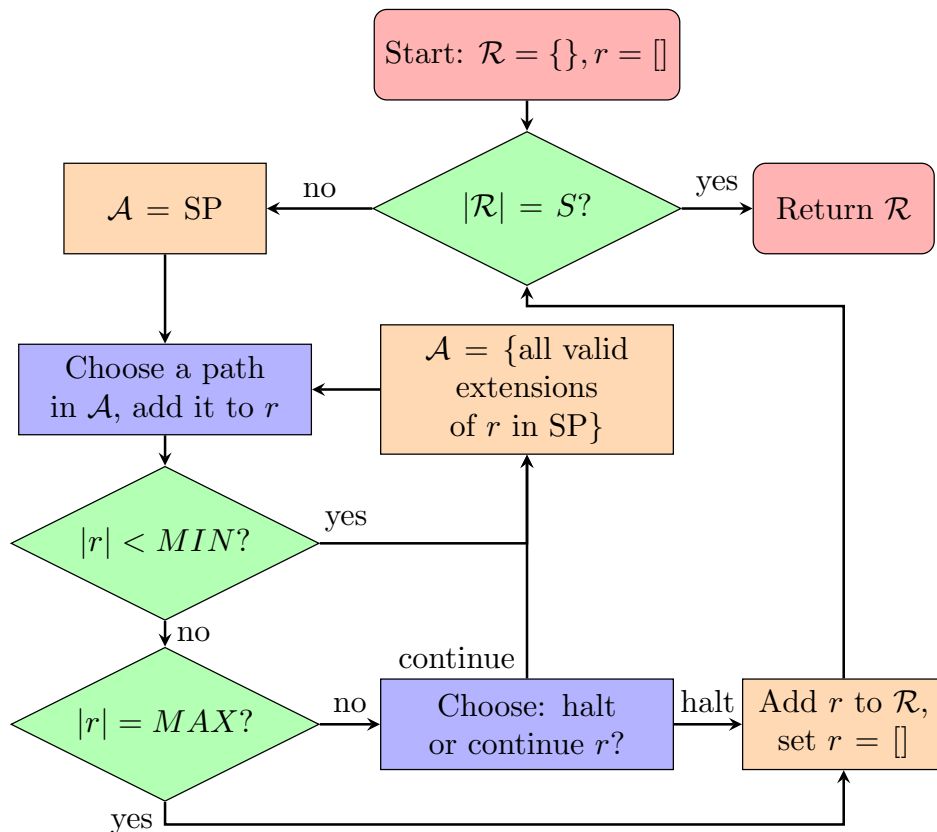


Figure 2.2: A flowchart of the transit network construction process defined by our MDP. Blue boxes indicate points where the timestep t is incremented and the agent selects an action. Red nodes are the beginning and ending of the process. Green nodes are hard-coded decision points. Orange nodes show updates to the state \mathcal{S} and action space \mathcal{A} .

to use policy gradient methods of deep reinforcement learning to learn policies for the TNDP.

Our policy $\pi_\theta(a|s)$ is a neural net parameterized by θ , which we train to maximize the cumulative return G_t on the construction MDP described in section 2.1. By then following this policy on the MDP for some city \mathcal{G} , we can obtain a transit network \mathcal{R} for that city. We refer to this learned policy as the Learned Constructor (LC). The policy can be used for planning in one of two modes: stochastic mode, where we randomly sample each action a_t from the distribution $\pi_\theta(\cdot|s_t)$, and greedy mode, where we “greedily” choose the highest-scored action under the policy, $a_t = \max_{a \in \mathcal{A}} \pi(a|s_t)$. Instead, the cost function’s constraint-violation term βC_c increases cost in proportion to the number of constraint violations, so that the algorithm will be more likely to keep solutions with fewer violations, eventually driving C_c to zero.

2.3 Policy Architecture

The policy π_θ is a neural net with three components: a Graph Attention Net (GAT) “backbone”, a halting module NN_{halt} , and an extension module NN_{ext} . The GAT outputs node embeddings \mathbf{y}_i , which are operated on by one of two policy “heads”, depending on the timestep: NN_{ext} for choosing among extensions when t is odd, and NN_{halt} for deciding whether to halt when t is even.

Figure 2.3 illustrates the three components’ role in the transit network construction

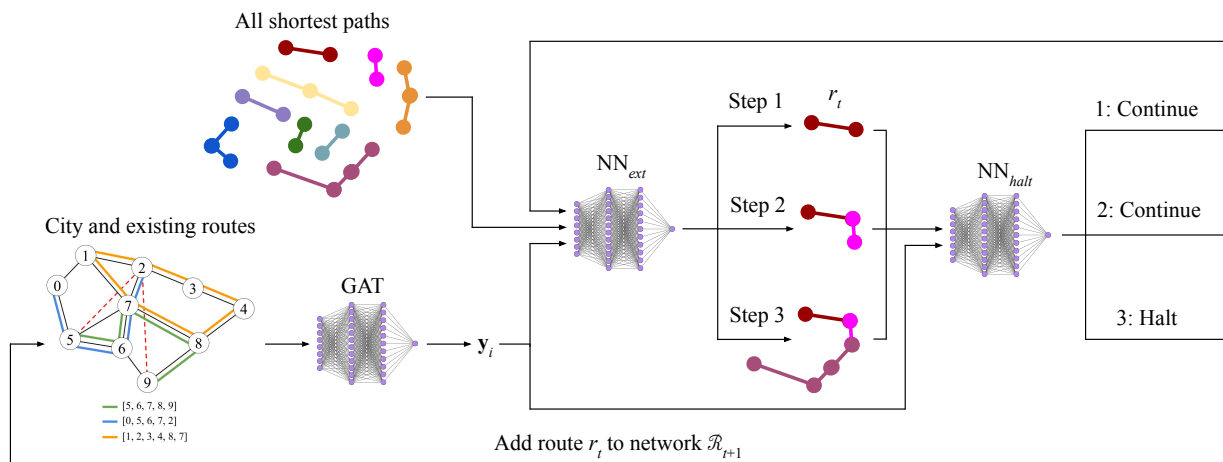


Figure 2.3: A schematic illustration of the role of each component of the policy net in the network construction process. This loop continues until $|\mathcal{R}_t| = S$, that is, we have the desired number of routes.

process.

2.3.1 Graph Attention Backbone

As described in section 1.2, we view the TNDP as a problem on graphs. This makes GNNs a natural design choice for a neural net architecture for this problem. As described in subsection 1.1.2, many GNN architectures have been proposed. Graph convolutional nets are among the earliest form of GNN architectures, and have been used successfully in many tasks - as has a much-simplified model linear model, the Simplified Graph Convolution.

However, these models assume a predefined adjacency matrix for the graph. This allows only the use of scalar edge features, and by design treats them as adjacencies that directly weight the contributions of a node's neighbours to its feature at the next GNN layer. In the

TNDP, we must deal not only with the fixed street graph of a city \mathcal{G} , but also with the route graph $G_{\mathcal{R}}$, which changes at each step of the construction MDP, and with its demand matrix, which can be viewed as a fully-connected graph with edge weights D_{ij} . These three graphs each have distinct edge sets, with edge weights signifying different things, but share the same node set \mathcal{N} . They can be viewed as forming a multi-layer graph. Graph convolutions are not well-suited to this kind of structure.

One way of dealing with this multi-layer graph is to treat it as a fully-connected simple graph, with edge features that combine the edge information from \mathcal{E}_s , $\mathcal{E}_{\mathcal{R}}$, and D . Such an edge feature \mathbf{e}_{ij} for the edge linking nodes i, j would have two binary features indicating whether or not i, j is in \mathcal{E}_s and $\mathcal{E}_{\mathcal{R}}$, and three scalar features, $\tau_{ij}, \tau_{rij}, D_{ij}$. This edge information is important to designing a good transit network, so we need a neural architecture that will make use of these rich edge features.

For this, we turned to Graph Attention Nets. A GAT is a graph neural net architecture that uses a multi-head attention mechanism [Vaswani et al., 2017] to determine the contribution made to a node’s feature by each of its neighbours. GATs can make use of multi-dimensional edge features, and the effect of edge features at each layer on the layer’s output is a learned function, rather than a pre-defined one as in graph convolutions. And they have been shown to perform well on diverse graph-related tasks. We therefore choose the GATv2 architecture proposed in Brody et al. [2021] for the layers of our policy net’s first stage. We note that a graph attention net operating on a fully-connected graph has

close parallels to a Transformer model Vaswani et al. [2017], but unlike Transformers this architecture enables the use of edge features that describe known relationships between elements.

We refer to this first stage as the “backbone” GAT of the neural net. It takes a matrix of n node features X and an $n \times n \times d_e$ tensor of edge features E as input, and applies a series of GAT layers and non-linearities to these. Each layer of the backbone applies the following operation:

$$H^l = \sigma(\text{GAT}_{\theta^l}(H^{l-1}, E)) \quad (2.5)$$

Where σ is a non-linear activation function, H^l is the matrix of node embeddings produced by the l -th layer, and $H^0 = X$. The output node embedding matrix Y is the output of the final L -th, layer, H^L . Along with the edge features E and a global state vector \mathbf{s} , these output node embeddings are given as input to the two policy heads.

2.3.2 Halting Head

The halting module NN_{halt} is a simple Multi-Layer Perceptron (MLP). It takes as input a vector formed by concatenating the following elements:

- the node embeddings of first and last nodes on the current route r_t ; or if $|r_t| = 0$, a placeholder vector whose contents are learned during training

- the mean of the node embeddings over the graph $\frac{1}{n} \sum_i y_i$,
- a vector \mathbf{s}_t , detailed in subsection 2.3.4, that encodes some global information about the state s_t ,
- the driving time of the route being planned, τ_{r_t} .

The MLP outputs a scalar z . We treat this scalar as the log-probability of halting, and apply the sigmoid function to h get the halting probability:

$$\pi_\theta(\text{halt}|s) = \sigma(z) = \frac{1}{1 + e^{-z}}, \quad \pi(\text{continue}) = 1 - \sigma(z) \quad (2.6)$$

2.3.3 Extension Head

The action space of all non-overlapping shortest paths starting from a given node i can be very large. To make learning a policy over this large action space tractable, we found it necessary to “factorize” the computation of probabilities for each shortest-path action. The extension head of our policy net thus outputs a scalar score o_{ij} for each node pair (i, j) in the graph at each step. From these, a score for each extension o_a is computed by summing over o_{ij} for all (i, j) that would become directly connected by appending path a to the current route r_t .

This should be a function of the time between nodes along the path, τ_{aij} , as well as the demand between i and j , and potentially of other features of \mathcal{G} and $\mathcal{G}_{\mathcal{R}}$. But since the paths

are all shortest paths, $\tau_{aij} = T_{ij}$ in every case, so the score o_{aij} gained by linking nodes i, j is independent of the chosen path a : $o_{aij} = o_{ij}$. Let these be computed by some function $f(\cdot)$:

$$o_{ij} = \begin{cases} f(T_{ij}, i, j, \mathcal{G}, \mathcal{G}_{\mathcal{R}}), & \text{if } i \neq j \\ 0, & \text{if } i = j \end{cases} \quad (2.7)$$

Assuming these node-pair scores are an accurate indication of the benefit of linking those nodes, the score of the path as a whole should simply be the sum of scores of the node pairs it links:

$$o_a = \sum_{k \in a} \sum_{l \in a} o_{kl} \quad (2.8)$$

Then, suppose we have a partially-planned route r and are considering paths $a \in \text{SP}$ to extend r . Each of these paths still links all the nodes along it, so can achieve score o_a . But appending a to r will also link every node in r to every node in a , so the benefit of extending r by a should depend on these as well. However, the time taken to get from node $i \in r$ to node $j \in a$ may be greater than T_{ij} , since $r|a$ is not necessarily a shortest path. So the shortest-path node-pair scores o_{ij} here are not appropriate. Instead, new node-pair scores $o_{(r|a)ij}$ should be computed based on the driving time $\tau_{(r|a)ij}$ that would result from joining a to r . Otherwise, the same function $f(\cdot)$ should be appropriate, with the new inter-node time:

$$o_{(r|a)ij} = \begin{cases} f(\tau_{(r|a)ij}, i, j, \mathcal{G}, \mathcal{G}_{\mathcal{R}}), & \text{if } i \neq j \\ 0, & \text{if } i = j \end{cases} \quad (2.9)$$

And the overall score should then be:

$$o_{(r|a)} = o_a + \sum_{i \in r} \sum_{j \in a} o_{(r|a)ij} \quad (2.10)$$

We design the extension policy head to compute the score function $f(\cdot)$. In this policy head, the function $f(\cdot)$ that computes node-pair scores is an MLP, called MLP_{ext1} , that takes as input T_{ij} or $\tau_{(r|a)ij}$ (as appropriate), the backbone GAT's embeddings y_i and y_j of nodes i and j , and the global state vector \mathbf{s} . For each path $a \in \text{SP}$, we sum these node-pair scores to get path scores o_a as in Equation 2.8, and when extending a route r , we compute the extension scores $o_{(r|a)}$ as in Equation 2.10. We can efficiently compute the node-pair scores in a batch by pairing all node embeddings y_i when $r_t = []$; and when $r_t \neq []$, we only compute scores $o_{(r|a)ij}$ for node pairs where exactly one of i or j is in r_t . The resultant scalar scores, o_a and $o_{(r|a)}$, are provided to the next stage of the extension policy head.

If $\alpha = 0.0$, then the benefit of choosing a path a to start or extend a route depends on its driving time τ_a , and generally on the state s . And if $0 < \alpha < 1$, then the benefit of a depends on these as well as on the edges it adds to $\mathcal{E}_{\mathcal{R}}$, and thus on $o_{(r|a)}$. So our architecture

ought to incorporate all of these factors. We achieve this with a final MLP, called MLP_{ext2} , that takes as input \mathbf{s}_t, τ_a , and the previous node-pair-based score (o_a or $o_{(r|a)}$, depending on whether $r_t = []$), and outputs a final scalar score \hat{o}_a for each candidate path. The extension policy is then the softmax of these values:

$$\pi_{\theta}(a|s) = \frac{e^{\hat{o}_a}}{\sum_{a' \in \mathcal{A}} e^{\hat{o}_{a'}}} \quad (2.11)$$

We thus treat the outputs of NN_{ext} as un-normalized log-probabilities of the possible actions during an extension step.

2.3.4 Features and Net Architecture Details

The policy net operates on three inputs: an $n \times 4$ matrix of node feature vectors X , an $n \times n \times 13$ tensor of edge features E , and a global state vector \mathbf{s} .

A node feature x_i is a vector with four elements: the (x, y) spatial coordinates of the node, and its in-degree and out-degree in the street graph.

An edge feature \mathbf{e}_{ij} is composed of the following elements:

- D_{ij} , the demand between the nodes
- $s_{ij} = 1$ if $(i, j, \tau_{ij}) \in \mathcal{E}_s$, 0 otherwise
- τ_{ij} if $s_{ij} = 1$, 0 otherwise
- $c_{ij} = 1$ if \mathcal{R} links i to j , 0 otherwise

- $c_{0ij} = 1$ if j can be reached from i over \mathcal{R} with no transfers, 0 otherwise
- $c_{1ij} = 1$ if one transfer is needed to reach j from i over \mathcal{R} , 0 otherwise
- $c_{2ij} = 1$ if two transfers are needed to reach j from i over \mathcal{R} , 0 otherwise
- self = 1 if $i = j$, 0 otherwise
- $\tau_{\mathcal{R}ij}$ if $c_{ij} = 1$, 0 otherwise
- τ_{rij} if $c_{0ij} = 1$ where r the route that provides the shortest direct trip between i and j , 0 otherwise
- T_{ij} , the shortest-path driving time between the nodes
- α and $1 - \alpha$, the weights of the two components of the cost function C

The global state vector \mathbf{s} is composed of:

- Average passenger trip time given current route set, $C_p(\mathcal{G}, \mathcal{R})$
- Total route time given current route set, $C_o(\mathcal{G}, \mathcal{R})$
- number of routes planned so far, $|\mathcal{R}|$
- number of routes left to plan, $S - |\mathcal{R}|$
- fraction of node pairs with demand $d_{ij} > 0$ that are not connected by \mathcal{R}
- α and $1 - \alpha$, the weights of the two components of the cost function C

Note that α and $1 - \alpha$ are included in both \mathbf{s} and \mathbf{e}_{ij} .

Neural net training is sensitive to extreme values in the inputs, so to stabilize training, it is common practice to normalize the inputs. We here do this by running the policy network over the validation set before training it. We compute the means μ and standard deviations σ of the numerical input feature values observed during this initial validation step, and store these as parameters of the policy network. Then, during training and when later evaluating the policy network, we normalize all numerical input features by subtracting μ and dividing by σ , so the resulting normalized inputs are centred near 0 and have standard deviation near 1. Boolean-valued features are not normalized, but provided as raw binary values.

We made use of the ReLU non-linearity [Fukushima, 1969] as the activation function throughout our policy net, but we note that we experimented with other activation functions such as GELU [Hendrycks and Gimpel, 2016], and found that this made little difference to performance. Unless otherwise specified, each neural net layer of each component outputs vectors of the common embedding dimension d_{embed} . Table 2.1 shows the hyperparameters we used for the policy net architecture. These were arrived at by a manual search.

2.4 Training The Policy Net

In our prior work [Holliday and Dudek, 2023, 2024], we trained the policy net using the REINFORCE with Baseline method proposed by Williams [1992], using a reward function that was 0 at all steps except the final step, where it was the negative of the cost function.

Hyper-Parameter	Value
# backbone layers	5
# heads in GAT multi-head attention	4
embedding dimension d_{embed}	64
# layers of MLP_{ext1}	3
# layers of MLP_{ext2}	3
hidden layer dimension of MLP_{ext2}	16
# layers of NN_{halt}	3

Table 2.1: Policy net architectural hyper-parameters

This was inspired by the similar approach taken by Kool et al. [2019]. However, REINFORCE has been built upon by a number of other policy gradient learning algorithms since its publication. Also, sparse reward functions like this one, which is zero at most timesteps, convey little information about the effect of each action, and so can make learning difficult.

For these reasons, in this thesis we train the policy net using the Proximal Policy Optimization (PPO) algorithm and a more dense reward function, described in subsection 2.4.1. PPO is a policy gradient method proposed by Schulman et al. [2017], because of its relative simplicity and because it remains a state-of-the-art method on many problems. PPO works by rolling out a number of steps h of a “batch” of episodes in parallel, and then computing an “advantage” for each timestep, $A_t = \sum_{t'=0}^{h-1} \gamma^{t'} R_{t+t'} + \gamma^h V(s_{t+h}) - V(s_t)$. This advantage weights the updates to the policy, such that actions with a positive advantage are made more likely, and those with a negative advantage are made less so. Updates to the policy are also weighted by the ratio of the current policy’s probability for the chosen action and that of the policy that actually chose

the action, to avoid the divergence that can plague off-policy learning. This is accomplished by attempting to maximize the CLIP objective defined by Schulman et al. [2017]:

$$L^{CLIP}(\theta) = \mathbb{E}_t \left[\min \left(\frac{\pi_\theta(a_t|s_t)}{\pi_{\theta_{\text{old}}}(a_t|s_t)} A_t, \text{clip} \left(\frac{\pi_\theta(a_t|s_t)}{\pi_{\theta_{\text{old}}}(a_t|s_t)}, 1 - \epsilon, 1 + \epsilon \right) A_t \right) \right] \quad (2.12)$$

Where θ_{old} are the policy parameters prior to the updates made in this training iteration. The “clip(x, y, z)” function returns y if $x < y$, z if $x > z$, and x otherwise. ϵ is a parameter usually set to a value in the range $[0, 0.5]$. Unlike Schulman et al. [2017], we do not include any entropy-maximization term in our training objective, as we found that doing so worsened the performance of the resulting policies.

The value function $V(s_t)$ is itself a small MLP neural net that is trained in parallel with the policy to predict the discounted return $G_t^h = \sum_{t'=1}^{h-1} \gamma^{t'} R_{t+t'} + \gamma^h V(s_{t+h})$. The input to $V(s_t)$ is a vector composed of α and several statistics of \mathcal{G} : the average of the node features $\frac{\sum_i \mathbf{x}_i}{n}$, the total demand $\sum_{i,j} D_{ij}$, the means and standard deviations of the elements of D and T , and the cost component weights α and $1 - \alpha$. Along with these, it takes the state vector \mathbf{s}_t .

After each batch of training episodes, the mean squared error of the value net’s estimates of the advantage $V(s_t)$ against the actual advantages A_t :

$$\text{Loss}_{\text{value}} = \frac{1}{Q} \sum_{i \in Q} [A_t - V(s_t)]^2 \quad (2.13)$$

where Q is the minibatch size.

We experimented with using an MLP that would compute the value estimate $V(s_t)$ based on the same node embeddings Y as NN_{ext} and NN_{halt} , but found that this performed slightly worse than using the separate MLP.

2.4.1 Reward Function

We use a reward function that is based on how the cost of the partial network $\mathcal{R}_t \cup \{r_t\}$ changes with each timestep. Specifically, we define the reward as:

$$R_t = C'(\mathcal{G}, \mathcal{R}_t \cup \{r_t\}) - C'(\mathcal{G}, \mathcal{R}_{t+1} \cup \{r_{t+1}\}) \quad (2.14)$$

Note that this means that on even timesteps (when halt-or-continue actions are taken), $R_t = 0$ because \mathcal{R}_t and r_t do not change as a result of a halt-or-continue action.

In the above equation, C' is a modified cost function that we define to serve as a good

basis for this reward, specifically:

$$C'_p(\mathcal{G}, \mathcal{R}) = \frac{\sum_{i,j} D_{ij}(\delta_{\mathcal{R}ij}\tau_{\mathcal{R}ij} + (1 - \delta_{\mathcal{R}ij})2 \max_{kl} T_{kl})}{\sum_{i,j} D_{ij}} \quad (2.15)$$

$$C'_c(\mathcal{G}, \mathcal{R}) = F_{un} + 0.1\delta'_v \quad (2.16)$$

$$C'(\mathcal{G}, \mathcal{R}) = \alpha w_p C'_p(\mathcal{G}, \mathcal{R}) + (1 - \alpha)w_o C_o(\mathcal{G}, \mathcal{R}) - \beta C'_c \quad (2.17)$$

$\delta_{\mathcal{R}ij}$ is a delta function that takes value 1 if \mathcal{R} provides a path from i to j , and 0 if not. δ'_v takes value 1 if $F_{un} > 0$, and 0 otherwise. The second term in the numerator of C'_p is meant to represent the high cost of failing to satisfy some demand, in a way that is proportional to the amount of demand that is unsatisfied, unlike F_{un} which reflects only how many node pairs are unconnected. Each desired trip that cannot be made over network \mathcal{R} is treated as taking time equal to twice the diameter of the street graph.

If \mathcal{R} satisfies the connectedness constraint of subsection 1.2.1, it connects all pairs of nodes, so C'_p simplifies to C_p . But during the MDP rollout, it is necessarily the case that the connectedness constraint is violated at some timesteps, before the network is complete. In these cases, C_p may increase from one timestep to the next as far-apart node pairs that were previously unconnected become connected by a new action. This would tend to penalize connecting those routes by increasing overall cost, when what we want is to reward the connection of new node pairs. We use C'_p instead because it decreases when a new node pair becomes connected, unless the connecting route is improbably circuitous.

It could be argued that simply increasing β would accomplish the same, but in practice we found that this was not the case: training with C'_p instead of C_p yielded better-performing models regardless of β 's value.

Similarly, we use C'_c instead of C_c because by the structure of the MDP, the number-of-stops constraint of subsection 1.2.1 is guaranteed to be satisfied when the MDP terminates, but before it terminates this will often not be the case. Penalizing the policy for these temporary violations of the number-of-stops constraint serves no purpose, and may swamp out useful learning signals. So we construct C'_c to be independent of the number-of-stops constraint 3, unlike C_c .

2.4.2 Training Data

To train the policy, we generate our own dataset of synthetic city graphs. The generation process begins by generating the nodes and street network using one of these processes chosen at random:

- 4-grid: Place n nodes in a rectangular grid as close to square as possible. Add edges from each node to its horizontal and vertical neighbours.
- 8-grid: The same as the above, but also add edges between diagonal neighbours.
- 4-nn: Sample n random 2D points uniformly in a square to give \mathcal{N} . Add street edges to each node i from its four nearest neighbours.

- Minimum spanning tree: Sample n points as above, treat them as a fully-connected graph J with edge weights as euclidean distances between points, and find the minimum spanning tree (MST) G of J . Then add more edges from J to G , in order of increasing weight, until a desired number of edges e is reached, where e is a linear function of n .
- Voronoi: Sample m random 2D points, and compute their Voronoi diagram Fortune [1995]. Take the shared vertices and edges of the resulting Voronoi cells as \mathcal{N} and \mathcal{E}_s . m is chosen so $|\mathcal{N}| = n$.

We note that the Minimum-spanning-tree process is the same process used to generate the Mumford benchmark cities [Mumford, 2013a], discussed further in subsection 2.5.2.

For each process except Voronoi, each edge in \mathcal{E}_s is then deleted with user-defined probability ρ . If the resulting street graph is not strongly connected, it is discarded and the process is repeated. Nodes are sampled in a $30\text{km} \times 30\text{km}$ square, and a fixed vehicle speed of $v = 15\text{m/s}$ is assumed to compute street edge weights $\tau_{ij} = \|(x_i, y_i) - (x_j, y_j)\|_2/v$. Finally, we generate the OD matrix D by setting diagonal demands $D_{ii} = 0$ and uniformly sampling off-diagonal elements $D_{ij}, i \neq j$ in the range $[60, 800]$.

The five different graph types were chosen to give a variety of spatial graphs that would reflect the variety in types of spatial layouts among real cities, the layouts of which are sometimes grid-like, other times more haphazard and random-seeming, but always with nodes connecting mostly to other nearby nodes. The demand-sampling process was chosen to match that used to generate the Mumford benchmark cities, as these were our main

evaluation target; this process also has the virtue of being very simple, although it loses the spatial structure of demand that can be present in real cities.

Our dataset consisted of $2^{15} = 32,768$ of these synthetic cities, each with $n = 20$ nodes. We make a 90:10 split of this dataset into training and validation sets.

In each iteration of training, we run learned construction with the policy net on one full MDP episode over each city in a “batch” that is sampled from the training set, and update the policy and value nets according to the PPO learning algorithm. After every ten iterations, the policy is run on the entire validation set, and the average cost C_v of the generated transit networks on the validation set is recorded. At the end of training, the parameters θ from with the lowest C_v are returned, giving the final policy π_θ .

In each episode of training, we sample a different cost weight α in the range $[0, 1]$ for each city, so that the policy net can learn to adapt its policy to the user’s preference for optimizing the passenger versus operator costs. S, m_{\min}, m_{\max} , and the constraint weight β are held constant across training. The values used for these parameters, and the sampling process for α , are presented in Table 2.2.

All neural net inputs are normalized so as to have unit variance and zero mean across the entire dataset during training. The scaling and shifting normalization parameters are saved as part of the policy net and are applied to new data presented to π_θ after training.

2.4.3 Training Parameters

Training was performed using the well-known Adam optimizer [Kingma and Ba, 2015]. The value function estimator used during training was an MLP with 3 layers and hidden-layer dimension 36, which is 2 times its input dimension.

In each epoch of training, we augmented the training dataset by applying a set of random transformations. These included rescaling the node positions by a uniformly-sampled random factor uniformly sampled in the range $[1 - a, 1 + a]$, rescaling the demand magnitudes by a random factor uniformly sampled in the range $[1 - b, 1 + b]$, mirroring node positions about the y axis with probability 0.5, and rotating the node positions by a random angle in $[0, 2\pi)$ about their geometric centre.

We also randomly sampled α separately for each training city in each batch. Each time α is sampled, it had equal probability of being set to 0, set to 1, and sampled uniformly in the range $[0, 1]$, so as to encourage the policy to learn to handle both extreme and intermediate α values.

This data augmentation lends greater variety to the finite dataset, increasing the performance of the resulting policy on new environments not seen during training.

Table 2.2 gives the hyper-parameters used during training. To find the values for decay and learning rate for the policy net, and node position and demand scaling ranges a and b , we ran an automatic hyperparameter search based on tree-structured Parzen estimation [Bergstra et al., 2013] using the Optuna library [Akiba et al., 2019]. Other

Hyper-Parameter	Value
Value function learning rate	5×10^{-4}
Value function weight decay	0.01
Policy learning rate	0.0016
Policy weight decay	8.4×10^{-4}
Number of training iterations	200
Discount rate γ	0.95
PPO CLIP threshold ϵ	0.2
Batch size	256
Horizon	120
Num. epochs	1
Constraint weight β	5.0
S	10
m_{\min}	2
m_{\max}	12
Adam α	0.001
Adam β_1	0.9
Adam β_2	0.999

Table 2.2: Training Hyper-Parameters

parameters were set through a manual search or based on recommended values from the literature.

Training proceeds for 200 iterations in batches of 256 cities, as we found that the policy stopped improving after this. A total of 51,200 episodes are rolled out during training. PPO has a parameter for the number of “epochs” per batch, that is, the number of training passes it makes over a batch of state transitions. Repeatedly iterating over the same batch can make training more efficient when computing the rewards requires costly simulation. But in our case, computing the rewards is much less costly than the forward and backward passes of the policy net itself, so we set the number of PPO epochs per batch to 1 so that more

diverse episodes will be seen across training.

The episode horizon for rollouts h is set to 120 because we find that with our settings of n, S, m_{\min}, m_{\max} , this meant that virtually every training episode would terminate within h steps. When an episode terminated in $t' < h$ steps, that episode was restarted from scratch with the same city \mathcal{G} and α and rolled out again, so that h distinct steps were recorded for each \mathcal{G}, α pair in the batch.

The search we performed for the value of n deserves some discussion. We experimented with training datasets of cities with $n = 20, 50$, and 100 , with S, m_{\min}, m_{\max} being increased in proportion to n . The time and memory requirements of training for a fixed number of epochs grew considerably with n . At $n = 100, S = 50$, this pushed the limits of what our commercial desktop computer could handle. To evaluate the different policies, we ran them on two of the benchmark cities described in subsection 2.5.2: the smallest, with $n = 15$, and the largest, with $n = 127$.

We were surprised to find that the policy trained on $n = 20$ performed best on both the $n = 15$ and $n = 127$ benchmark graphs, while increasing the training set n to 50 and then to 100 made the policy successively worse on both benchmark graphs. This goes against our expectations that increasing n in the training set ought to produce a policy that performs better at larger n . Based on these results, we chose keep $n = 20$ in our training process, and did not investigate this mystery further, but it does warrant further inquiry. In particular, it would be interesting to train a model with n starting at 20 and gradually increasing.

2.5 Experiments

2.5.1 Training

In these experiments, we trained ten different policy net models π_{θ_k} with ten different random seeds k using the procedure described in section 2.4. Figure 2.4 shows the cost achieved on the validation set and the reward over each training episode averaged over these ten runs. The costs achieved by the policy decreases rapidly over the first 50 training batches. Improvement then slows considerably, and has levelled off by about 200 batches, at which point we halt training. Over the course of training, the cost on the validation set drops by about 70%.

We see also that the validation cost and the training rewards follow the mirrored trends over training. This is plausible, given that the two sets are sampled from the same distribution of synthetic cities. It shows that the policy net is not simply memorizing the best actions to perform on the specific examples in the training set, but is learning some policy that is effective across city graphs from this distribution.

2.5.2 Evaluation

We evaluate the trained policies on five benchmark cities from two different benchmarks: Mandl Mandl [1980], and Mumford Mumford [2013b]. Both benchmarks are widely used to evaluate TNDP algorithms John et al. [2014], Kılıç and Gök [2014], Hüselmann et al. [2023]. The Mandl dataset is one small synthetic city, while the Mumford dataset consists

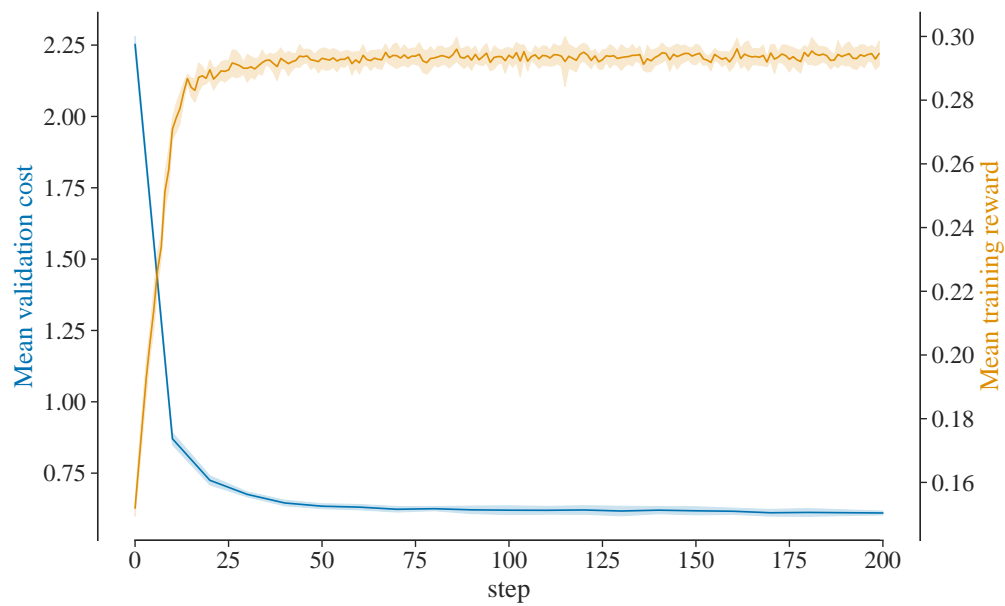


Figure 2.4: Mean cost on the validation set, and mean reward during training, achieved by our policy net over five epochs of training. The curves show the mean over ten training runs with different random seeds, and the shaded areas shows one standard deviation over the ten seeds.

City	# nodes n	# street edges $ \mathcal{E}_s $	# routes S	m_{\min}	m_{\max}	Area (km ²)
Mandl	15	20	6	2	8	352.7
Mumford0	30	90	12	2	15	354.2
Mumford1	70	210	15	10	30	858.5
Mumford2	110	385	56	10	22	1394.3
Mumford3	127	425	60	12	25	1703.2

Table 2.3: Statistics of the five benchmark problems used in our experiments. The area is estimated assuming all vehicles travel at 15 meters per second.

of four synthetic cities, labelled Mumford0 through Mumford3, and it gives values of S , m_{\min} , and m_{\max} to use when benchmarking on each city. The values n , S , m_{\min} , and m_{\max} for Mumford1, Mumford2, and Mumford3 are taken from three different real-world cities and their existing transit networks, giving the dataset a degree of realism. Details of these benchmarks, and the parameters we use when evaluating on them, are given in Table 2.3.

As noted in subsection 1.2.2, in all of our experiments, we set the transfer penalty used to compute average trip time C_p to $p_T = 300\text{s}$ (five minutes), the typical value used these benchmarks [Mumford, 2013b].

The data files that define both benchmarks are obtained from Mumford [2013a]. These files provide, for each city, the node positions \mathbf{p}_i on an arbitrary scale, as well as the driving time τ_{ij} in seconds of all street edges and the demand matrix D . To convert the node positions from their arbitrary scale to a scale of meters, we assumed a fixed driving speed for vehicles of 15 meters per second, which equates to 54 kilometers per hour, a reasonable average speed for a city bus. We used this to compute a scaling factor for the node positions

as follows:

$$f = \frac{1}{|\mathcal{E}_s|} \sum_{(i,j,\tau_{ij}) \in \mathcal{E}_s} \frac{\tau_{ij} * 15\text{m/s}}{\|\mathbf{p}_i - \mathbf{p}_j\|_2} \quad (2.18)$$

and then multiplied the positions by this factor to get approximate positions in meters $\mathbf{p}'_i = f\mathbf{p}_i$. Figure 2.5 shows the Mandl and Mumford benchmark cities based on these scaled node positions \mathbf{p}'_i .

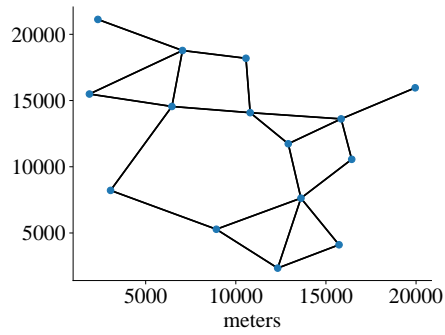
To evaluate a trained policy on one of these cities \mathcal{G} , we sampled 100 networks from the policy by running it for 100 separate episodes on \mathcal{G} . We then chose the network \mathcal{R} among these for which $C(\mathcal{G}, \mathcal{R})$ was lowest. We refer to this as the LC-100 algorithm, “LC” standing for “learned construction”. We also separately evaluate each policy “greedily” by running one episode on \mathcal{G} where instead of sampling a_t according to $\pi(\cdot|s_t)$, we deterministically take actions $a_t = \operatorname{argmax}_a \pi_\theta(a|s_t)$. We can also view this as using the policy $\pi_{\theta_G}(a|s_t) = 1 \iff a = \operatorname{argmax}_{a'} \pi_\theta(a'|s_t), 0$ otherwise. We refer to this as the “LC-Greedy” algorithm.

To provide a point of comparison, we also ran experiments on this benchmark with a purely random policy π_{random} , which gives equal probability to all actions:

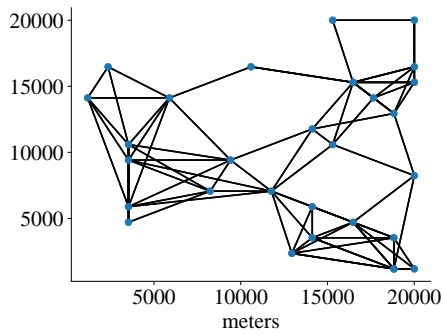
$$\pi_{\text{random}}(a|s_t) = \frac{1}{|\mathcal{A}_t|} \forall a \in |\mathcal{A}_t| \quad (2.19)$$

We followed a similar procedure to “LC-100” using this policy, which we refer to as “RC-100” for “random construction”.

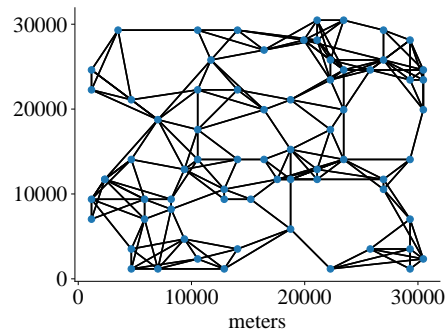
The trade-off parameter α in the cost function $C(\mathcal{G}, \mathcal{R})$ reflects the range of possible



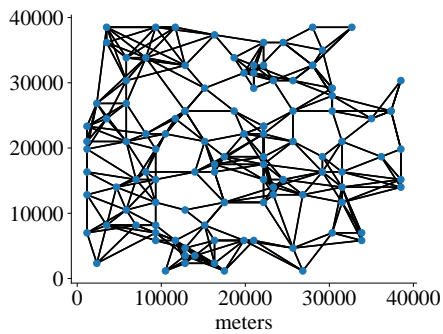
(a) Mandl



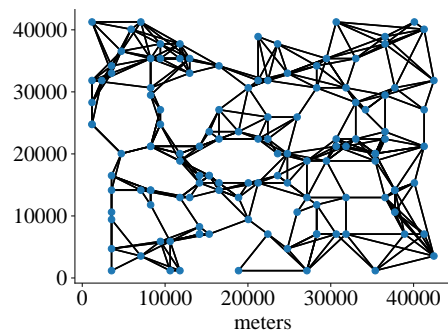
(b) Mumford0



(c) Mumford1



(d) Mumford2



(e) Mumford3

Figure 2.5: The Mandl benchmark city and the four Mumford benchmark cities.

preferences a user may have over minimizing passenger cost C_p versus operator cost C_o . An TNDP algorithm should be sensitive to this parameter, producing networks that reflect the user’s preference. To assess this, we ran each algorithm on each benchmark city with eleven values of α , ranging from $\alpha = 0.0$ to $\alpha = 1.0$ in increments of 0.1. Additionally, as LC-100 and RC-100 are both stochastic algorithms, and as the training process is itself stochastic, we repeated each run 10 times with 10 different random seeds k and, if a learned policy was needed, we used the parameters θ_k trained with random seed k .

Figure 2.6 shows the results of this evaluation. Each sub-figure shows, for one benchmark city, C_p and C_o for the transit networks produced by each algorithm over the values of α . As there is necessarily a trade-off between C_p and C_o , these (C_p, C_o) points form a curve for each algorithm that indicates how good of a trade-off it can achieve between C_p and C_o across values of α . As we seek to minimize both quantities, the down-and-leftward direction represents strict improvement.

On Mandl and Mumford0, LC-100 dominates the random policy RC-100, producing networks for some values of α that dominate all of the networks produced by RC-100. On Mumford1, RC-100 fails to generate any valid networks at all. On Mumford2 and Mumford3, the two largest cities, the situation is a little more complex. There, RC-100’s networks for the different α values are tightly clustered in an area with high C_o and low C_p . While these networks have much higher C_o than any of LC-100’s or LC-Greedy’s networks, making them worse for most values of α , at the extreme of $\alpha = 1.0$ (where C_o is irrelevant) RC-100’s

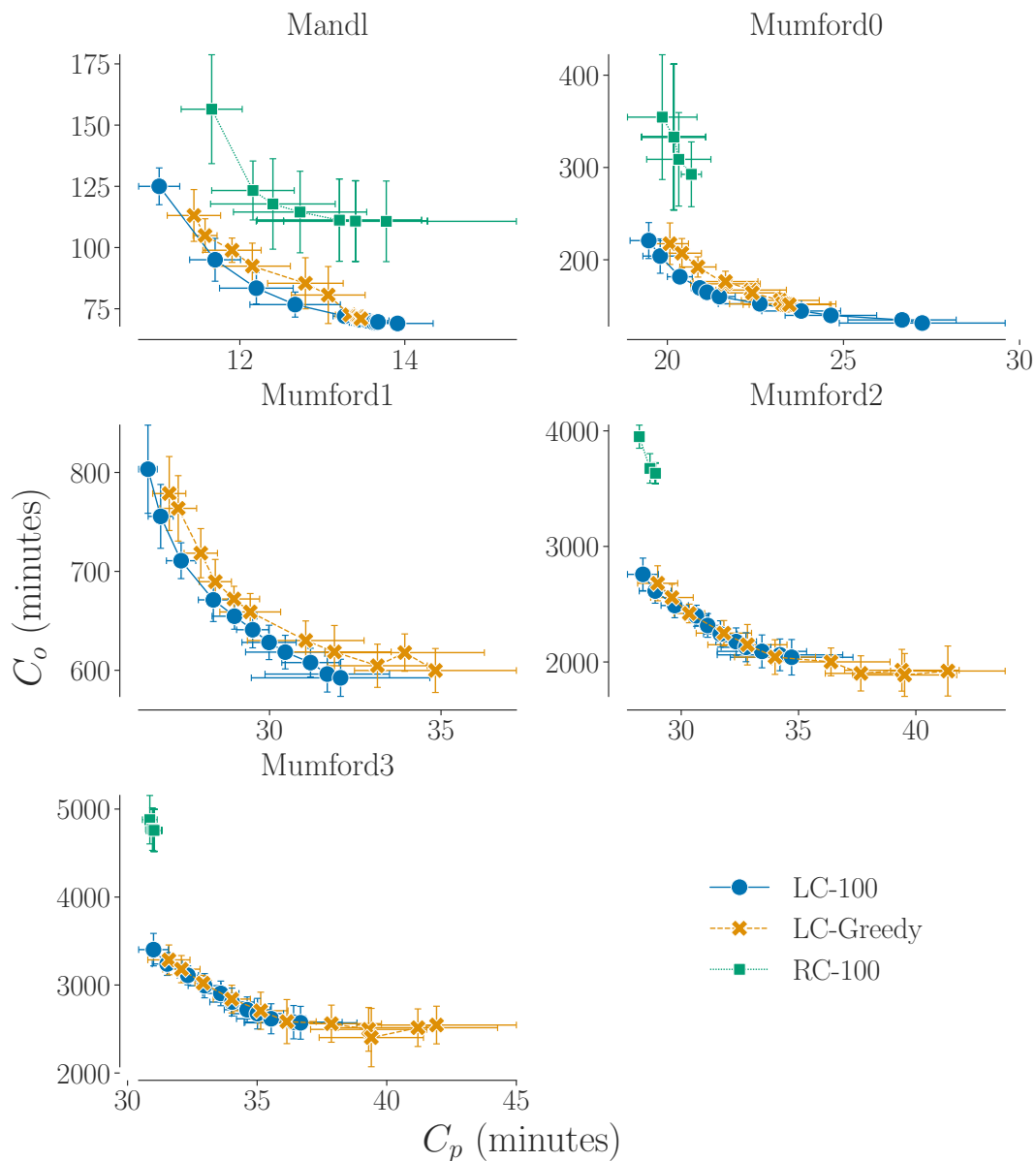


Figure 2.6: Values of average trip time C_p (on the x-axis) and total route time C_o (on the y-axis), across values of α from 0 at lower-right to 1 at upper-left, in increments of 0.1. Each point is the mean over 10 random seeds for one value of α (excluding those that generated invalid networks), and bars around each point indicate one standard deviation. Lines link pairs of points with consecutive α values. Note that RC-100 is not shown for Mumford1 because none of its generated networks were valid for that city.

mean C_p is slightly lower than that of LC-100 and LC-Greedy, though within one standard deviation of LC-100.

This is surprising. Naïvely, we would expect that the policy net would learn to match the performance of π_{random} by simply matching its probabilities: $\pi_{\theta}(\cdot|s_t, \alpha) = \pi_{\text{random}}$. Yet it fails to do so. To test whether this failure was due to the policy’s having been trained over the full range of α values, we trained ten additional policy nets with ten random seeds in the same manner as described in section 2.4, except that we held $\alpha = 1.0$ throughout training. The first set of policies we trained in this way did not perform any better at $\alpha = 1.0$ than our existing policies. We then tried adjusting the batch size and minibatch size, learning rate, and number of training iterations. Finally we found that setting the batch size and minibatch size to 16, while leaving the other values unchanged from Table 2.2, allowed us to train policies at $\alpha = 1.0$ that achieved considerably lower C_p . We called these the $\pi_{\theta_{\alpha=1}}$ policies.

We then tried training policies over the full range of α with this batch size and minibatch size, but found that these policies performed considerably worse overall than the ones trained with batch size 256. So the smaller batch size is beneficial at $\alpha = 1.0$ but not over the whole range of α .

We evaluated the $\pi_{\theta_{\alpha=1}}$ policies with the LC-100 algorithm over the five benchmark cities. Figure 2.7 shows the results at $\alpha = 1.0$, in comparison with those from π_{θ} and π_{random} . We see that, indeed, the $\pi_{\theta_{\alpha=1}}$ policies outperform both RC-100 and our variable- α policies on

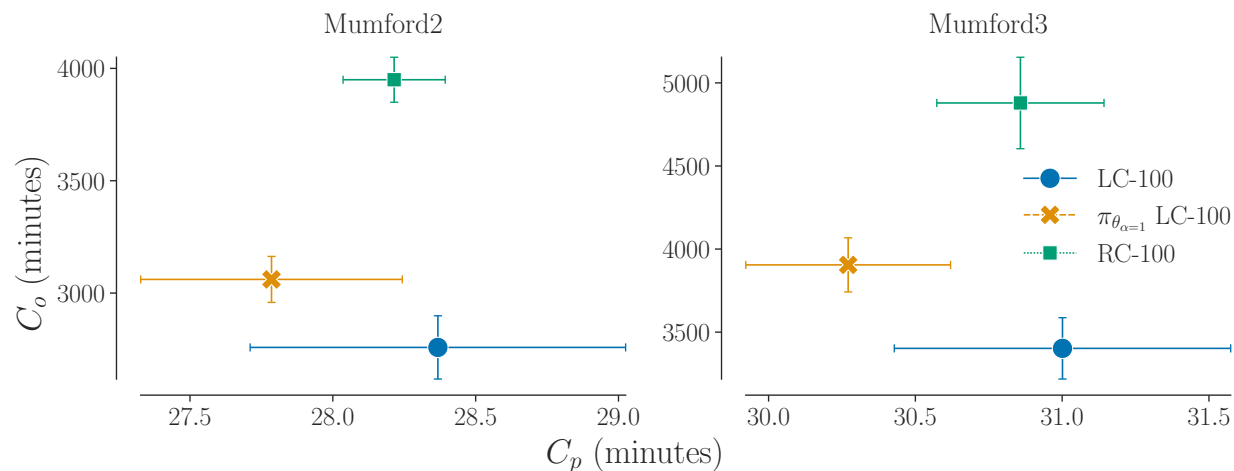


Figure 2.7: Values of average trip time C_p (on the x-axis) and total route time C_o (on the y-axis) of solutions from LC-100 with π_θ , LC-100 with $\pi_{\theta_{\alpha=1}}$, and RC-100, all with $\alpha = 1.0$.

all five benchmark cities. This shows that while training our policies over the full range of α gives good performance over the range, it does mean that the policies don't perform as well at the extremes of α as is possible. While they are capable of learning a better-than-random policy at $\alpha = 1.0$, they fail to fully learn the best policies at both $\alpha = 1.0$ and $\alpha < 1.0$, as this is a more challenging learning goal than $\alpha = 1.0$ alone.

Comparing LC-100 and LC-Greedy in Figure 2.6, we observe that on Mandl, Mumford0, and Mumford1, LC-100 dominates LC-Greedy, its curve being lower and to the left of it. On Mumford2 and Mumford3, again the situation is more complex: LC-100 performs a bit better for $\alpha = 1.0$, but LC-Greedy achieves lower C_o at $\alpha \leq 0.4$, and in between their performance is comparable. Overall, LC-100 is biased slightly towards favouring C_p over C_o , in comparison with LC-Greedy.

The reason may be related to the high performance of RC-100 at $\alpha = 1.0$. RC-100 is

a uniformly random policy, while LC-Greedy is a purely deterministic policy; LC-100, as a non-uniform stochastic policy, can be seen as being “in between” RC-100 and LC-Greedy. Formally, we can think of this in terms of the temperature parameter, $temp$, of the softmax function. π_{random} is what we would get by taking π_{θ} (for which $temp = 1$ in our experiments) and setting $temp = \infty$; whereas π_{θ_G} is the limit of π_{θ} as $temp \rightarrow 0$. So it may be the case that our policies are somehow favouring C_o over C_p , and the shift towards more stochasticity in the policy as we go from π_{θ_G} to π_{θ} to π_{random} gradually relaxes this preference for actions that favour C_o , which automatically improves C_p due to the trade-off between the two.

We must also consider how often each algorithm produce invalid transit networks that violate one or more of the constraints listed in subsection 1.2.1. LC-100 produced no invalid networks with any of the learned policies. Across the 110 trials (10 random seeds and 11 α values) for each city, however, LC-Greedy produced invalid networks in two trials on Mumford2, and in six trials on Mumford3. Meanwhile, RC-100 produced invalid networks in 36 of 110 trials on Mumford1, 11 of 110 on Mumford2, and in all 110 trials on Mumford1. Figure 2.8 shows how many of the ten generated networks for each α and benchmark city violated a constraint.

Using LC-Greedy, one of the ten trained policies generated an invalid network for 4 of the 11 values of α on Mumford3, and at $\alpha = 0.1$ there were two invalid networks. On Mumford2, just 2 of the 11 α values got an invalid network from one model in LC-Greedy mode. On the other benchmark cities, all LC-Greedy networks were valid. This is a low failure rate, but

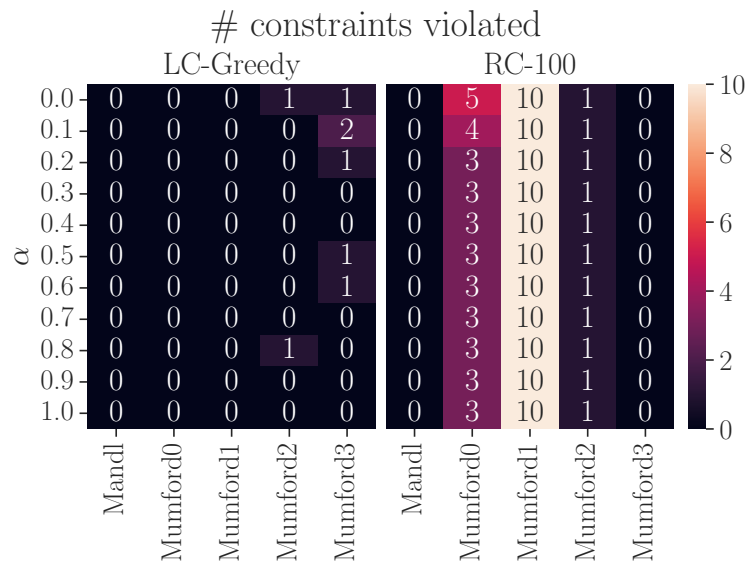


Figure 2.8: Of the ten runs with different random seeds for each benchmark city and α , these heat maps show the number of solutions produced by each algorithm that violated one or more network constraints. LC-100 is not shown, as it produced no constraint violations in any case.

as most of the α values where constraint violations occur are ≤ 0.5 , it casts doubt on the apparent superiority of LC-Greedy over LC-100 at low α that we concluded from Figure 2.6. LC-100 is more reliable than LC-Greedy, and so one would be justified in using it regardless of the value of α .

RC-100, meanwhile, produced many invalid networks, but mostly on Mumford0 and Mumford1 (in fact, it failed to produce any valid network on Mumford1). On the larger Mumford2 and Mumford3 cities, it produced valid networks except with one random seed on Mumford2. Perhaps this is because of the much larger values of S specified on those cities made it easier to obtain full network coverage, so as not to violate the connectedness constraint.

Comparing our learned policy with a random policy shows that, while the TNDP is very challenging, there are regularities in its structure across different instances, enough so that heuristics can be learned from training on small instances that generalize well to much larger instances.

2.5.3 Comparison with State of the Art Methods

While the comparison of our learned policies with a random policy shows that they learn something useful, existing methods for the TNDP provide a more rigorous benchmark of performance. Table 2.4 compares LC-100's performance with that of a selection of other methods that have been benchmarked on the Mumford cities. Apart from ours, all of the

methods presented in this table are metaheuristic improvement methods that perform some search of the space of complete transit networks. Mumford [2013b] use the multi-objective genetic algorithm SEAMO2 [Valenzuela, 2002, Mumford, 2004] to achieve their results, running it on the Mumford cities for 200 generations with a population size (the number of networks considered in parallel) of 200. Thus, a total of 40,000 transit networks are proposed, and their costs evaluated, over a single run. By comparison, LC-100 considers 100 networks, and LC-Greedy considers just 1. Despite this considerable gap in the scope of search, on the largest two cities (Mumford2 and Mumford3) LC-100 outperforms Mumford [2013b] at $\alpha = 1$, and LC-Greedy outperforms Mumford [2013b] at $\alpha = 0$.

The improvement in performance of our method relative to that of Mumford [2013a] as n increases may be explainable by the constant number of networks that their algorithm considers in their evaluation. As n and S grow, so does the space of possible transit networks. A fixed number of networks (40,000 in Mumford’s case) will then cover a smaller fraction of this search space, so we would expect the quality of the best of these to decrease relative to the quality of the best possible network for that city. Meanwhile, if there are heuristics for this problem that generalize well across values of n and S , then the relative quality of networks found via this heuristic may remain constant, or decline less quickly, as n and S grow. These results are more evidence that the heuristics learned by our policies generalize well to large problem instances, and make clear that our method holds real promise for the TNDP.

City	Method	C_p at $\alpha = 1$	C_o at $\alpha = 0$
Mandl	LC-100	11.00	69
	LC-Greedy	11.44	71
	Mumford [2013b]	10.27	63
	John et al. [2014]	10.25	63
	Ahmed et al. [2019]	10.18	63
	Hüsselmann et al. [2023]	10.19	63
Mumford0	LC-100	19.47	131
	LC-Greedy	20.07	152
	Mumford [2013b]	16.05	111
	John et al. [2014]	15.40	95
	Ahmed et al. [2019]	14.09	94
	Hüsselmann et al. [2023]	14.34	94
Mumford1	LC-100	26.46	592
	LC-Greedy	27.07	600
	Mumford [2013b]	24.79	568
	John et al. [2014]	23.91	462
	Ahmed et al. [2019]	21.69	408
	Hüsselmann et al. [2023]	21.94	465
Mumford2	LC-100	28.37	2040
	LC-Greedy	29.00	1924
	Mumford [2013b]	28.65	2244
	John et al. [2014]	27.02	1875
	Ahmed et al. [2019]	25.19	1330
	Hüsselmann et al. [2023]	25.31	1545
Mumford3	LC-100	31.00	2571
	LC-Greedy	31.59	2486
	Mumford [2013b]	31.44	2830
	John et al. [2014]	29.50	2301
	Ahmed et al. [2019]	28.05	1746
	Hüsselmann et al. [2023]	28.03	2043

Table 2.4: A comparison of our algorithms with a selection of methods from recent literature, in terms of C_p achieved when $\alpha = 1$ and C_o achieved when $\alpha = 0$. Values for LC-100 and LC-Greedy are means over 10 random seeds. Bold values are the best on the environment.

2.6 Summary

While our learned policies outperform the first method to show results on the Mumford benchmark, they are themselves outperformed by the more recent work of John et al. [2014], Ahmed et al. [2019], and Hüsselmann et al. [2023]. All three of these use metaheuristic improvement methods, and so are more exhaustive and computationally costly than LC-100 and LC-Greedy: John et al. [2014] and Hüsselmann et al. [2023]’s methods both take about two days on the largest city, Mumford3, using desktop hardware, while Ahmed et al. [2019]’s method takes ten hours. By contrast, LC-100 and LC-Greedy take less than five minutes to run on Mumford3 on commercial hardware. But as Table 2.4 shows, the greater cost pays off in the quality of solutions found. Observing this, we next sought ways of combining our learned policies with improvement metaheuristics, in the hope that this combination could improve on the performance of both.

Chapter 3

Neural Nets as Initialization

Procedures

The quality of solutions found by a metaheuristic improvement algorithm is usually highly dependent on its initial solution, the place in solution space where it begins the search. A poor starting point in a wide “valley” of equally low-quality solutions, or at the peak of a sub-optimal maximum, can cause the algorithm to search fruitlessly, never finding a hill to climb. A good starting point, on or near the steep slope of a high-quality region, can allow it to find excellent solutions very quickly.

Existing metaheuristic algorithms for the TNDP generally use simple construction heuristics to produce an initial transit network [Nikolić and Teodorović, 2013, Mumford, 2013a, John et al., 2014, Ahmed et al., 2019, Hüsselmann et al., 2023]. Most such

heuristics greedily maximize or minimize some quantity, such as demand directly served or constraints violated. They may involve many random restarts to find an initial network with no constraint violations. These algorithms are engineered to be simple and fast at the expense of output quality, since the metaheuristic search that follows bears the burden of achieving high quality.

The neural net policy architecture we developed in Chapter 2 is comparable in speed to these initialization algorithms: the LC-100 algorithm described in subsection 2.5.2 runs in under 60 seconds on a desktop computer with a commercial GPU, whereas most initialization algorithms take seconds to minutes to run, and in at least one case, take hours [Kılıç and Gök, 2014]. But its outputs appear to be much higher-quality, as it exceeds the performance of at least Mumford [2013a]’s metaheuristic algorithm on the Mandl and Mumford benchmarks. This raises the question: do transit networks produced by the learned policy serve as good initial networks for improvement metaheuristics?

To answer this question, we conducted experiments with two metaheuristic algorithms for the TNDP, using different initialization procedures and comparing the performance of the algorithms’ output transit networks. The two metaheuristic algorithms we considered were a simple evolutionary algorithm (modified slightly from the algorithm of Nikolić and Teodorović [2013]), and the hyper-heuristic algorithm of Ahmed et al. [2019]. We chose the former for its ease of implementation and fast running-time, and the latter because it was a recent algorithm whose authors reported state-of-the-art results on the Mumford

benchmark, and because, not being an evolutionary algorithm, it would make for an interesting comparison with the first algorithm.

For each of the two algorithms, we performed experiments with three different initialization procedures:

- The initialization procedure used in the original work (which is different for the two algorithms),
- The initialization procedure used by John et al. [2014],
- LC-100 with the learned policies π_θ from Chapter 2.

This allows us to compare, for each algorithm, our learned initialization procedure LC-100 with two human-designed procedures: one chosen by the authors of the algorithm, and one from a different algorithm (that of John et al. [2014]). This will give some indication of the extent to which the original initialization procedures for each algorithm are especially suited to that algorithm. In the following sections, we describe the two algorithms and their initialization procedures, and then present the experimental details and our results.

3.1 Evolutionary Algorithm

The metaheuristic improvement algorithm we used in these experiments is an evolutionary algorithm. Evolutionary algorithms are a broad class of improvement algorithms in which a population of solutions undergo repeated stages of random modification and selection. The

modification step explores the solution space, while the selection step filters out low-quality solutions from the population. Over many iterations, the quality of the population’s solutions rises, and finally one can select the best solution from among them.

Our evolutionary algorithm is based on that of Nikolić and Teodorović [2013], with several modifications to the algorithm that we found improved its performance on the Mumford benchmark cities. We chose this algorithm because its ease of implementation and short running times (with appropriate parameters) aided prototyping and experimentation.

The algorithm operates on a population of transit networks $B = \{\mathcal{R}_b | 1 \leq b \leq |B|\}$, and performs alternating stages of mutation and selection. In the mutation stage, the algorithm applies two “mutators”, type 1 and type 2, to equally-sized subsets of the population chosen at random; if the mutated network \mathcal{R}'_b has lower cost than its “parent” \mathcal{R}_b , it replaces its parent in B : $\mathcal{R}_b \leftarrow \mathcal{R}'_b$. This is repeated F times in the stage. Then, in the selection stage, networks either “die” or “reproduce”, with probabilities inversely related to their cost $C(\mathcal{G}, \mathcal{R}_b)$. After I repetitions of mutation and selection, the algorithm returns the best network found over all iterations.

Both mutators begins by selecting, uniformly at random, a route r in \mathcal{R}_b and a terminal node i on that route. The type-1 mutator then selects a random node $j \neq i$ in \mathcal{N} , and replaces r with the shortest path between i and j , SP_{ij} . The probability of choosing each node j is proportional to the amount of demand directly satisfied by SP_{ij} . The type-2 mutator chooses with probability p_d to delete i from r ; otherwise, it adds a random node j

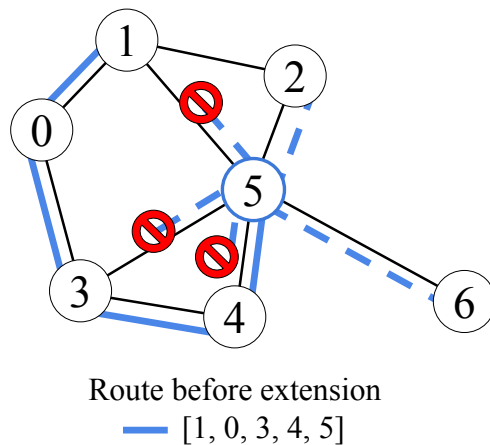


Figure 3.1: A schematic of which extensions of a route are allowed by the type-2 mutator. Here, the mutator will extend a route from its terminal at node 5 to a neighbouring node. Nodes 1, 2, 3, 4, and 6 are neighbours of node 5, but nodes 1, 3, and 4 are already on the route, so may not be chosen. This leaves nodes 2 and 6 as valid choices, so one of these two will be chosen randomly.

in i 's street-graph neighbourhood to r (before i if i is the first node in r , and after i if i is the last node in r), making j the new terminal. Following Nikolić and Teodorović [2013], we set the deletion probability $p_d = 0.2$ in our experiments.

As shown in Figure 3.1, we disallow the type-2 mutator from choosing extending nodes that are already on the route, to avoid violating the simple-path constraint described in subsection 1.2.1. The number-of-routes constraint is respected by construction, since the type-1 mutator replaces each route it deletes with another route. Violations of the connectedness and number-of-stops constraints may occur, but the cost function's constraint-violation term βC_c means that the algorithm will be more likely to keep solutions with fewer violations, and so ought eventually to drive C_c to zero.

The parameters of this algorithm are the population size $|B|$, the number of mutations per mutation stage F , and the number of iterations of mutation and selection stages I . In addition to these, the algorithm takes as input the city \mathcal{G} being planned over, the set of shortest paths through the city’s street graph SP , and the cost function C . The full procedure is given in Algorithm 1.

We note that Nikolić and Teodorović [2013] describe their algorithm as a “bee colony optimization” algorithm. As noted in Sörensen [2015], “bee colony optimization” is merely a relabelling of the components of one kind of evolutionary algorithm. It is mathematically identical to this older, well-established metaheuristic. To avoid confusion and the spread of unnecessary terminology, we here describe the algorithm as an evolutionary algorithm.

3.2 Hyper-Heuristic with Great Deluge

The Sequence-Based Selection Hyper-heuristic algorithm for the TNDP proposed by Ahmed et al. [2019] is an improvement metaheuristic that operates on a single network, unlike evolutionary algorithms which operate on a population of multiple networks. The term “hyper-heuristic” in the literature denotes an adaptive mechanism within a metaheuristic algorithm that keeps track of how successful each low-level heuristic has been at improving a solution, and uses this record to preferentially select more successful low-level heuristics as the algorithm proceeds.

At a high level, Ahmed et al. [2019]’s algorithm (henceforth denoted HH) has these

Algorithm 1 Evolutionary Algorithm

```

1: Input: city graph  $\mathcal{G} = (\mathcal{N}, \mathcal{E}_s, D)$ ; set of shortest paths in city graph SP; cost function
    $C$ ; population size  $|B|$ ; number of iterations  $I$ ; number of mutations per iteration  $F$ 
2: Construct initial network:  $\mathcal{R}_0 \leftarrow \text{initialize}(\mathcal{G})$ 
3:  $\mathcal{R}_b \leftarrow \mathcal{R}_0 \forall b \in \text{integers } 1 \text{ through } |B|$ 
4:  $\mathcal{R}_{\text{best}} \leftarrow \mathcal{R}_0$ 
5: for  $i = 1$  to  $I$  do
6:   // Mutation stage
7:   for  $j = 1$  to  $F$  do
8:     for  $b = 1$  to  $|B|$  do
9:       if  $b \leq |B|/2$  then
10:         $\mathcal{R}'_b \leftarrow \text{type\_1\_mut}(\mathcal{R}_b)$ 
11:       else
12:         $\mathcal{R}'_b \leftarrow \text{type\_2\_mut}(\mathcal{R}_b)$ 
13:        if  $C(\mathcal{G}, \mathcal{R}'_b) < C(\mathcal{G}, \mathcal{R}_b)$  then
14:           $\mathcal{R}_b \leftarrow \mathcal{R}'_b$ 
15:       Randomly shuffle network indices  $b$ 
16:   // Selection stage
17:    $C_{\text{max}} \leftarrow \max_b C(\mathcal{G}, \mathcal{R}_b)$ 
18:    $C_{\text{min}} \leftarrow \min_b C(\mathcal{G}, \mathcal{R}_b)$ 
19:   for  $b = 1$  to  $|B|$  do
20:     if  $C(\mathcal{G}, \mathcal{R}_b) < C(\mathcal{G}, \mathcal{R}_{\text{best}})$  then
21:        $\mathcal{R}_{\text{best}} \leftarrow \mathcal{R}_b$ 
22:   // Select surviving networks
23:    $O_b \leftarrow \frac{C_{\text{max}} - C(\mathcal{G}, \mathcal{R}_b)}{C_{\text{max}} - C_{\text{min}}}$ 
24:    $s_b \sim \text{Bernoulli}(1 - e^{-O_b})$ 
25:   // Set survivor reproduction probabilities
26:    $p_b \leftarrow \frac{O_b s_b}{\sum_{b'} O_{b'} s_{b'}}$ 
27:   if  $\exists b \in [1, |B|]$  s.t.  $s_b = 1$  then
28:     // Replace non-survivors with survivors' offspring
29:     for  $b = 1$  to  $|B|$  do
30:       if  $s_b = 0$  then
31:          $k \sim P(k)$ , where  $P(k = b') = p_{b'}$ 
32:          $\mathcal{R}_b = \mathcal{R}_k$ 
33: return  $\mathcal{R}_{\text{best}}$ 

```

components: a set H of seven low-level heuristics, a cost function $C(\mathcal{G}, \mathcal{R})$, a 7×7 transition matrix $Tran$, a 7×2 “sequence-construction matrix” Seq , and an acceptance rule.

Each of the seven low-level heuristics applies a different class of random modification to the existing network by applying some operation to one or two random routes involving adding, deleting, or rearranging random nodes on the routes. For example, one heuristic removes a node on a route; another selects a route and inserts a random node in \mathcal{N} at a random position; another exchanges two nodes between two routes. All seven heuristics have in common that they modify at most two routes by altering either one or two total nodes, and that their selections of which routes and nodes to alter are made uniformly at random. Also, each heuristic can modify routes in ways that violate the constraints described in subsection 1.2.1.

The cost function is much like the one we describe in subsection 1.2.2, but the scaling parameters w_o and w_p are not used, and separate weights are used for C_p and C_o :

$$C_{HH}(\mathcal{G}, \mathcal{R}, \alpha, \beta, \gamma) = \alpha C_p(\mathcal{G}, \mathcal{R}) + \gamma C_o(\mathcal{G}, \mathcal{R}) + \beta C_c(\mathcal{G}, \mathcal{R}) \quad (3.1)$$

The authors set the constraint-violation penalty $\beta = \infty$. This way, if a modification violates any constraints, the algorithm will reject it. Also, as their low-level heuristics may cause a route to violate the simple-path constraint, their C_c term differs from ours in that $C_c > 0$ if that constraint is violated, so these routes will be rejected as well.

Starting from some initial network \mathcal{R}_0 , HH works by repeatedly assembling sequences of the heuristics in H and applying them to its current network \mathcal{R} to get a modified network \mathcal{R}' . To assemble a sequence of heuristics, it selects the first, h_0 , uniformly randomly, and selects subsequent heuristics stochastically according to $Tran$, such that $P(h_i = k) = \frac{Tran_{h_{i-1},k}}{\sum_l Tran_{h_{i-1},l}}$. After selecting each heuristic, it decides stochastically according to Seq whether to end the sequence and apply it to \mathcal{R} : $P(end) = \frac{Seq_{h_i,0}}{Seq_{h_i,0} + Seq_{h_i,1}}$. This process repeats until end is chosen; then the sequence $[h_0, \dots, h_{last}]$ is applied to \mathcal{R} , yielding \mathcal{R}' .

The algorithm then applies an acceptance rule to determine whether to accept the \mathcal{R}' as its new current solution, replacing \mathcal{R} . If \mathcal{R}' is accepted, $Tran$ and Seq are updated to increase the likelihood of each of the choices that formed the sequence. The sequence is then cleared, and the algorithm repeats this process, continuing until a time limit $Limit$ is reached, at which point the lowest-cost network \mathcal{R}_{best} found over the course of the run is returned. In essence, the algorithm continually learns over its run which heuristics perform well when following which others, and which heuristics do or do not provide a good end to a sequence. For the full details of the algorithm, we refer the reader to Ahmed et al. [2019].

Ahmed et al. [2019] experiment with multiple acceptance rules, and find that the Great Deluge rule provides the best performance. This rule accepts a network \mathcal{R}' if it strictly improves on the current network \mathcal{R} ; otherwise, it accepts \mathcal{R}' if its cost $C(\mathcal{G}, \mathcal{R}')$ is below a threshold $L_\tau = f_0 + \Delta f(1 - \frac{\tau}{Limit})$, where τ is the running time so far, and f_0 and Δf are user-defined parameters. This amounts to a linearly-decreasing acceptance threshold on

cost, which starts at $f_0 + \Delta f$ and ends at f_0 .

As Ahmed et al. [2019] did not provide a reference implementation, we implemented HH with the Great Deluge acceptance rule ourselves, based on their publication. The authors report that speed is one of the advantages of their algorithm over others, claiming that they are able to run HH for 365,000 iterations on the Mumford3 city with $Limit = 63.5$ minutes, and for 524,000 iterations on Mumford2 with $Limit = 55$ minutes, on commercial desktop hardware - where each iteration corresponds to adding one heuristic to the current sequence. We found that our implementation was much slower, requiring upwards of 10 hours to run for 365,000 iterations on Mumford3 on our high-end desktop hardware. This is most likely due to our implementation being written in Python, an interpreted language that is slow for some purposes, unlike the authors' implementation which was written in C++ [C. Mumford, personal communication, December 2024].

Regarding the parameters of the acceptance rule, the authors describe f_0 as “the final expected objective value” and Δf as “the maximum change in the objective value”. They state that the initial threshold is the cost of the initial network, implying $L_0 = f_0 + \Delta f = C(\mathcal{G}, \mathcal{R}_0)$, but provide no other information about the values of f_0 and Δf used in their experiments, or how to choose such values. We attempted to inquire with the authors about this question, but the only author we could reach was unable to provide an answer. We then performed some preliminary experiments with different values of f_0 and Δf , but because of the slowness of our implementation, we were not able to search very extensively. Although we

were unable to find values of f_0 and Δf that replicated the state-of-the-art results reported by Ahmed et al. [2019], we found that setting $f_0 = 0$ and $\Delta f = C(\mathcal{G}, \mathcal{R}_0)$ gave results that were at least better than those of our evolutionary algorithm described in Algorithm 1.

3.3 Initialization procedures

3.3.1 Demand-Maximizing Shortest Paths

In their original work, Nikolić and Teodorović [2013] construct \mathcal{R}_0 by greedily selecting routes from SP, the set of all shortest paths in the street graph, that maximize the amount of directly-satisfied demand - that is, ignoring demand satisfied by transfers to or from other routes. After each route is selected, the demands it satisfies directly are zeroed out, and not considered in the selection of subsequent routes. No attempt is made to avoid constraint violations: Nikolić and Teodorović [2013] ignore the constraints we outline in subsection 1.2.1, and we rely on the βC_c term in the cost function to encourage the evolutionary algorithm itself to remove them. We refer to this initialization procedure as Nikolić (2013). It generates initial networks that have relatively low C_p (and C_o , since the routes are all shortest paths), but which may not be valid.

3.3.2 Validity-Maximizing Shortest Paths followed by Repair

To initialize HH, Ahmed et al. [2019] use a two-stage procedure that aims only to find an initial network \mathcal{R}_0 with no constraint violations. In the first stage, a transit network is constructed by first finding the set SP of all shortest paths between all node pairs in $\mathcal{N} \times \mathcal{N}$. This is filtered to remove paths r for which $|r| < m_{\min}$ or $|r| > m_{\max}$, leaving a set of candidate routes we will call \mathbb{P} . Then, starting with an empty network $\mathcal{R}_0 = \{\}$, routes are added one at a time from \mathbb{P} according to which route minimizes the number of constraint violations:

$$\mathcal{R} \leftarrow \mathcal{R} \cup \left\{ \arg \min_{r \in \mathbb{P}} C_c(\mathcal{R} \cup \{r\}) \right\} \quad (3.2)$$

This repeats until the desired number of routes are obtained ($|\mathcal{R}| = S$).

If $C_c(\mathcal{R}) = 0$ at the end of the first stage, the second stage, called the “repair” stage, begins. It enters a loop where it selects a random heuristic from the seven heuristics in H , and applies it to \mathcal{R} to get \mathcal{R}' ; \mathcal{R}' replaces \mathcal{R} if $C_c(\mathcal{R}') \leq C_c(\mathcal{R})$, and is discarded otherwise. This loop repeats until $C_c(\mathcal{R}) = 0$. The resulting network becomes \mathcal{R}_0 , the initial network for HH. We refer to this initialization procedure as Ahmed (2019).

Ahmed (2019) ignores the quality of \mathcal{R}_0 in terms of C_p and C_o , in favour of ensuring that it is a valid network. We note that each low-level heuristic in H is more likely to create new constraint violations than to repair existing ones, and as a result, we found that the repair procedure is very time-consuming for large graphs: On Mumford2 and Mumford3, it took

between 10 and 20 hours, as long or longer than the HH algorithm itself.

3.3.3 Growing Routes based on Diverse Edge Weights

The initialization procedure used by John et al. [2014] is intended for multi-objective optimization algorithms that require a diverse set of initial solutions. It therefore attempts to produce not a single network, but a diverse set of networks that both achieve low C_p and C_o while also satisfying all constraints. To generate a set of M networks, it first generates a set of M different weighted street graphs $\{\mathcal{N}, \mathcal{E}_s, W^m\}$, where W^m is a set of weights of edges in \mathcal{E}_s . Then, each of these weighted street graphs is used to construct a network in two stages. The first stage assembles routes and adds them to \mathcal{R} until all nodes in \mathcal{N} are covered by \mathcal{R} . If $|\mathcal{R}| < S$ at the end of the first stage, the second stage is carried out to add more routes to connect node pairs that are not yet directly connected, until $|\mathcal{R}| = S$. We refer to this initialization procedure as John (2014).

Pre-calculation stage: Weighted Street Graphs

A diverse set of M weighted street graphs are first computed using scalar parameters λ_1 and λ_2 , each of which has M values $\{(\lambda_1^0, \lambda_2^0), (\lambda_1^1, \lambda_2^1), \dots, (\lambda_1^M, \lambda_2^M)\}$ different specified by the user. The weight w_{ij}^m of edge (i, j) in the m th weight set W^m is computed as a weighted sum of the normalized edge drive time and the normalized demand:

$$w_{ij}^m = \lambda_{1,m} \frac{\tau_{ij}}{\max_{k,l \in \mathcal{E}_s} \tau_{kl}} + \lambda_{2,m} \left(1 - \frac{D_{ij}}{\max D} \right) \quad (3.3)$$

Each weighting W^m is used in one run of the first and second stages in order to select edges to include in routes, with lower weights being preferred.

First stage: Score-based route assembly

We define $\mathcal{N}_{\mathcal{R}} \subset \mathcal{N}$ as the set of nodes visited by at least one route $r \in \mathcal{R}$; if $i \notin \mathcal{N}_{\mathcal{R}}$, then i is not served by the transit network.

Using weight set W^m , this stage constructs one route at a time and adds it to \mathcal{R} . Each route is constructed in steps, starting from $r = []$; at each step one edge is selected from \mathcal{E}_s and added to r . The step first assembles a set \mathcal{E}_c of candidate edges, where $\mathcal{E}_c \subset \mathcal{E}_s$. If $|\mathcal{E}_c| > 0$, the candidate edge with the lowest score (breaking ties randomly) is selected: $(i, j) = \arg \min_{(i,j) \in \mathcal{E}_c} w_{ij}^m$, and it is appended to r at the appropriate place. If $\mathcal{E}_c = \{\}$ (there are no valid extensions for r) and $|r| < m_{\min}$, r is reset to $[]$ and construction starts again; if $\mathcal{E}_c = \{\}$ and $|r| \geq m_{\min}$, or if $|r| = m_{\max}$, r is considered finished and is added to \mathcal{R} . Then, if $\mathcal{N}_{\mathcal{R}} \neq \mathcal{N}$, construction of a new route begins; if $\mathcal{N}_{\mathcal{R}} = \mathcal{N}$, all nodes are covered by transit, and the first stage ends.

At the start of the first stage, when $r = []$ and $\mathcal{R} = \{\}$, all edges are candidates: $\mathcal{E}_c = \mathcal{E}_s$.

When starting subsequent routes (that is, when $r = []$ and $|\mathcal{R}| > 0$), candidate edges are

those which connect a served node to an unserved node:

$$\mathcal{E}_c = \{i, j | (i, j, \tau_{ij}) \in \mathcal{E}_s, i \in \mathcal{N}_{\mathcal{R}}, j \notin \mathcal{N}_{\mathcal{R}}\} \quad (3.4)$$

In steps after a route's first edge is selected, when $r = [s, \dots, e]$, \mathcal{E}_c is formed from the set of edges from either end of r that do not connect to nodes already on r :

$$\mathcal{E}_c = \{i, j | (i, j, \tau_{ij}) \in \mathcal{E}_s, j \in \{s, e\}, i \notin r\} \quad (3.5)$$

Furthermore, if any extensions of r would extend service to an unserved node, one of those extensions must be chosen. That is, if $\exists k \in \{j | (i, j) \in \mathcal{E}_c\}$ s.t. $k \notin \mathcal{N}_{\mathcal{R}}$, we update the candidate set:

$$\mathcal{E}_c \leftarrow \{i, j | (i, j) \in \mathcal{E}_c, j \notin \mathcal{N}_{\mathcal{R}}\} \quad (3.6)$$

Second stage: Growing network to required size

If at this point $|\mathcal{R}| < S$, the second stage begins. This stage begins by building a collection $\mathcal{P}_{\mathcal{R}}$ of node pairs that are not directly linked by any route in \mathcal{R} :

$$\mathcal{P}_{\mathcal{R}} = \{i, j | i \in \mathcal{N}, j \in \mathcal{N}, \nexists r \in \mathcal{R} \text{ s.t. } i \in r \text{ and } j \in r\} \quad (3.7)$$

It iterates over the pairs $(i, j) \in \mathcal{P}_{\mathcal{R}}$ in descending order of D_{ij} . For each pair, it uses Yen’s k -shortest-path algorithm [Yen, 1970] with $k = 10$ and W^m as the edge weights to find the ten lowest-weight paths between i and j through \mathcal{E}_s . It iterates over these ten paths until it finds one, r , for which $m_{\min} \leq |r| \leq m_{\max}$ and $\tau_{rij} < \tau_{\mathcal{R}ij}$; if it finds such an r , it adds r to \mathcal{R} . After finding or failing to find r for (i, j) , it repeats this process with the next node pair, until $|\mathcal{R}| = S$.

Finally, the procedure returns \mathcal{R} for use as \mathcal{R}_0 by the outer algorithm.

Adaptation to single-objective setting

In his doctoral thesis [John, 2016], John describes setting λ_1 and λ_2 to values ranging from 0 to 1 in increments of 0.05, giving 21 unique values for each, and pairing all combinations of these to give 441 $(\lambda_{1,m}, \lambda_{2,m})$ pairs, so that his initialization algorithm produces 441 transit networks. We are concerned in this chapter with initializing single-objective metaheuristic algorithms, each of which requires only a single initial solution. We therefore adapt John’s algorithm to this setting by specifying only a single weight pair (λ_1, λ_2) to compute a single set of street edge weights W , and generating a single network from this. We discuss the specific choice of values of λ_1 and λ_2 in subsection 3.4.1.

3.4 Experiments

As in Chapter 2, both the initialization methods and the metaheuristic improvement methods that use them are evaluated on the Mandl [Mandl, 1980] and Mumford [Mumford, 2013b] benchmark cities, over the same range of α values - from $\alpha = 0$ to $\alpha = 1$ in steps of 0.1 - and the same ten random seeds.

3.4.1 Initialization Results

We began by running each of the three pre-existing initialization methods - Nikolić (2013), John (2014), and Ahmed (2019) - over the range of random seeds and α values and comparing the results with those from LC-100 and LC-Greedy, as presented in section 2.5. Figure 3.2 shows the results of each.

To choose values of λ_1 and λ_2 in John (2014), we observed that, like $1 - \alpha$ and α , λ_1 and λ_2 are weights that control the linear trade-off between a term related to route travel time ($\lambda_1, 1 - \alpha$) and a term related to demand (λ_2, α). While the terms are not identical, a relatively high λ_1 will (like $1 - \alpha$) prioritize shorter routes, while a high λ_2 will (like α) prioritize satisfying demand directly, without transfers. This analogy suggests setting $\lambda_1 = 1 - \alpha$ and $\lambda_2 = \alpha$, and so that was how we set these parameters to obtain the results for John (2014) presented in Figure 3.2.

We note that at most α values, John (2014) creates the same network regardless of random seed; this is because randomness only enters into the algorithm if there is a tie in

the scores of candidate edges, which happens rarely. As a result, most of the points shown for John (2014) in Figure 3.2 have no error bars. Also, on the Mandl city, John created the same network for several adjacent values of α - the changes in λ_1, λ_2 were in those cases too small to induce any change in outcome for this very small city, so these points are “stacked” in the plot, giving the appearance of fewer than 10 points.

We observe from this figure, however, that setting $\lambda_1 = 1 - \alpha$ and $\lambda_2 = \alpha$ does not lead John (2014) to make an appropriate trade-off between C_p and C_o as we would hope. Surprisingly, for the three largest cities, Mumford1, 2, and 3, the values imposed by $\alpha = 0.0$ - that is, $\lambda_1 = 1.0, \lambda_2 = 0.0$ - appear to perform best or near-best in terms of both C_p and C_o , with both cost metrics tending to grow as α grows. For this reason, in the subsequent experiments in which we use John (2014) to initialize different metaheuristic improvement methods, we always set $\lambda_1 = 1.0, \lambda_2 = 0.0$, regardless of α .

Broadening our attention to the full set of methods in Figure 3.2, we observe that both John (2014) and Ahmed (2019) produce network or sets of networks that are dominated by LC-100 and LC-Greedy. Ahmed (2019)’s networks are biased towards low C_o and high C_p , relative to those from LC-100 and LC-Greedy, whereas John (2014)’s networks strike a more even balance.

From these results we might expect that one of LC-100 or LC-Greedy would provide better performance than John (2013) and Ahmed (2019) when used to initialize a metaheuristic improvement process. These results provide key context for interpreting the results of the

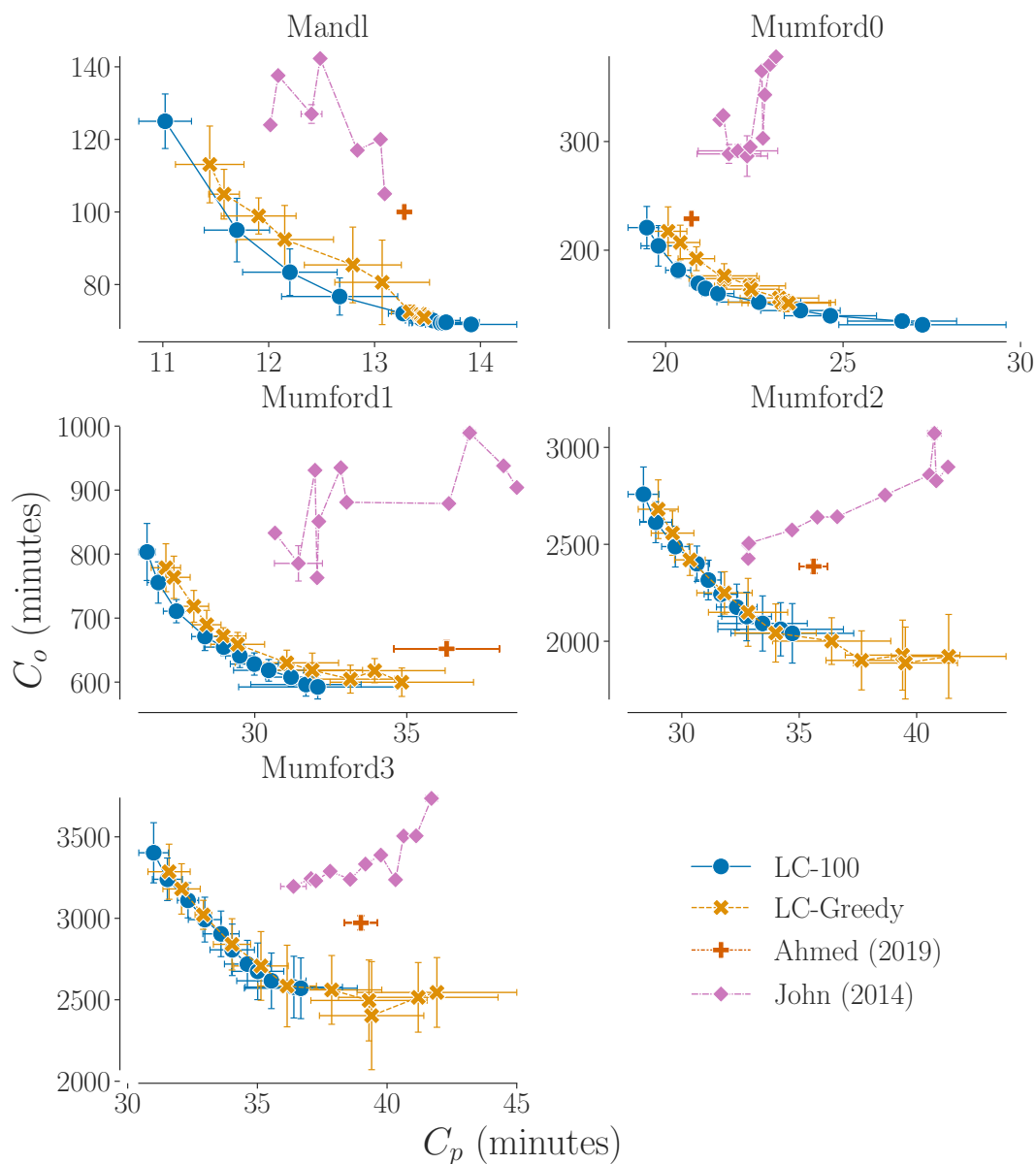


Figure 3.2: Results for the initialization methods. Nikolic (2013) is excluded as all of its networks are invalid. Curves for LC-100 and John (2014) show values of average trip time C_p (on the x-axis) and total route time C_o (on the y-axis) across values of α from 0 to 1 in increments of 0.1. Ahmed (2019) does not depend on α , so only one point is shown for it. Each point is the mean over 10 random seeds for one value of α and one method, and bars around each point indicate one standard deviation.

next section.

3.4.2 Metaheuristic Improvement Results

Evolutionary Algorithm (EA)

Figure 3.3 shows the results obtained by running EA after initializing it by four different methods: LC-100, LC-Greedy, Nikolić (2013) (its original initialization procedure), and John (2014). On Mandl and Mumford0, the performance of all methods is very similar. But Mumford1, John (2014) is dominated by the rest, and on Mumford2 and Mumford3, LC-100 shows better performance especially at low values of α , though it also performs best by a small margin at $\alpha = 1.0$.

To allow a clearer comparison between the different initializations, we used the means of C_p and C_o computed for each α value of each method, shown in Figure 3.3, to compute a hypervolume (also known as an S-metric) for each method. The hypervolume is a metric commonly used to evaluate a set of solutions in a multi-objective context. Each solution in a set can be viewed as a point x in a d -dimensional space, where d is the number of different objectives we care about - in this context, $d = 2$, the two objectives being C_p and C_o . Given some reference point p in this space, we can define a hyper-rectangle for each solution point x with opposite corners at p and x , which has a “hyper-volume” $v = \prod_{i \leq d} |p_i - x_i|$. The hypervolume $v(X)$ of the set X is simply the hypervolume of the shape formed by taking the union of these hyper-rectangles for each point $x \in X$. Assuming that we want to minimize

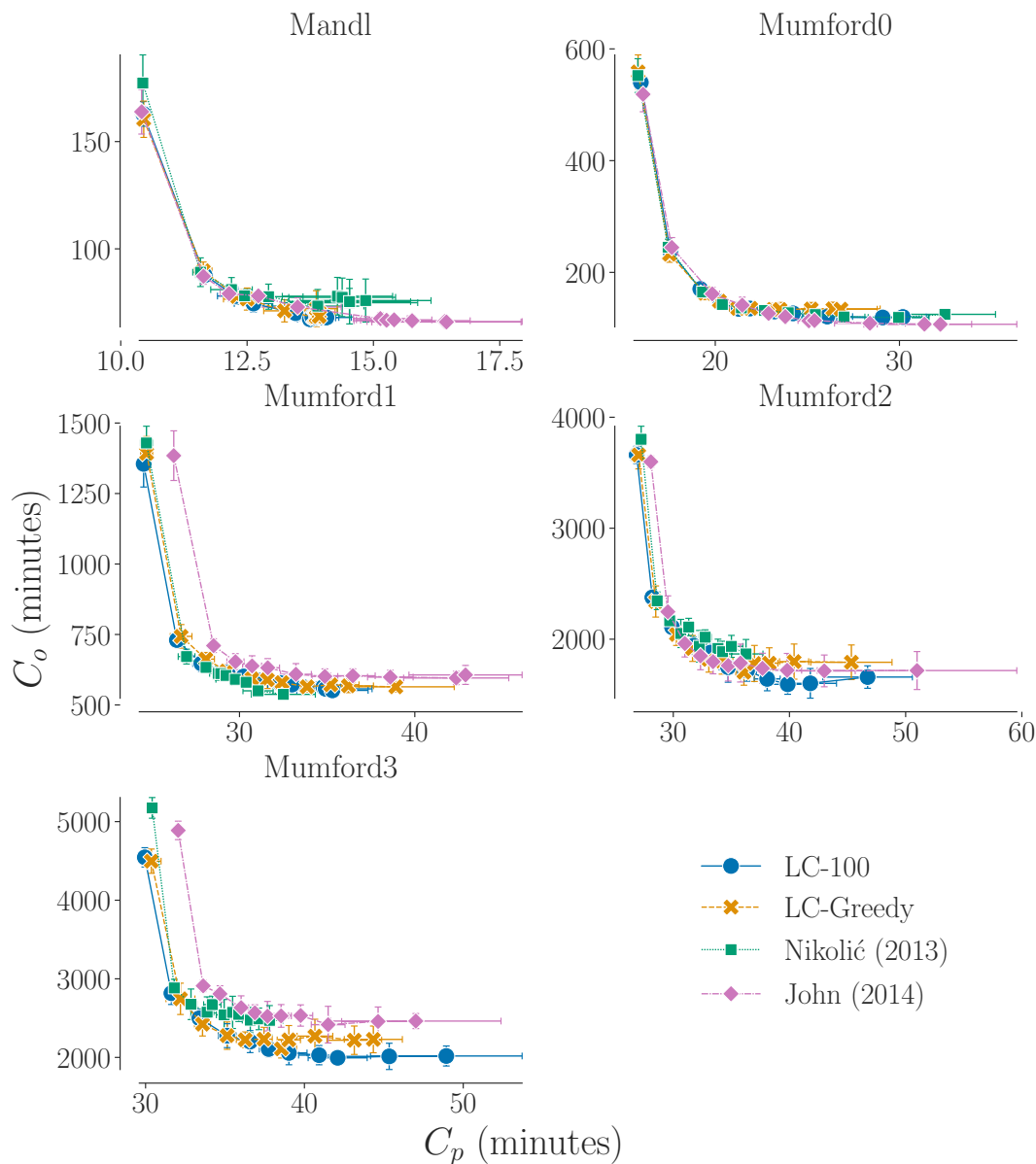


Figure 3.3: Results for EA with four different initialization methods. Each curve shows values of average trip time C_p (on the x-axis) and total route time C_o (on the y-axis) across values of α from 0 at lower-right to 1 at upper-left, in increments of 0.1. Each point is the mean over 10 random seeds for one value of α and one method, and bars around each point indicate one standard deviation. Lines link pairs of points for the same method and consecutive α values.

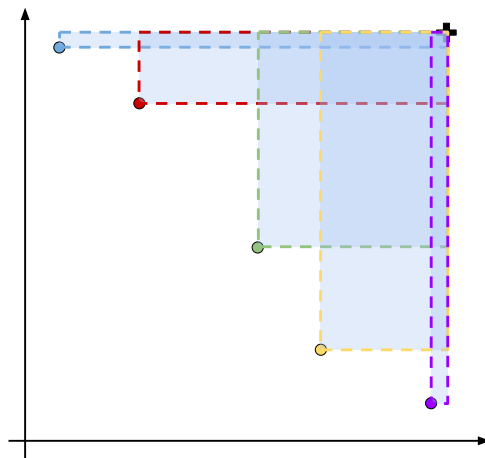


Figure 3.4: A schematic of a hypervolume computed based on five points in two dimensions. The point p , represented by + sign, is chosen to be ϵ greater than the largest magnitude of any point on each dimension. Then, we can define an axis-aligned rectangle for each point x with x at one corner and p at the other. The hypervolume of the set of five points is then the area of the union of these five rectangles, shown as the total shaded area.

each objective, we can choose p_i to be a point greater on each dimension than any point in the Pareto set X' of X : the set $X' \subset X$ such that no point $x \in X'$ is dominated by any other point $x' \in X'$. Then, the hypervolume $v(X)$ grows as the set of solution points in X improves. Figure 3.4 illustrates this concept.

Figure 3.5 compares the hypervolumes achieved by EA with the four initialization methods. Each method's hypervolume is computed with respect to the same reference point $p = (C_p^{max} + \epsilon, C_o^{max} + \epsilon)$, where C_p^{max} and C_o^{max} are the largest values of the mean C_p and C_o observed across all methods and values of α , and ϵ is a very small constant, which we set to 10^{-5} minutes. This metric makes it clearer that on Mumford1, 2, and 3, LC-100 and LC-Greedy outperform John (2014), and they outperform Nikolić (2013) on the largest

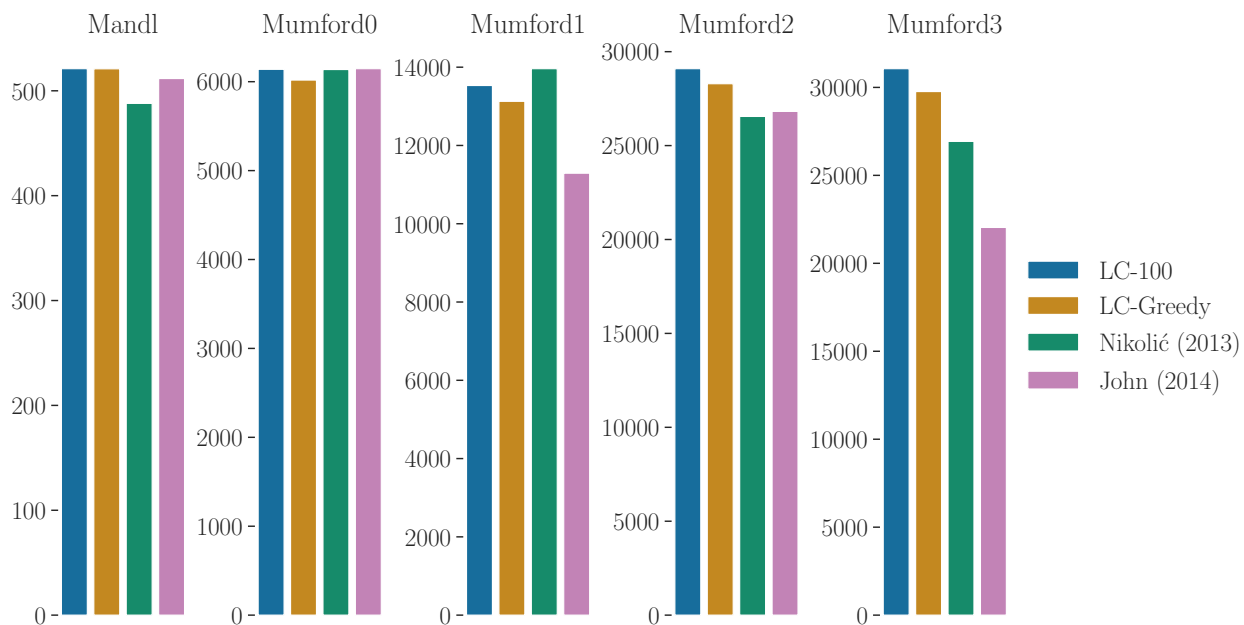


Figure 3.5: Hypervolumes achieved by EA with different initializations.

two cities, Mumford2 and 3. LC-100 performs slightly better than LC-Greedy across the Mumford cities.

Hyper-Heuristic with Great Deluge (HH)

In their experiments, Ahmed et al. [2019] set a time limit, *Limit*, for the HH algorithm to run based on the number of nodes n in the target city. To constrain the time taken to run these experiments, we instead set a limit of 500,000 iterations for all experiments, which is in between the numbers of iterations that occurred in their experiments on Mumford2 and on Mumford3. The form of the Great Deluge acceptance rule is changed accordingly: the threshold equation $L_\tau = f_0 + \Delta f(1 - \frac{\tau}{Limit})$ becomes $L_\tau = f_0 + \Delta f(1 - \frac{i}{500,000})$, where i is the

number of iterations so far. Assuming constant time per iteration, this keeps the behaviour identical to the original time-limited HH.

As shown in Figure 2.8, some of LC-Greedy’s networks for Mumford3 have constraint violations. In these cases, we apply the repair stage of Ahmed (2019) to it to obtain a valid network, before running HH.

Figure 3.6 shows the results obtained by running HH over the range of α values with four different initialization methods. As in the case of EA, we see here that LC-100 and LC-Greedy dominate the non-learned methods on Mumford2 and Mumford3, while all methods perform very similarly on Mandl, Mumford0, and Mumford1, which are smaller. We also observe that, unlike EA, HH initialized with LC-Greedy dominates LC-100 at lower values of α on Mumford2 and Mumford3, though LC-100 still dominates at higher values of α . So unlike EA, HH appears to preserve the relative advantages of LC-100 and LC-Greedy.

Figure 3.7 shows the hypervolumes attained by HH with these four initialization methods. Confirming what we observe in the Figure 3.6, LC-Greedy and LC-100 attain the largest hypervolumes on Mumford2 and 3, but this figure reveals that they perform best on Mumford1 as well. Interestingly, despite LC-Greedy’s better performance at low α , LC-100 obtains a slightly larger hypervolume than LC-Greedy on each city.

We also note that with Ahmed (2019), we have the HH algorithm as originally described by Ahmed et al. [2019]. But the performance we obtain with this on both C_p and C_o is significantly worse than the results reported in that work on Mumford1, 2, and 3. On

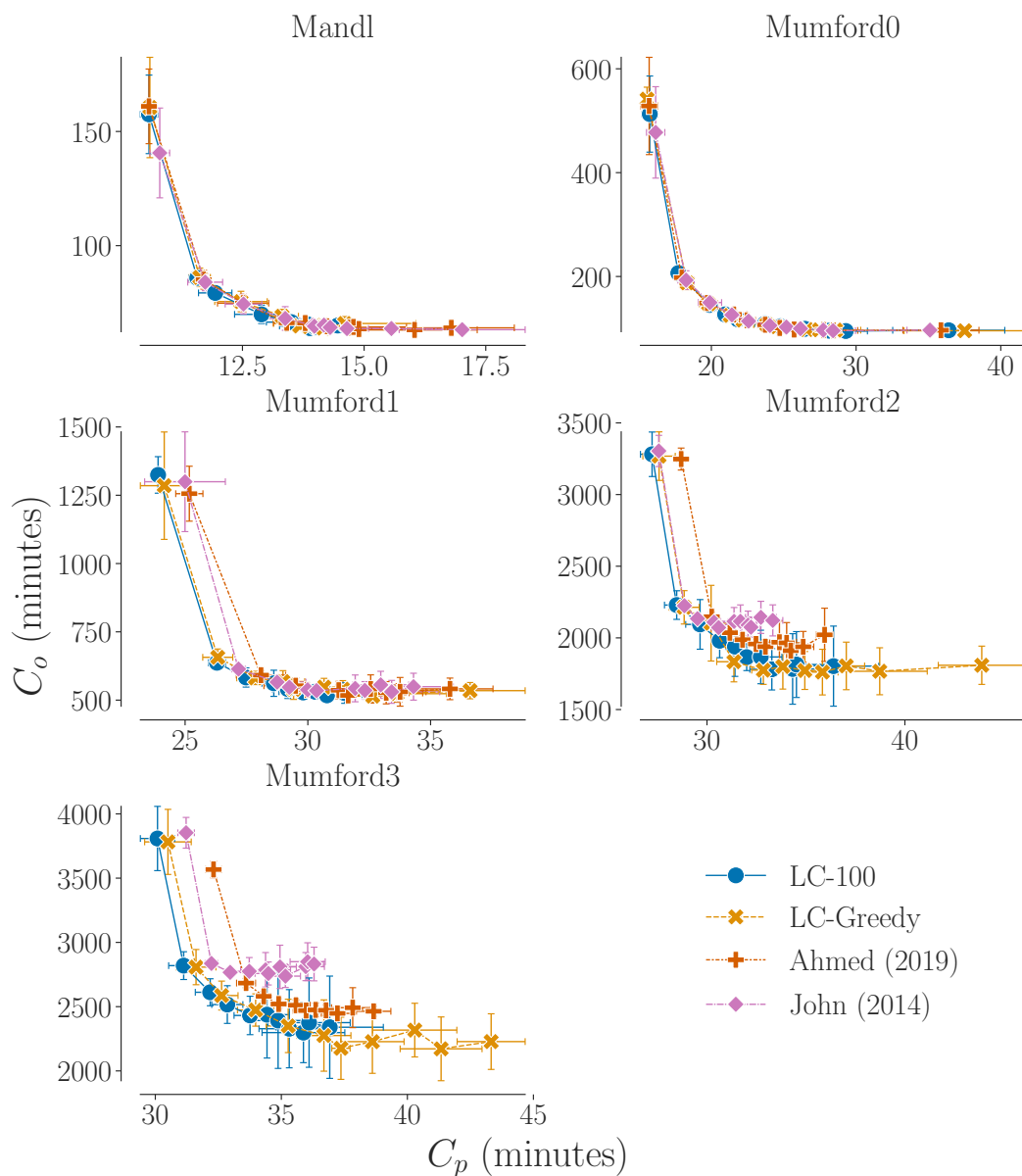


Figure 3.6: Results for HH with three different initialization methods. Each curve shows values of average trip time C_p (on the x-axis) and total route time C_o (on the y-axis) across values of α from 0 at lower-right to 1 at upper-left, in increments of 0.1. Each point is the mean over 10 random seeds for one value of α and one method, and bars around each point indicate one standard deviation. Lines link pairs of points for the same method and consecutive α values.

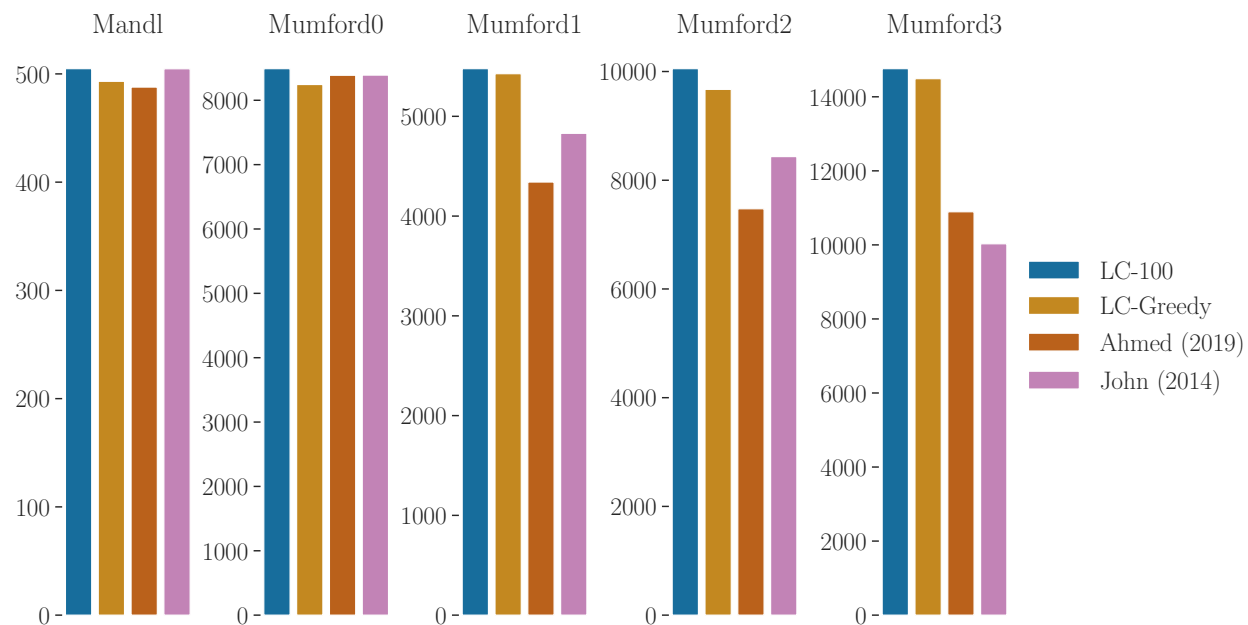


Figure 3.7: Hypervolumes achieved by HH with different initializations.

Mumford3, the mean result we obtained at $\alpha = 1.0$ is about 16% greater in C_p , and at $\alpha = 0.0$, it is about 37% greater in C_o .

3.5 Summary

Across both sets of experiments, we see that using our learned policies to construct initial transit networks for metaheuristic improvement methods improve the results of those methods when optimizing transit networks, compared with the use of various human-engineered construction algorithms. This is particularly true on large city graphs with 100 nodes or more, that is, graphs more like those of real-world cities: on the largest benchmark city, our initialization increased the hypervolume of solutions across α by 15%

versus the best other initialization method when using an evolutionary algorithm, and by 36% versus the best other method when using the hyperheuristic algorithm.

Having found that our learned policies can help with the second of Fan and Mumford's three factors in metaheuristic optimization, we turned next to the third factor: the choice of moves in search space. We will explore whether the neural policies we have trained to construct transit networks can be repurposed to modify existing networks in a way that is useful to a metaheuristic algorithm.

Chapter 4

Neural Nets as Low-Level Heuristics

The third factor that Fan and Mumford list as essential to the performance of a metaheuristic improvement algorithm is the set of neighbourhood moves that are available during search. This move set is dictated by the operations used to modify solutions during the algorithm's run. These operators are heuristics about what kinds of neighbourhood moves should be considered. They are commonly referred to as the low-level heuristics, because they operate at the "low" level of modifying networks directly, by comparison with the metaheuristic (such as evolution or annealing) which operates at the "high" level of deciding which modified networks to keep and which to discard. In the context of evolutionary algorithms specifically, these heuristics are also often called "mutators", by analogy with mutation's role in biological evolution. In this chapter, we consider whether the neural net policies described in Chapter 2 can enact good low-level heuristics within a

metaheuristic algorithm.

We designed the following neural-policy-based heuristic. To modify a network \mathcal{R} , it selects a random route $r \in \mathcal{R}$ and deletes it from \mathcal{R} to get $\mathcal{R}' = \mathcal{R} \setminus \{r\}$, and then runs learned construction with policy π_θ starting from \mathcal{R}' . Since $|\mathcal{R}'| = S - 1$, this constructs just one new route r' and adds it to \mathcal{R}' to get the modified network: $\mathcal{R} \leftarrow \mathcal{R}' \cup \{r'\}$.

To evaluate this learned low-level heuristic, we use it in a modified version of the evolutionary algorithm described in Chapter 3, where it replaces the type-1 mutator. We replace the type-1 mutator because its space of changes (replacing one route by a shortest path) is similar to that of the learned heuristic (replacing one route by a new route composed of shortest paths), while the type-2 mutator’s space of changes is quite different (lengthening or shortening a route by one node).

We refer to this modified algorithm as NEA, for “neural evolutionary algorithm”, and the unmodified algorithm with the type-1 mutator as EA.

In Chapter 3, we found that using LC-100 to generate \mathcal{R}_0 in the evolutionary algorithm improved its performance, so this was how we initialized both EA and NEA, except where otherwise mentioned. For NEA, we use the same policy π_θ in the LC-100 initialization as in the learned heuristic.

4.1 Comparison with Baseline Evolutionary Algorithm

We run each algorithm under consideration on all five of these synthetic cities over eleven different values of α , ranging from 0.0 to 1.0 in increments of 0.1. This lets us observe how well the different methods perform under a range of possible preferences, from the extremes of the operator perspective ($\alpha = 0.0$, caring only about C_o) and passenger perspective ($\alpha = 1.0$, caring only about C_p) to a range of intermediate perspectives. The constraint weight is set as $\beta = 5.0$ in all experiments, the same value used in training the policies. We found that this was sufficient to prevent any of the constraints in subsection 1.2.1 from being violated by any transit network produced in our experiments.

Because these algorithms are stochastic, for each city we perform ten runs of each algorithm with ten different random seeds. For algorithms that make use of a learned policy, ten separate policies were trained with the same set of random seeds (but using the same training dataset), and each was used when running algorithms with the corresponding random seed. The values reported are statistics computed over the ten runs.

We first compared our neural evolutionary algorithm (NEA) with our baseline evolutionary algorithm (EA). We also compare both with the initial networks from LC-100, to see how much improvement each algorithm makes over the initial networks. In the EA and NEA runs, the same parameter settings of $B = 10, I = 400, F = 10$ were used, following the values used in Nikolić and Teodorović [2013].

Table 4.1 displays the mean and standard deviation of the cost $C(\mathcal{G}, \mathcal{R})$ achieved by each

algorithm on the Mandl and Mumford benchmarks for $\alpha = 0.0$ (commonly referred to as the “operator perspective” in the literature), $\alpha = 1.0$ (commonly referred to as the “passenger perspective”), and $\alpha = 0.5$ (which we refer to as the “balanced perspective”). We see that on Mandl, the smallest of the five cities, EA and NEA perform virtually identically for the operator and passenger perspectives, while NEA offers a slight improvement for the balanced perspective. But for the larger cities of the Mumford dataset, NEA performs considerably better than EA for both the operator and balanced perspectives. On Mumford3, the largest of the five cities, NEA solutions have 13% lower average cost for the operator perspective and 5% lower for the balanced perspective than EA.

For the passenger perspective NEA’s advantage over EA is smaller, but it still outperforms EA on Mumford1 and Mumford3 and performs comparably on Mumford2. NEA’s networks have 1% lower average cost on Mumford3 than EA’s, but the average costs of NEA and EA are within one standard deviation of each other.

Figure 4.1 displays the average trip time C_p and total route time C_o achieved by each algorithm on the three largest Mumford cities, the three which are each based on a real city’s statistics, over eleven α values evenly spaced over the range $[0, 1]$ in increments of 0.1. There is a necessary trade-off between C_p and C_o , and as we would expect, as α increases, C_o increases and C_p decreases for each algorithm’s output. We also observe that for intermediate values of α , NEA pushes C_o much lower than LC-100, at the cost of increases in C_p . This behaviour is desirable, because as the figure shows, NEA achieves an overall larger range

α	Environment	LC-100	EA	NEA
0.0	Mandl	0.697 \pm 0.011	0.687 \pm 0.016	0.687 \pm 0.016
	Mumford0	0.842 \pm 0.021	0.770 \pm 0.022	0.771 \pm 0.028
	Mumford1	1.795 \pm 0.057	1.672 \pm 0.039	1.373 \pm 0.063
	Mumford2	1.375 \pm 0.103	1.118 \pm 0.068	0.950 \pm 0.063
	Mumford3	1.405 \pm 0.102	1.103 \pm 0.070	0.955 \pm 0.062
0.5	Mandl	0.560 \pm 0.003	0.548 \pm 0.007	0.543 \pm 0.009
	Mumford0	0.926 \pm 0.005	0.854 \pm 0.015	0.853 \pm 0.018
	Mumford1	1.307 \pm 0.027	1.243 \pm 0.032	1.101 \pm 0.016
	Mumford2	1.054 \pm 0.033	0.917 \pm 0.043	0.855 \pm 0.023
	Mumford3	1.046 \pm 0.038	0.885 \pm 0.027	0.844 \pm 0.027
1.0	Mandl	0.334 \pm 0.008	0.317 \pm 0.002	0.318 \pm 0.003
	Mumford0	0.749 \pm 0.021	0.614 \pm 0.007	0.619 \pm 0.011
	Mumford1	0.601 \pm 0.006	0.557 \pm 0.006	0.549 \pm 0.005
	Mumford2	0.535 \pm 0.012	0.507 \pm 0.003	0.507 \pm 0.007
	Mumford3	0.508 \pm 0.009	0.491 \pm 0.006	0.485 \pm 0.007

Table 4.1: Final cost $C(\mathcal{G}, \mathcal{R})$ achieved baseline experiments for three different α values. Values are averaged over ten random seeds; the \pm value is the standard deviation of $C(\mathcal{G}, \mathcal{R})$ over the seeds.

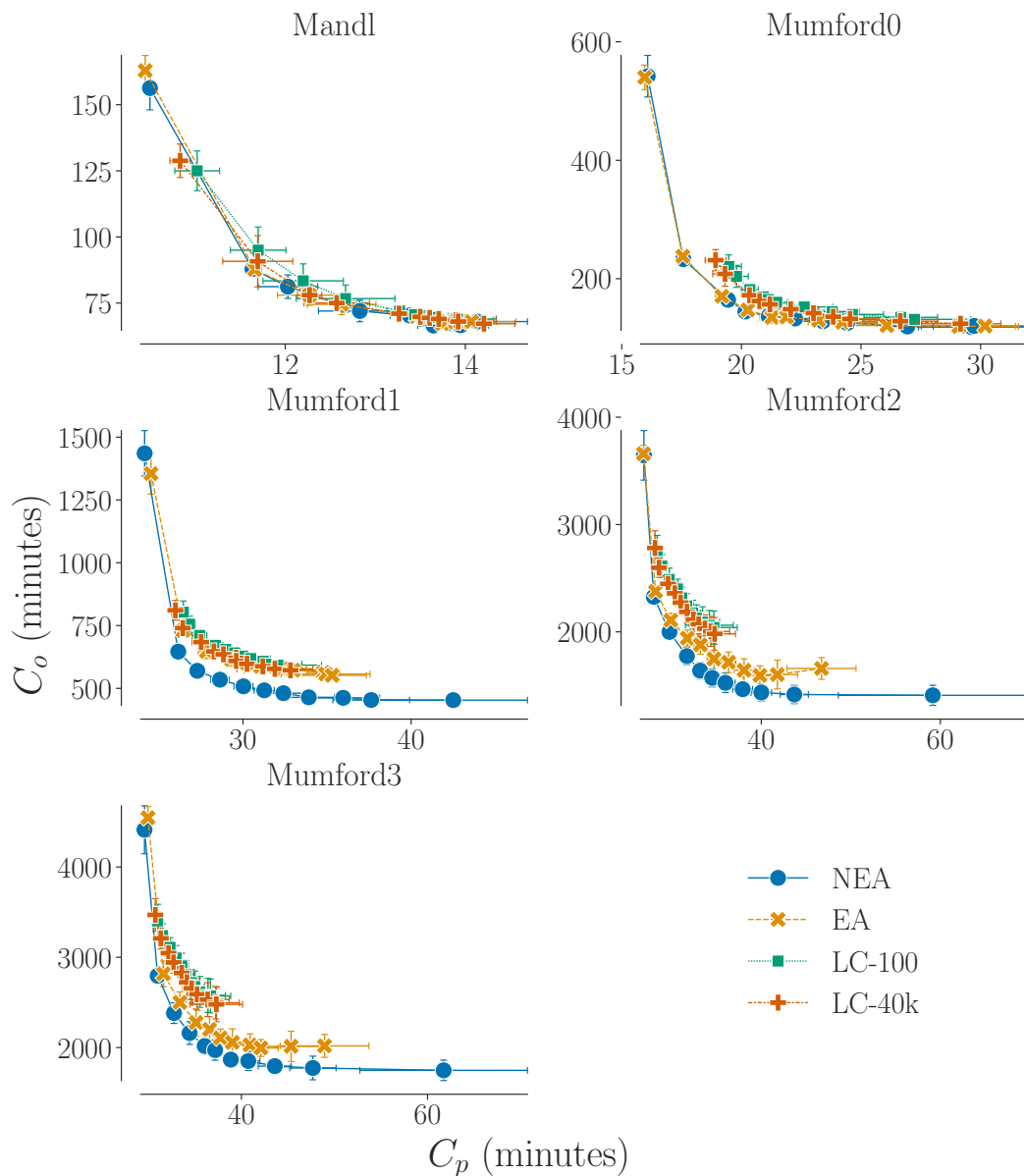


Figure 4.1: Values of average trip time C_p (on the x-axis) and total route time C_o (on the y-axis) achieved by NEA, EA, LC-100, and LC-40k, across values of α from 0 at lower-right to 1 at upper-left, in increments of 0.1. Each point is the mean over 10 random seeds for one value of α , and bars around each point indicate one standard deviation. Lines link pairs of points with consecutive α values.

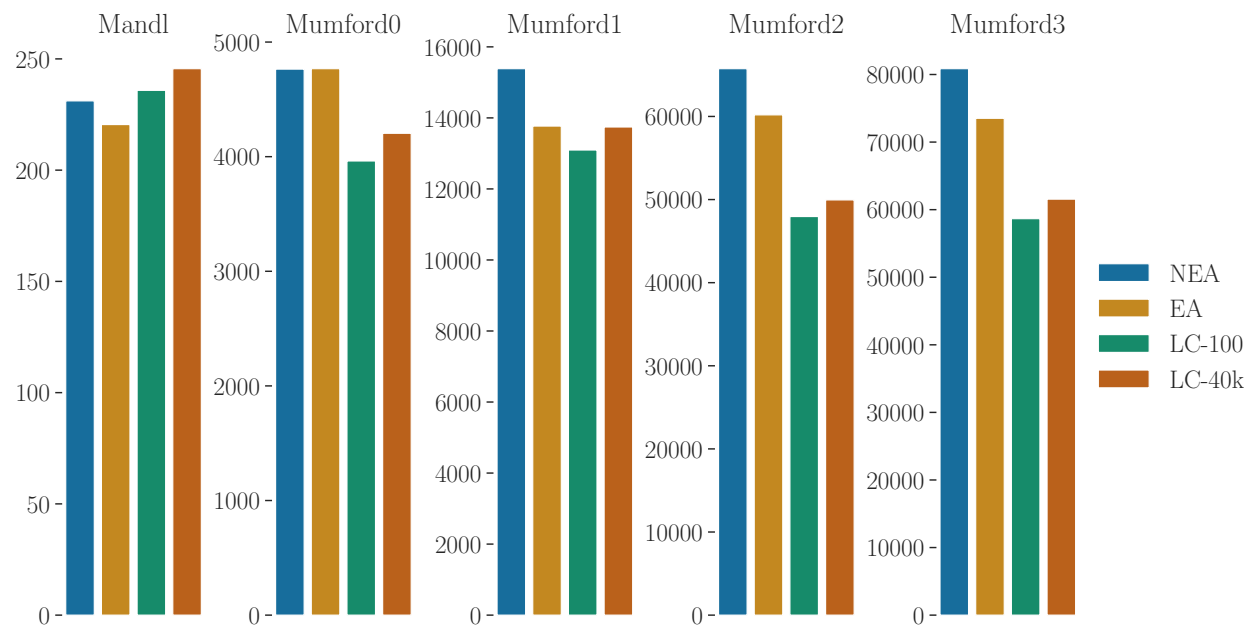


Figure 4.2: Hypervolumes achieved by LC-100, LC-Greedy, EA, and NEA.

of outcomes than LC-100 - for any network \mathcal{R} from LC-100, there is some value of α for which NEA produces a network \mathcal{R}' which dominates \mathcal{R} . Figure 4.1 also shows results for an additional algorithm, LC-40k, which we discuss in section 4.2.

We observe a common pattern on all Mumford1, 2, and 3: EA and NEA perform very similarly at $\alpha = 1.0$ (the leftmost point on each curve), but a significant performance gap forms as α decreases - consistent with what we see in Table 4.1. We also observe that LC-100 favours reducing C_p over C_o , with its points clustered higher and more leftwards than most of the points with corresponding α values on the other curves. Both EA and NEA achieve only very small decreases in C_p on LC-100's initial networks at $\alpha = 1.0$, and they do so by increasing C_o considerably.

Figure 4.2 corroborates what we observe in Table 4.1 and Figure 4.1: introducing the neural mutator improves the performance of the evolutionary algorithm by a significant margin on the three largest benchmark cities, across the range of α values.

4.2 Ablation Studies

To better understand the contribution of various components of our method, we performed three sets of ablation studies. These were conducted over the three realistic Mumford cities (1, 2, and 3) and over eleven α values evenly spaced over the range $[0, 1]$ in increments of 0.1.

4.2.1 Effect of number of samples

We note that over the course of the evolutionary algorithm, with our parameter settings $B = 10, I = 400, F = 10$, a total of $B \times I \times E = 40,000$ different transit networks are considered. By comparison, LC-100 only considers 100 networks. It could be that NEA’s superiority to LC-100 is only due to its considering more networks. To test this, we ran LC-40k, in which we sample 40,000 networks from the learned-construction algorithm, and pick the lowest-cost network. Comparing LC-100 and LC-40k in Figure 4.1, we see that across all three cities and all values of α , LC-40k performs very similarly to LC-100, improving on it only slightly in comparison with the larger improvements given by EA or NEA. Figure 4.2 shows further that taking the best of 40,000 samples instead of 100 makes only a slight

improvement to the quality of the networks found, in comparison with the improvement of NEA over EA. From this we conclude that the number of networks considered is not on its own an important factor in EA's and NEA's performance: much more important is the evolutionary algorithm that guides the search of possible networks.

4.2.2 Contribution of type-2 mutator

We next considered the impact of the type-2 mutator heuristic on NEA. This low-level heuristic is the same between EA and NEA and is not a learned function. To understand how important it is to NEA's performance, we ran "all-1 NEA", a variant of NEA in which only the neural mutator is used, and not the type-2 mutator.

The results are shown in Figure 4.3, along with the curve for NEA as in Figure 4.1, for comparison. It is clear that NEA and all-1 NEA perform very similarly in most scenarios. The most notable difference is at $\alpha = 1.0$, where we see that all-1 NEA underperforms NEA, achieving higher values of C_p . It appears that the minor adjustments to existing routes made by the type-2 mutator are more important at extremes of α , where the neural net policy has been pushed to the extremes of its behaviour.

On Mumford3, we observe that the curves do not overlap as cleanly: NEA seems to slightly outperform all-1 NEA at most α values. So the contribution of the type-2 mutator appears to grow as the city gets larger and more challenging. This may be because as the city gets larger, the space of possible routes grows larger, so the neural mutator's changes get

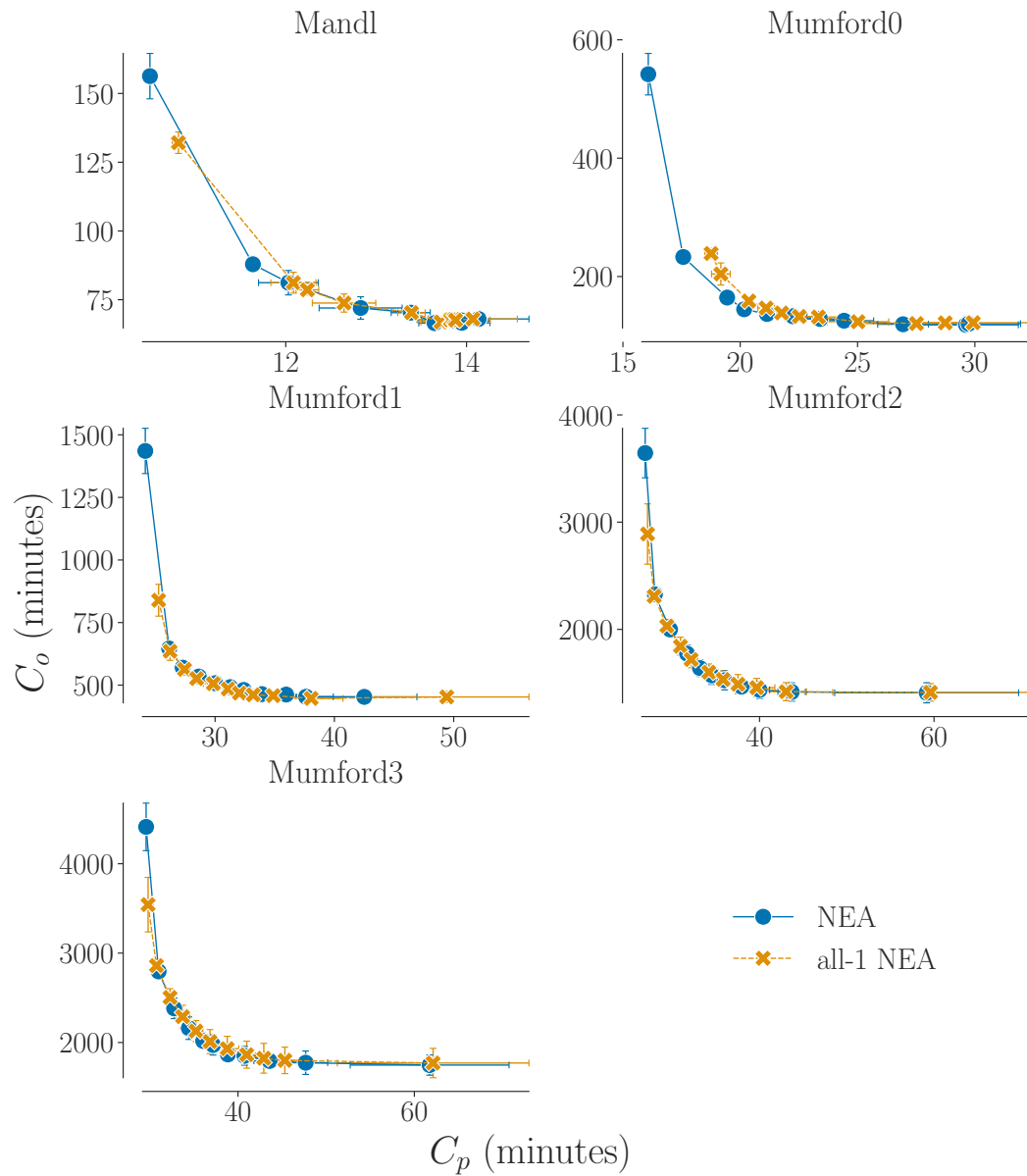


Figure 4.3: Values of average trip time C_p (on the x-axis) and total route time C_o (on the y-axis) achieved by all-1 NEA, plotted along with EA and NEA (repeated from Figure 4.1) for comparison.

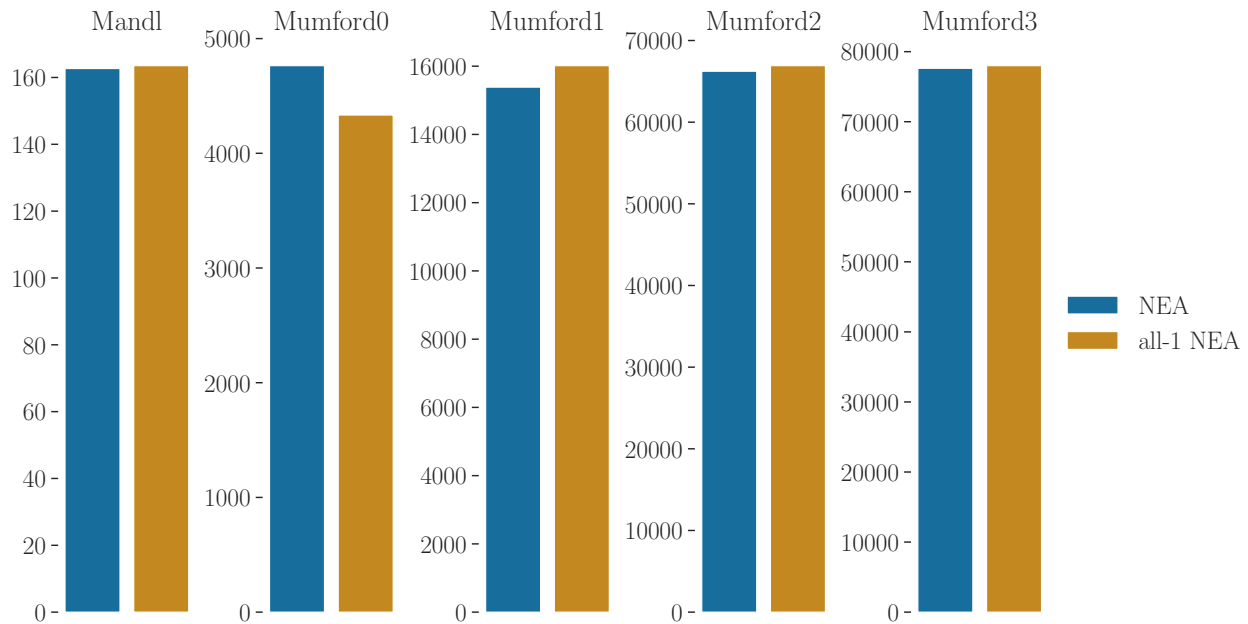


Figure 4.4: Hypervolumes achieved by NEA vs NEA with only the type-1 mutator.

more dramatic in comparison with the single-node adjustments of the type-2 mutator. The type-2 mutator’s class of changes becomes more distinct from those of the neural mutator, possibly making it more important.

Figure 4.4 compares the hypervolumes of NEA and all-1 NEA across the five benchmark cities, and confirms that their performance is overall extremely similar, except on Mumford0 where NEA has a more pronounced edge. This suggests that keeping the type-2 mutator is not a disadvantage on large cities, and may help on smaller ones. The differences are very small in any case, so we retain this mutator in NEA in future experiments. This does confirm, however, that between the two mutators, the primary contributor to the NEA’s quality is the neural mutator.

4.2.3 Importance of learned heuristics

We note that the type-1 mutator used in EA and the neural mutator used in NEA differ in the space of changes each is capable of making. The type-1 mutator can only add shortest paths as routes, while the neural mutator may compose new routes from multiple shortest paths. It may be that this structural difference, as opposed to the quality of the heuristics learned by the policy π_θ , is part of NEA's advantage over EA.

To test this conjecture, we ran a variant of NEA in which the learned policy π_θ is replaced by the uniformly-random policy π_{random} , previously described in Chapter 2. We call this variant the random-construction evolutionary algorithm (RC-EA). Since we wanted to gauge the performance of this variant in isolation from the learned policy, we used RC-100 to generate the initial network \mathcal{R}_0 , instead of LC-100 with π_θ .

The results are shown in Figure 4.5, along with the same NEA curves as in Figure 4.1. For most values of α , RC-EA performs less well than NEA, and Figure 4.6 confirms that its hypervolume is significantly smaller on each city. But at the extreme of $\alpha = 1.0$ it performs better than NEA, decreasing average trip time C_p by between one and two minutes versus NEA on each city - an improvement of about 3.7% on Mumford1 and about 4.5% on Mumford2 and Mumford3.

RC-EA's poor performance at low α makes sense: π_{random} , which replaces routes with composites of shortest paths, is biased towards making long routes. Unlike π_θ , which can learn to increase its halting probability with decreasing α , π_{random} 's halting probability is

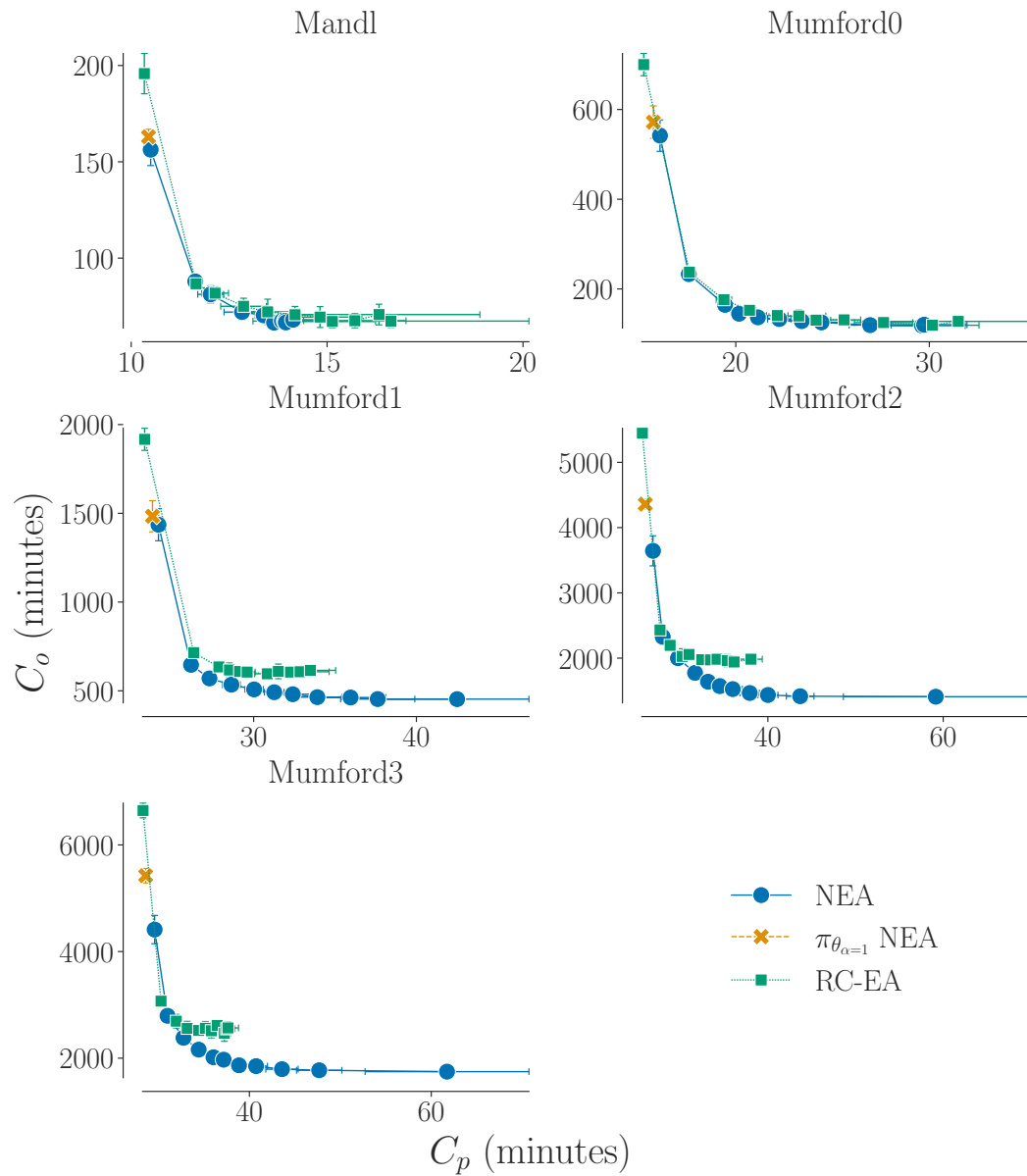


Figure 4.5: Trade-offs between average trip time C_p (on the x-axis) and total route time C_o (on the y-axis) achieved by RC-EA, plotted along with NEA (repeated from Figure 4.1) for comparison.

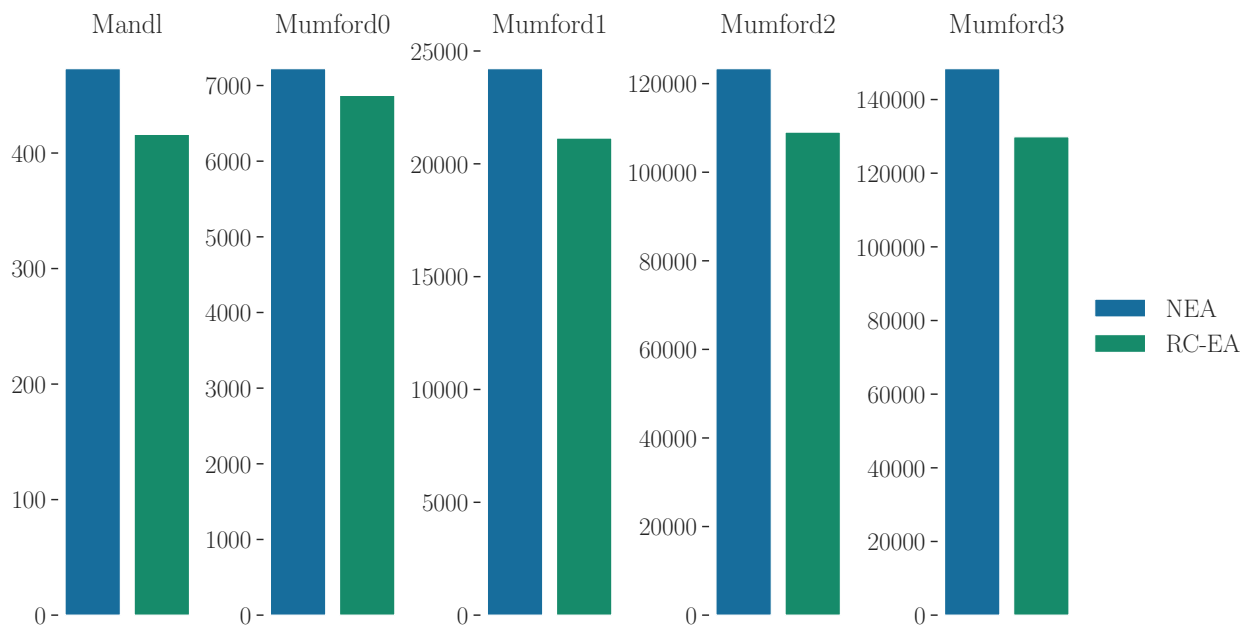


Figure 4.6: Hypervolumes achieved by NEA and RC-EA with only the type-1 mutator.

fixed and independent of α . This is an advantage over NEA at $\alpha = 1.0$ but a disadvantage at α less than about 0.8. It is interesting, though, that RC-EA outperforms NEA at $\alpha = 1.0$, as these two share the same space of possible actions. This calls to mind what we observed in subsection 2.5.2, which was that the superior performance at $\alpha = 1.0$ of π_{random} over π_{θ} on the transit network construction task. In that instance, we established that this was because π_{θ} , being trained over a range of α values, had not learned to perform as well as possible at the extreme of $\alpha = 1.0$. With parameters $\theta_{\alpha=1}$ trained with only $\alpha = 1.0$, $\pi_{\theta_{\alpha=1}}$ outperformed π_{random} at $\alpha = 1.0$.

To test whether the same thing was happening here, we ran another set of NEA experiments, this time using the same policy parameters $\theta_{\alpha=1}$ that were trained in

subsection 2.5.2, both for the LC-100 initialization and for NEA’s neural mutator. These experiments were run only at $\alpha = 1.0$, as we would not expect $\pi_{\theta_{\alpha=1}}$ to perform well for values of α it never saw during training. The results are displayed in Figure 4.5 alongside those of RC-EA. We observe that for all four Mumford cities, NEA with $\pi_{\theta_{\alpha=1}}$ at $\alpha = 1.0$ achieves lower C_p than NEA with π_{θ} , but not quite as low as RC-EA. Evidently, π_{random} still offers advantages over our learned models in the context of this evolutionary algorithm.

In principle, our policy could learn to perform as well as RC-EA by simply learning to choose actions uniformly at random. Yet that is evidently not the policy it has learned. In fact, as we observe in Figure 2.7, $\pi_{\theta_{\alpha=1}}$ does outperform π_{random} in the context of a construction process (LC-100 and RC-100), which is nearly the same process as the MDP in which $\pi_{\theta_{\alpha=1}}$ was trained. So $\theta_{\alpha=1}$ learned some policy that was better than a uniformly-random policy in its training context. But Figure 4.5 shows that this superiority does not translate to the evolutionary algorithm, which is quite different from the training context. This difference in context may explain why NEA $\pi_{\theta_{\alpha=1}}$ does not perform as well as RC-EA at $\alpha = 1.0$.

To test this would require designing a different training process, one where the MDP would more closely resemble the improvement process of EA than the construction process of LC-100 and LC-Greedy. This would be worthwhile but would require a major investment of time, and so lies beyond the scope of this thesis. Furthermore, as Figure 4.6 confirms, NEA with π_{θ} performs better than RC-EA when considering the whole range of α , so we

do not think this a critical flaw in our approach. For now we merely note that composing shortest paths is a good heuristic for route construction at high α , but is worse than simply choosing shortest paths at low α ; so the advantage of NEA comes primarily from what the policy π_θ learns during training.

4.3 Comparison with State of the Art Methods

While conducting the experiments of section 4.1, we observed that after 400 iterations the cost of NEA’s best-so-far network $\mathcal{R}_{\text{best}}$ was still decreasing from one iteration to the next. In order to make a fairer comparison with other methods from the literature on the Mandl and Mumford benchmarks, we performed a further set of experiments where we ran NEA with $I = 4,000$ instead of 400, for the operator perspective ($\alpha = 0.0$) and the passenger perspective ($\alpha = 1.0$). In addition, because we observed better performance from RC-EA for α near 1.0, we also ran RC-EA with $I = 4,000$ for $\alpha = 1.0$, and we include these results in the comparison.

Table 4.2 and Table 4.3 present the results of these experiments on the Mandl and Mumford benchmarks, alongside results reported on these benchmarks in comparable recent work. As elsewhere, the results we report for NEA and RC-EA are averaged over ten runs with different random seeds; the same set of ten trained policies used in the experiments of section 4.1 and section 4.2 are used here in NEA. Results from other work are as reported in that work. In addition to the average trip time C_p and total route time C_o , the tables

present metrics of how many transfers between routes were required by the networks. These are labelled d_0 , d_1 , d_2 , and d_{un} . d_i with $i \in \{0, 1, 2\}$ is the percentage of all passenger trips that required i transfers between routes; while d_{un} is the percentage of trips that require more than 2 transfers ($d_{un} = 100 - (d_0 + d_1 + d_2)$).

Before discussing these results, a brief word should be said about computation time. On a desktop computer with a 2.4 GHz Intel i9-12900F processor and an NVIDIA RTX 3090 graphics processing unit (used to accelerate our neural net computations), NEA takes about 10 hours for each 4,000-iteration run on Mumford3, the largest environment, while the RC-EA runs take about 6 hours. By comparison, John et al. [2014] and Hüsselmann et al. [2023] both use a variant of NSGA-II, a genetic algorithm, with a population of 200 networks, which in both cases takes more than two days to run on Mumford3. Hüsselmann et al. [2023]’s DBMOSA variant, meanwhile, takes 7 hours and 52 minutes to run on Mumford3. Kılıç and Gök [2014] report that their procedure takes eight hours just to construct the initial network for Mumford3, and don’t report the running time for the subsequent optimization.

These reported running times are mainly a function of the metaheuristic algorithm used, rather than the low-level heuristics used in the algorithm. Genetic algorithms like NSGA-II, with large populations as used in some of these methods, are very time-consuming because of the large number of networks they must modify and evaluate at each step. But their search of solution space is correspondingly more exhaustive than single-solution methods such as simulated annealing, or an evolutionary algorithm with a small population ($B = 10$) as we

use in our own experiments. It is therefore to be expected that they would achieve lower final costs in exchange for their greater run-time. We are interested here in the quality of our low-level heuristics, rather than that of the metaheuristic algorithm, and this must be kept in mind as we discuss the results of this section.

Caveat for Ahmed et al. (2019)

In these comparisons, we include results from Ahmed et al. [2019], but we wish to state a caveat to these. While they reported results that set a new state of the art on these benchmarks, they do not provide the values used for the two parameters to their algorithm. In our earlier work Holliday and Dudek [2023], theirs was one of several methods we implemented in order to test our proposed initialization scheme. We discovered parameter values on our own that gave results comparable to other work up to 2019, but after much effort and correspondence with one of the authors of Ahmed et al. [2019], we were unable to replicate their state-of-the-art results.

Passenger-perspective results

Table 4.2 shows the passenger perspective results alongside results from other work. On each city except Mumford3, the hyper-heuristic method of Ahmed et al. [2019] performs best, while on Mumford3 the NSGA-II variant of Hüsselmann et al. [2023] performs best. RC-EA and NEA both perform poorly on the smallest two cities, Mandl and Mumford0,

City	Method	$C_p \downarrow$	C_o	$d_0 \uparrow$	d_1	d_2	$d_{un} \downarrow$
Mandl	Mumford [2013b]	10.27	221	95.38	4.56	0.06	0
	John et al. [2014]	10.25	212	-	-	-	-
	Kılıç and Gök [2014]	10.29	216	95.5	4.5	0	0
	Ahmed et al. [2019]	10.18	212	97.17	2.82	0.00	0
	Hüsselmann et al. [2023] DBMOSA	10.27	179	95.94	3.93	0.13	0
	Hüsselmann et al. [2023] NSGA-II	10.19	197	97.36	2.64	0	0
	NEA	10.47	157	91.89	7.55	0.52	0.04
	RC-EA	10.32	194	94.15	5.74	0.11	0
Mumford0	Mumford [2013b]	16.05	759	63.2	35.82	0.98	0
	John et al. [2014]	15.4	745	-	-	-	-
	Kılıç and Gök [2014]	14.99	707	69.73	30.03	0.24	0
	Ahmed et al. [2019]	14.09	722	88.74	11.25	0	0
	Hüsselmann et al. [2023] DBMOSA	15.48	431	65.5	34.5	0	0
	Hüsselmann et al. [2023] NSGA-II	14.34	635	86.94	13.06	0	0
	NEA	16.00	550	49.74	43.85	6.38	0.02
	RC-EA	14.96	722	63.21	36.36	0.43	0
Mumford1	Mumford [2013b]	24.79	2038	36.6	52.42	10.71	0.26
	John et al. [2014]	23.91	1861	-	-	-	-
	Kılıç and Gök [2014]	23.25	1956	45.1	49.08	5.76	0.06
	Ahmed et al. [2019]	21.69	1956	65.75	34.18	0.07	0
	Hüsselmann et al. [2023] DBMOSA	22.31	1359	57.14	42.63	0.23	0
	Hüsselmann et al. [2023] NSGA-II	21.94	1851	62.11	37.84	0.05	0
	NEA	24.07	1450	33.04	45.64	18.89	2.43
	RC-EA	23.01	1924	39.57	49.66	10.46	0.32
Mumford2	Mumford [2013b]	28.65	5632	30.92	51.29	16.36	1.44
	John et al. [2014]	27.02	5461	-	-	-	-
	Kılıç and Gök [2014]	26.82	5027	33.88	57.18	8.77	0.17
	Ahmed et al. [2019]	25.19	5257	56.68	43.26	0.05	0
	Hüsselmann et al. [2023] DBMOSA	25.65	3583	48.07	51.29	0.64	0
	Hüsselmann et al. [2023] NSGA-II	25.31	4171	52.56	47.33	0.11	0
	NEA	26.52	4017	32.74	49.94	16.42	0.90
	RC-EA	25.45	5536	41.18	52.96	5.84	0.02
Mumford3	Mumford [2013b]	31.44	6665	27.46	50.97	18.79	2.81
	John et al. [2014]	29.5	6320	-	-	-	-
	Kılıç and Gök [2014]	30.41	5834	27.56	53.25	17.51	1.68
	Ahmed et al. [2019]	28.05	6119	50.41	48.81	0.77	0
	Hüsselmann et al. [2023] DBMOSA	28.22	4060	45.07	54.37	0.56	0
	Hüsselmann et al. [2023] NSGA-II	28.03	5018	48.71	51.1	0.19	0
	NEA	29.18	5122	30.70	52.27	16.17	0.87
	RC-EA	28.09	6830	38.6	57.02	4.35	0.03

Table 4.2: Passenger-perspective results. C_p is the average passenger trip time. C_o is the total route time. d_i is the percentage of trips satisfied with number of transfers i , while d_{un} is the percentage of trips satisfied with 3 or more transfers. Arrows next to each quantity indicate which of increase or decrease is desirable. Bolded values in C_p , d_0 , and d_{un} columns are the best on that environment.

but their relative performance improves as the size of the city increases. On both Mumford2 and Mumford3, RC-EA’s performance is very close to that of Hüsselmann et al. [2023]’s and Ahmed et al. [2019]’s, and better than all other methods listed, despite the relatively under-powered metaheuristic that drives it.

RC-EA also outperforms Hüsselmann et al. [2023]’s DBMOSA, which uses the same low-level heuristics as their NSGA-II with a faster but less-exhaustive metaheuristic. That RC-EA exceeds DBMOSA’s performance on Mumford2 and Mumford3 is evidence that the low-level heuristics used in RC-EA are better for the passenger perspective than those proposed by Hüsselmann et al. [2023]. This is especially the case given that DBMOSA is still a more sophisticated metaheuristic algorithm than ours, with ten different low-level heuristics and a hyper-heuristic that adapts the rate at which each low-level heuristic is applied over the run - though we acknowledge that DBMOSA is a multi-objective optimization algorithm, which may account for its relative weakness here.

NEA does not perform as well as RC-EA on the passenger perspective (aligning with what we observed in section 4.2), but still shows good performance on Mumford2 and 3, outperforming all of these methods that were published prior to 2019.

4.3.1 Operator-perspective results

Table 4.3 shows the operator-perspective results alongside results from other work. Kılıç and Gök [2014] do not report results for the operator perspective and as such we do not

include their work in Table 4.3. Similarly to the passenger-perspective results, our methods underperform on the smallest cities (Mandl and Mumford0) but perform well on larger ones. Strikingly, NEA achieves the lowest value of total route time C_o out of all methods on Mumford3, improving even on Ahmed et al. [2019], and outperforms all other methods on Mumford1 and Mumford2 as well. Evidently, the learned policy functions very well as a low-level heuristic at low values of α , where the premium is on keeping routes short.

4.3.2 Transfer Statistics

The metrics d_0 to d_{un} reveal that both RC-EA and NEA favour higher numbers of transfers relative to most of the other methods, particularly Hüsselmann et al. [2023]. This is true for both the passenger and operator perspectives. For the operator perspective, this matches our intuitions: shorter routes will deliver fewer passengers directly to their destinations and will require more transfers. But we were surprised to observe this in the passenger perspective case as well.

Compared to Hüsselmann et al. [2023]’s DBMOSA, RC-EA achieves lower average trip time C_p on Mumford2 and Mumford3 for the passenger perspective, despite the fact that it requires more passenger trips to make 1 and 2 transfers. Still, RC-EA’s networks require fewer transfers overall than NEA’s, which matches our intuition that fewer transfers should result in lower average trip time C_p . It seems that the process of compositing shortest paths to form routes biases those routes towards directness and efficiency, to a degree that

City	Method	$C_o \downarrow$	C_p	$d_0 \uparrow$	d_1	d_2	$d_{un} \downarrow$
Mandl	Mumford [2013b]	63	15.13	70.91	25.5	2.95	0.64
	John et al. [2014]	63	13.48	-	-	-	-
	Ahmed et al. [2019]	63	14.28	62.23	27.16	9.57	1.03
	Hüsselmann et al. [2023] DBMOSA	63	13.55	70.99	24.44	4.00	0.58
	Hüsselmann et al. [2023] NSGA-II	63	13.49	71.18	25.21	2.97	0.64
	NEA	68	14.13	57.28	30.56	11.84	0.31
Mumford0	Mumford [2013b]	111	32.4	18.42	23.4	20.78	37.40
	John et al. [2014]	95	32.78	-	-	-	-
	Ahmed et al. [2019]	94	26.32	14.61	31.59	36.41	17.37
	Hüsselmann et al. [2023] DBMOSA	98	27.61	22.39	31.27	18.82	27.51
	Hüsselmann et al. [2023] NSGA-II	94	27.17	24.71	38.31	26.77	10.22
	NEA	120	29.73	15.25	31.14	28.58	25.03
Mumford1	Mumford [2013b]	568	34.69	16.53	29.06	29.93	24.66
	John et al. [2014]	462	39.98	-	-	-	-
	Ahmed et al. [2019]	408	39.45	18.02	29.88	31.9	20.19
	Hüsselmann et al. [2023] DBMOSA	511	26.48	25.17	59.33	14.54	0.96
	Hüsselmann et al. [2023] NSGA-II	465	31.26	19.70	42.09	33.87	4.33
	NEA	437	49.37	13.92	21.51	22.42	42.15
Mumford2	Mumford [2013b]	2244	36.54	13.76	27.69	29.53	29.02
	John et al. [2014]	1875	32.33	-	-	-	-
	Ahmed et al. [2019]	1330	46.86	13.63	23.58	23.94	38.82
	Hüsselmann et al. [2023] DBMOSA	1979	29.91	22.77	58.65	18.01	0.57
	Hüsselmann et al. [2023] NSGA-II	1545	37.52	13.48	36.79	34.33	15.39
	NEA	1365	61.67	8.34	15.33	18.71	57.62
Mumford3	Mumford [2013b]	2830	36.92	16.71	33.69	33.69	20.42
	John et al. [2014]	2301	36.12	-	-	-	-
	Ahmed et al. [2019]	1746	46.05	16.28	24.87	26.34	32.44
	Hüsselmann et al. [2023] DBMOSA	2682	32.33	23.55	58.05	17.18	1.23
	Hüsselmann et al. [2023] NSGA-II	2043	35.97	15.02	48.66	31.83	4.49
	NEA	1697	66.04	8.26	13.46	16.66	61.63

Table 4.3: Operator perspective results. C_p is the average passenger trip time. C_o is the total route time. d_i is the percentage of trips satisfied with number of transfers i , while d_{un} is the percentage of trips satisfied with 3 or more transfers. Arrows next to each quantity indicate which of increase or decrease is desirable. Bolded values in C_o , d_0 and d_{un} columns are the best on that environment.

outweighs the cost imposed by having more transfers. Each transfer is less impactful on riders if the routes they’re transferring between are more direct.

Meanwhile, since both the learned heuristic of NEA and the unlearned heuristic of RC-EA suffer from high transfer counts, it seems the difference between these and the other results from the literature may be a result of the evolutionary algorithm itself. At any rate, these results are not out of line with those of Mumford [2013b] and Kılıç and Gök [2014] on the largest cities, so we do not consider this a major strike against our learned heuristics. Indeed, we expect that these results could be improved by explicitly including d_0 in the reward function used to train the policy π_θ , and this would reduce the number of transfers required by NEA’s networks.

4.4 Summary

In this chapter, we proposed a low-level heuristic that uses the learned neural policies described in Chapter 2 to modify an existing transit network, in a way that exploits the construction heuristics learned by the policy to prefer better neighbourhood moves to worse ones. We showed that an evolutionary algorithm that used this heuristic as one of its mutators, which we call a Neural Evolutionary Algorithm, could achieve performance competitive with, and in some cases better than, state-of-the-art metaheuristic improvement methods for the TNDP, while running in approximately 80% less wall-clock time. And we performed several ablation studies to understand the contribution of

different parts of the Neural Evolutionary Algorithm, finding that its performance versus a variant without the neural mutator was indeed due mainly to the learned policy.

Up to now, we have evaluated these methods on synthetic cities, whose only connection to real cities is in coarse statistics like the number of nodes and number of required routes. In the next chapter, we discuss the use of this neural evolutionary algorithm in a more realistic scenario, with geography and travel demand closely based on real data from an existing city.

Chapter 5

Application to a Realistic Scenario

Over the past three chapters, we developed a hybrid method composed of an evolutionary algorithm that uses a learned neural policy both to initialize the algorithm and to select some of the neighbourhood moves made during each mutation step. We have evaluated our method's performance on a set of synthetic benchmark cities. While some of these synthetic cities have statistics n , S , m_{\min} , and m_{\max} based on those of a real-world city, all the particulars - the spatial layout of the nodes \mathcal{N} , the road network \mathcal{E}_s that connects them, and the travel demands D - are entirely synthetically generated, with no reference to the actual spatial and demand characteristics of their corresponding real cities. In this chapter, we describe how we then applied our method to a more realistic instance of the TNDP, based closely on real data from the city of Laval in Quebec, Canada.

Laval is a suburb of the major city of Montreal, located on an island north of the island

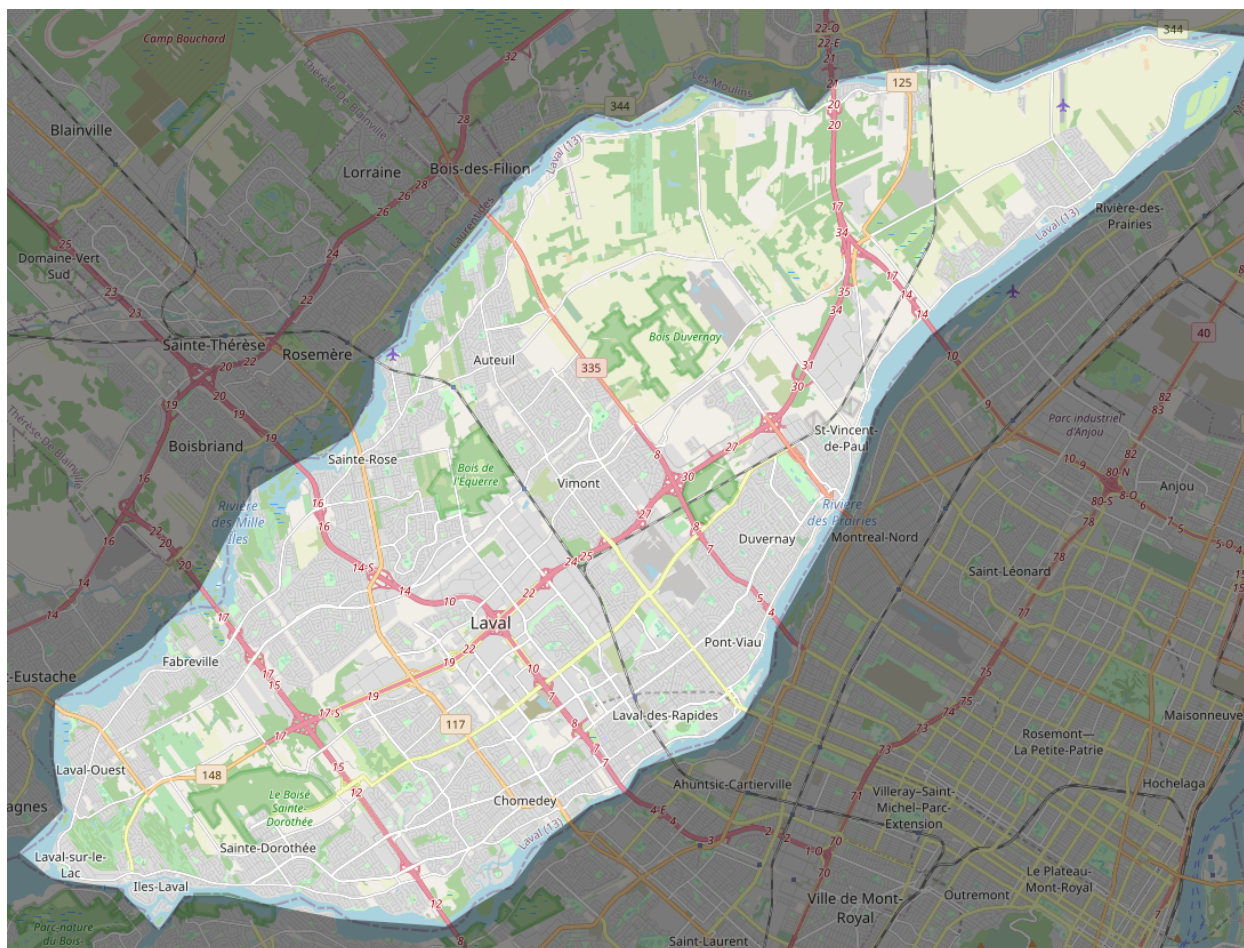


Figure 5.1: A map of the city of Laval, Quebec, taken from Google [2024].

of Montreal. As of the 2021 census, it had a total population of 429,555 [Statistics Canada, 2023]. Public transit in Laval is provided primarily by the bus network of the Société de Transport de Laval; additionally, one line of the Montreal underground metro system has three stops in Laval.

5.1 Representing Laval

To apply our learned policy π_θ to Laval, we first had to assemble a city graph $\mathcal{G} = (\mathcal{N}, \mathcal{E}_s, D)$ to represent it using the data sources that were available to us. Our model of the Laval is based on several sources: geographic data on Census Dissemination Areas (CDAs) for 2021 from Statistics Canada [Statistics Canada, 2021], a GIS representation of the road network of Laval provided to us by the Société de Transport de Laval, an OD dataset [Agence métropolitaine de transport, 2013] provided by Quebec’s Agence Métropolitaine de Transport, and publicly-available GTFS data from 2013 [Société de Transport de Laval] that describes Laval’s existing transit system.

5.1.1 Street graph

The real city of Laval contains 2,618 unique transit stop facilities. Taking each of these to be a node yielded a very large graph. The experiments in this chapter were run on a compute cluster node with an NVidia A100 GPU with 40 GB of VRAM; our neural policies needed more memory than this to run on the entire 2,618-node graph, creating a technical hurdle. It is also likely that such a representation would be more fine-grained than necessary: the demand for travel within the service areas of nearby transit stops is likely to be very similar. For these reasons, we instead made use of a coarsened graph, where the nodes correspond to CDAs. CDAs are designed so as to enclose populations that are roughly homogeneous (among other factors), making them a sensible granularity at which to analyze

travel demands. Laval contains 632 distinct CDAs, and a graph size of $n = 632$ makes it feasible for us to apply our neural policies with the hardware we have available.

The street graph $(\mathcal{N}, \mathcal{E}_s)$ was derived from the 2021 census data by taking the centroid of each CDA within Laval to be a node in \mathcal{N} , and adding a street edge (i, j, τ_{ij}) for node pair (i, j) if their corresponding CDAs shared a border. To compute drive times τ_{ij} , we found all points in the road network within the CDAs of i and j , computed the shortest-path driving time over the road network from each of i 's road-network points to each of j 's, and set τ'_{ij} as the median of these driving times. We did this so that τ'_{ij} would reflect the real drive times given the existing road network. By this approach, $\tau'_{ij} \neq \tau'_{ji}$ in general, but as our method treats cities as undirected graphs, it expects that $\tau_{ij} = \tau_{ji} \forall i, j \in \mathcal{N}$. To enforce this, as a final step we set:

$$\tau_{ij} = \tau_{ji} = \max(\tau'_{ij}, \tau'_{ji}) \forall i, j \in \mathcal{N} \quad (5.1)$$

5.1.2 Existing transit

The existing transit network in Laval has 43 bus routes that operate during morning rush hour from 7 to 9 AM. To compare networks from our algorithm to the this network, we had to translate it to a network that runs over $(\mathcal{N}, \mathcal{E}_s)$ as defined in subsection 5.1.1. To do this, we mapped each stop on an existing bus route to the node in \mathcal{N} of the CDA that contained the stop. We will refer to this translated transit system as the Société de Transport de Laval

(STL) network, after the city’s transit agency, the Société de Transport de Laval.

The numbers of stops on the routes in the STL network range from 2 to 52. To ensure a fair comparison, we set $m_{\min} = 2$ and $m_{\max} = 52$ when running our algorithm. Unlike the routes in our algorithm’s networks, many of STL’s routes are not symmetric (that is, they follow a different path in each direction between terminals), and several are unidirectional (they go only one way between terminals). We maintained the constraints of symmetry and bidirectionality on our own algorithm since this was how our policies are trained, so relaxing the constraints might harm their performance. But we did not enforce these constraints upon the STL network, as doing so would require major changes to it, making it a much less realistic point of comparison. Given that uni-directional streets are a common feature in real cities, it would be good to train future policies without these two constraints, but we leave this for future work.

Since these constraints were not obeyed by STL, when reporting total route time C_o in this section, we calculated it for bidirectional routes by summing the travel times of both directions, instead of just one direction as in the preceding sections. This allows a fair comparison of C_o between STL and other networks.

In addition, there is an underground metro line, the Montreal Orange Line, which has three stops in Laval. As with the existing bus lines, we mapped these three stops to their containing CDAs and treat them as forming an additional route. We added this metro route to both the STL network and the networks \mathcal{R} produced by our algorithm when evaluating

them, to reflect that unlike the bus routes, it is not feasible to change the metro line and so it represents a constant of the city.

5.1.3 Demand matrix

Finally we assembled the demand matrix D from the OD dataset. The entries in the OD dataset correspond to trips reported by residents of Laval who were surveyed about their recent travel behaviour. Each entry has latitude and longitude coordinates \mathbf{l}_o and \mathbf{l}_d for the trip's approximate origin and destination, as well as an "expansion factor" $expf$ giving the estimated number of actual trips corresponding to that surveyed trip. It also indicates the mode of travel, such as car, bicycle, or public transit, that was used to make the trip.

Many entries in the OD dataset refer to trips that begin or end in Montreal. For our purposes, we "redirected" all trips made by public transit that enter or leave Laval to one of several "crossover points" that we defined. These crossover points are the locations of the three Orange Line metro stations in Laval, and the locations of the last or first stop in Laval of each existing bus route that goes between Laval and Montreal.

For each trip between Laval and Montreal, we identified the crossover point that has the shortest distance to either of \mathbf{l}_o or \mathbf{l}_d , and overwrote the Montreal end-point of the trip by this crossover point. This process was automated with a simple computer script. The idea is that if the Laval end of the trip is close to a transit stop that provides access to Montreal, the rider will choose to cross over to the Montreal transit system as soon as

possible, as most locations in Montreal will be easier to access once in the Montreal transit system. Trips that go between Laval and Montreal by means other than public transit were not included in D , as we judge that most such trips cannot be induced to switch modes to transit.

Having done this remapping, we initialized D with all entries set to 0. Then for each entry in the OD dataset, we found the CDAs that contain $\mathit{mathbf{fl}}_o$ and \mathbf{l}_d , associated them with the matching nodes i and j in \mathcal{N} , and updated $D_{ij} \leftarrow D_{ij} + \mathit{expf}$. D then had the estimated demand between every pair of CDAs. To enforce symmetric demand, we then assigned $D_{ij} \leftarrow \max(D_{ij}, D_{ji}) \forall i, j \in \mathcal{N}$. The resulting demand matrix D contains 548,159 trips, of which 63,104 are trips between Laval and Montreal that we redirected.

We then applied a final filtering step. The STL network does not provide a path between all node pairs i, j for which $D_{ij} > 0$, and so it violates the connectedness constraint of subsection 1.2.1. This is because D at this point includes all trips that were made within Laval by any mode of transport, including to and from areas that are not served by the STL network. These areas may be unserved because they are populated by car owners unlikely to use transit if it were available. To ensure a fair comparison between the STL network and our algorithm’s networks, we set to 0 all entries of D for which the STL network does not provide a path. We expected this to cause our system to output transit networks that are “closer” to the existing transit network, in that they satisfy the same travel demand as before. This will reduce the scope of the changes required to go from the existing network

# nodes n	# street edges $ \mathcal{E}_s $	# demand trips	# routes S	m_{\min}	m_{\max}	Area (km ²)
632	4,544	548,159	43	2	52	520.1

Table 5.1: Statistics and parameters of the Laval scenario

to a new one proposed by our system.

Table 5.1 contains the statistics of, and parameters used for, the Laval scenario.

The final set of routes in our STL network is shown in Figure 5.3. We observe that the three major bus terminals, shown in black, are highly connected, with many discrete routes visiting them, although a large fraction of the bus routes connected to Le Carrefour and Montmorency connect them quickly to each other. The Montmorency bus terminal is located at the Montmorency metro station on the orange line, so it is likely that these routes are meant to provide access to and from the orange line. The same is true of the Cartier terminal, which is located at the Cartier orange line station: many routes connect to this node from diverse locations around the Laval graph, probably because of its co-location with the metro station, which is also the closest metro station to Montreal itself. Connecting Laval’s residents to Montreal via the orange line is clearly a priority for the STL’s planners.

5.2 Enforcing constraint satisfaction

In the experiments on the Mandl and Mumford benchmark cities described in Chapter 4, the EA and NEA algorithms never produced networks that violated any of the constraints

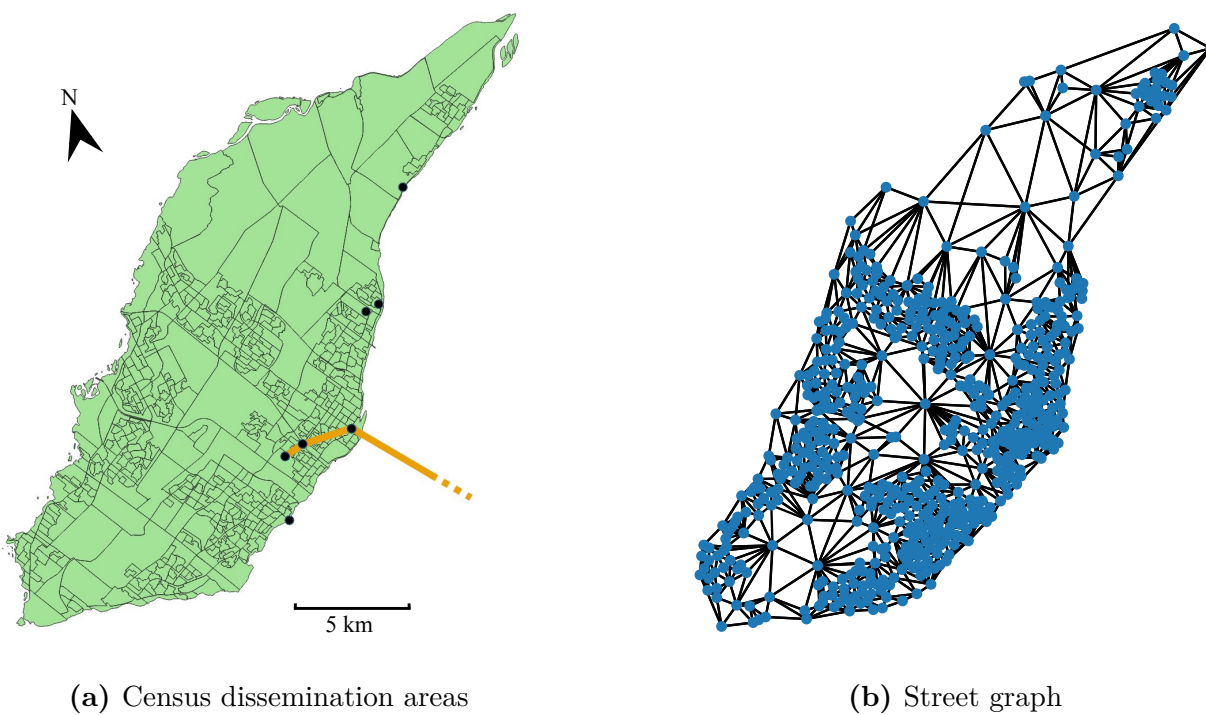


Figure 5.2: Figure 5.2a shows a map of the Census Dissemination Areas of the city of Laval, with “crossover points” used to remap inter-city demands shown as black circles, and the Montreal Metro Orange Line shown in orange. Figure 5.2b shows the street graph constructed from these dissemination areas.

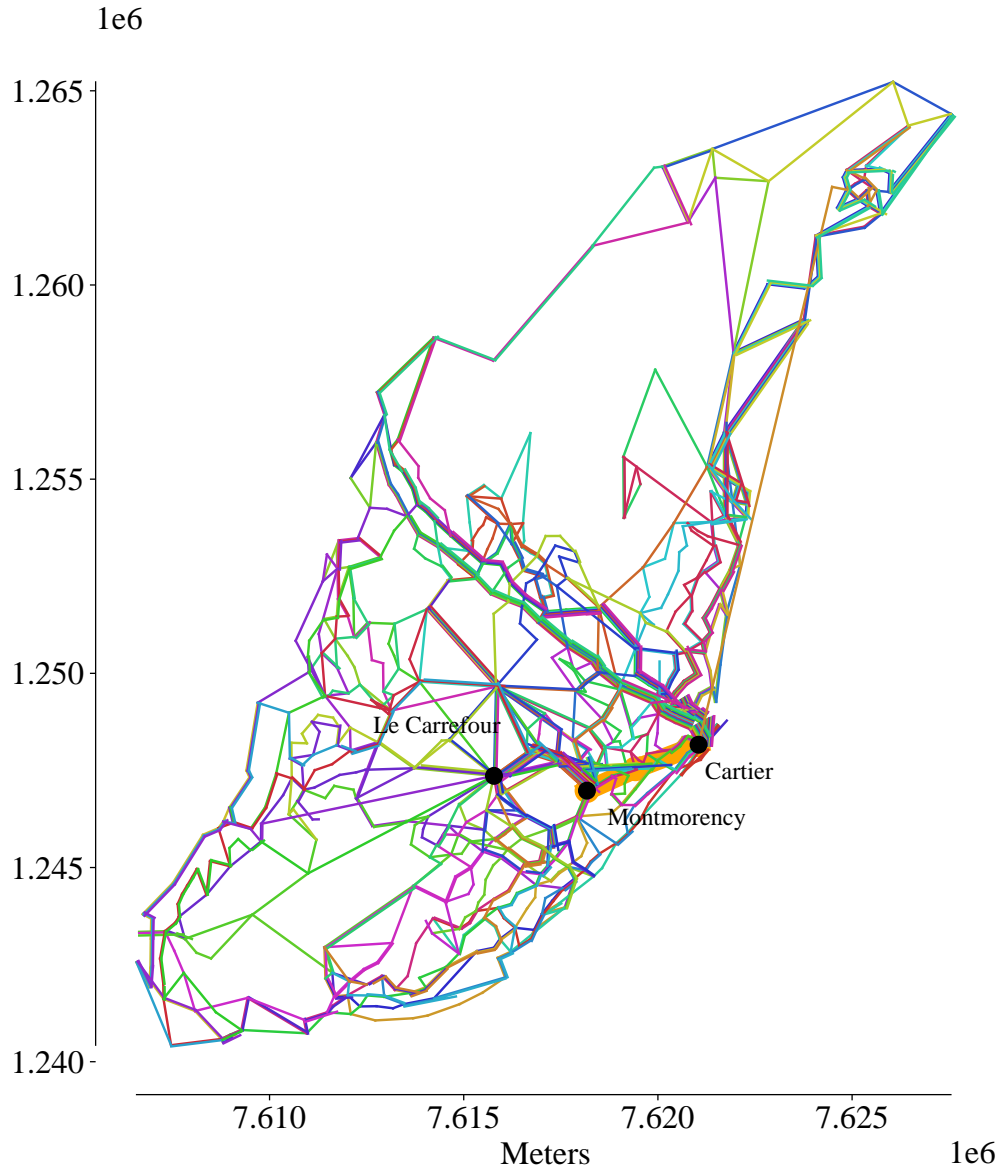


Figure 5.3: The routes of our STL network. Routes that go along a single edge are placed next to each other, so thicker “rainbow” edges show multiple parallel routes. The thick orange line shows the Orange Line subway of the Montreal Metro, with its stations as orange circles, and the black circles show the nodes of the CDAs containing Laval’s three major bus terminals: Le Carrefour, Montmorency, and Cartier.

on networks outlined in subsection 1.2.1. However, Laval’s city graph, with 632 nodes, is considerably larger than even the largest Mumford city, which has only 127 nodes. In our initial experiments on Laval, we found that both EA and NEA consistently produced networks that violated the connectedness constraint, providing no transit path for some node pairs (i, j) for which $D_{ij} > 0$.

To remedy this, we modified the MDP described in section 2.1 to enforce reduction of unsatisfied demand. Let $c_1(\mathcal{G}, \mathcal{R})$ be the number of node pairs i, j with $D_{ij} > 0$ for which network \mathcal{R} provides no transit path, and let $\mathcal{R}'_t = \mathcal{R}_t \cup \{r_t\}$, the network formed from the finished routes and the in-progress route r_t . We applied the following changes to the action space \mathcal{A}_t whenever $c_1(\mathcal{R}_t) > 0$:

- When the timestep t is even and \mathcal{A}_t would otherwise be $\{\text{continue, halt}\}$, the halt action is removed from \mathcal{A}_t . This means that if $c_1(\mathcal{G}, \mathcal{R}'_t) > 0$, the current route must be extended if it is possible to do so without violating another constraint.
- When t is odd, if \mathcal{A}_t contains any paths that would reduce $c_1(\mathcal{G}, \mathcal{R}'_t)$ if added to r_t , then all paths that would *not* reduce $c_1(\mathcal{G}, \mathcal{R}'_t)$ are removed from \mathcal{A}_t . This means that if it is *possible* to connect some unconnected trips by extending r_t , then *not* doing so is forbidden.

With these changes to the MDP, we found that both LC-100 and NEA produced networks that connected all desired passenger trips, with no constraint violations - even when the

policy π_θ was trained without these changes. The results reported in this section are obtained using this variant of the MDP.

5.3 Results

We performed experiments evaluating both the NEA and RC-EA algorithms on the Laval city graph. These experiments were conducted on different hardware than those in the previous chapters: specifically, they were run on an academic compute cluster node, using one NVidia A100 GPU with 40 GB of GPU RAM.

Three sets of NEA experiments were performed with different α values representing different perspectives: the operator perspective ($\alpha = 0.0$), the passenger perspective ($\alpha = 1.0$), and a balanced perspective ($\alpha = 0.5$). RC-EA experiments are only run at $\alpha = 1.0$ since we observed in subsection 4.2.3 that RC-EA did not perform well at other α . As before, we perform ten runs of each experiment with ten different random seeds and ten different learned policies π_θ , and report statistics over these ten runs; the same per-seed parameters θ are used as in the experiments of Chapter 4. We also run the STL network on the Laval city graph \mathcal{G} in the same way that we run the networks from our other algorithms to measure their performance, but since the STL network is a single, pre-determined network that does not depend on α , we run it only once.

The parameters of NEA were the same as in the Mumford experiments in section 4.1: $I = 400$, $B = 10$, $F = 10$, and transfer penalty $p_T = 300$ s.

α	Method	$C_p \downarrow$	$C_o \downarrow$	$d_0 \uparrow$	d_1	d_2	$d_{un} \downarrow$
N/A	STL	124.61	23954	14.48	22.8	20.88	41.83
0.0	LC-100	104.36 ± 3.69	19175 ± 316	14.25 ± 0.64	21.38 ± 1.15	21.81 ± 1.23	42.57 ± 2.49
	NEA	113.44 ± 12.34	18171 ± 486	14.70 ± 1.14	20.62 ± 2.10	22.17 ± 1.72	42.52 ± 3.38
0.5	LC-100	82.44 ± 9.38	21452 ± 1482	13.56 ± 0.61	24.23 ± 2.73	25.01 ± 3.13	37.20 ± 5.63
	NEA	83.74 ± 5.32	19978 ± 1015	13.68 ± 0.80	24.01 ± 1.88	25.23 ± 1.85	37.08 ± 3.48
1.0	LC-100	68.29 ± 4.13	27871 ± 3871	15.89 ± 1.41	29.70 ± 3.74	27.60 ± 1.16	26.81 ± 5.77
	NEA	60.43 ± 1.03	42600 ± 1269	20.29 ± 0.82	33.82 ± 2.24	27.51 ± 0.93	18.39 ± 3.16
	RC-EA	58.46 ± 0.24	47810 ± 900	21.26 ± 0.46	38.98 ± 0.86	26.87 ± 0.50	12.88 ± 0.74

Table 5.2: Performance of networks from LC-100 and NEA at three α values, RC-EA at $\alpha = 1.0$, and the STL network. Bolded values are best for the corresponding α , except where STL performs better than all methods at that α , in which case no values are bolded. C_p is the average passenger trip time. C_o is the total route time. d_i is the percentage of trips satisfied with number of transfers i , while d_{un} is the percentage of trips satisfied with 3 or more transfers. All values are averaged over ten random seeds, with one standard deviation following “±”, except for those in the STL row.

The results of the Laval experiments are shown in Table 5.2. The results for the initial networks produced by LC-100 are presented as well, to show how much improvement the NEA makes over its initial networks. Figure 5.4 highlights the trade-offs each method achieves between average trip time C_p and total route time C_o , and how they compare to the STL network.

We see that for each value of α , NEA’s network outperforms the STL network: it achieves 52% lower C_p at $\alpha = 1.0$, 24% lower C_o at $\alpha = 0.0$, and at $\alpha = 0.5$, 33% lower C_p and 17% lower C_o . At both $\alpha = 0.0$ and $\alpha = 0.5$, NEA strictly dominates the existing transit system, achieving both lower C_p and lower C_o .

Comparing NEA’s results to LC-100, we see that at $\alpha = 0.0$, NEA decreases C_o and

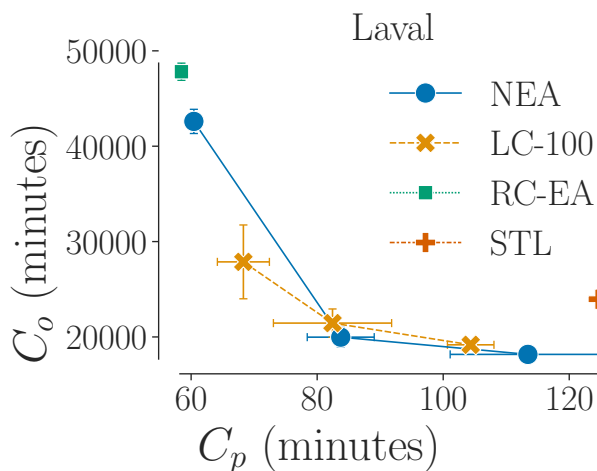


Figure 5.4: Average trip time C_p versus total route time C_o achieved by LC-100 and NEA at $\alpha = 0.0$ (bottom-right), 0.5 (middle), and 1.0 (top-left), as well as for RC-EA at $\alpha = 1.0$ and the STL network itself (independent of α). Except for STL, each point is a mean value over 10 random seeds, and bars show one standard deviation.

increases C_p relative to LC-100; and for $\alpha = 1.0$, the reverse is true. In both cases, NEA improves over the initial network on the objective being optimized, at the cost of the other, as we would expect. In the balanced case ($\alpha = 0.5$), we see that NEA decreases C_o by 7% while increasing C_p by 1.6% relative to LC-100. This matches what we observed in Figure 4.1, as discussed in section 4.1. NEA improves on the STL network by a considerable margin at all three α values, even though RC-EA outperforms NEA at $\alpha = 1.0$.

Looking at the transfer percentages d_0 , d_1 , d_2 , and d_{un} , we see that as α increases, the overall number of transfers shrinks, with d_0 , d_1 and d_2 growing and d_{un} shrinking. This is as expected, since fewer transfers implies reduced passenger travel times. By the same token, at $\alpha = 1.0$ RC-EA performs best on these metrics, as it does on average trip time

Terminal	Has metro station	# routes in: STL	NEA $\alpha = 0.0$	NEA $\alpha = 0.5$	NEA $\alpha = 1.0$
Le Carrefour	No	25	5.0	6.8	21.0
Montmorency	Yes	29	2.9	3.9	9.2
Cartier	Yes	38	1.2	1.1	4.1
Total		92	9.1	11.7	34.3

Table 5.3: Counts of the number of routes that visit each bus terminal in each network. For NEA, counts are the average over the ten networks computed at that α value.

C_p . At $\alpha = 1.0$, NEA outperforms the STL network by these metrics as well. At $\alpha = 0.5$, surprisingly, NEA's d_0 is lower than at the other α values, and lower than the STL network's d_0 by 0.8% of trips. But NEA's d_{un} is lower than STL's by 4.8% of trips, while d_1 and d_2 are both higher, meaning that NEA's networks let more passengers reach their destination in 2 or fewer transfers than the STL network. It is only at $\alpha = 0.0$ that STL's network requires fewer transfers overall than NEA's networks, and this is reasonable given that at $\alpha = 0.0$ the goal is strictly to minimize route length regardless of transfers.

5.3.1 Visual Inspection

Figure 5.5, Figure 5.6, and Figure 5.7 show one of the networks produced by NEA for each of $\alpha = 0.0$, $\alpha = 0.5$, and $\alpha = 1.0$. These networks were chosen among the ten networks for each α value based on their (C_p, C_o) being closest to the mean (C_p, C_o) of the ten networks, so that the network displayed would be representative of the algorithm's performance.

One thing we can observe in these figures is that the NEA $\alpha = 0.0$ and NEA $\alpha = 0.5$ networks have many fewer routes that connect directly to the three large bus terminals. To

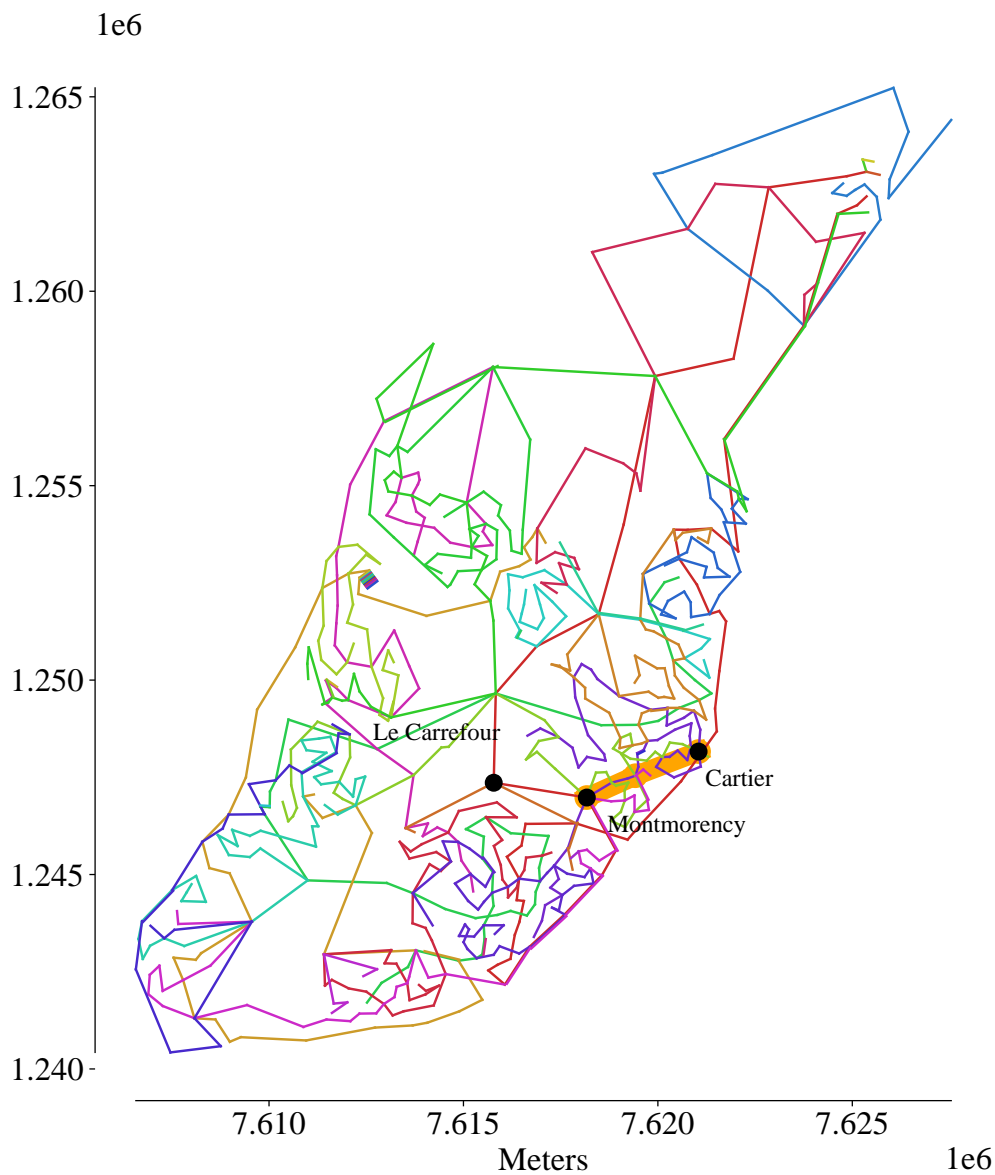


Figure 5.5: The routes of one of NEA's generated networks at $\alpha = 0.0$. The heavy orange line and its circles represent the orange line metro and its stops, while the black dots represent existing bus terminals.

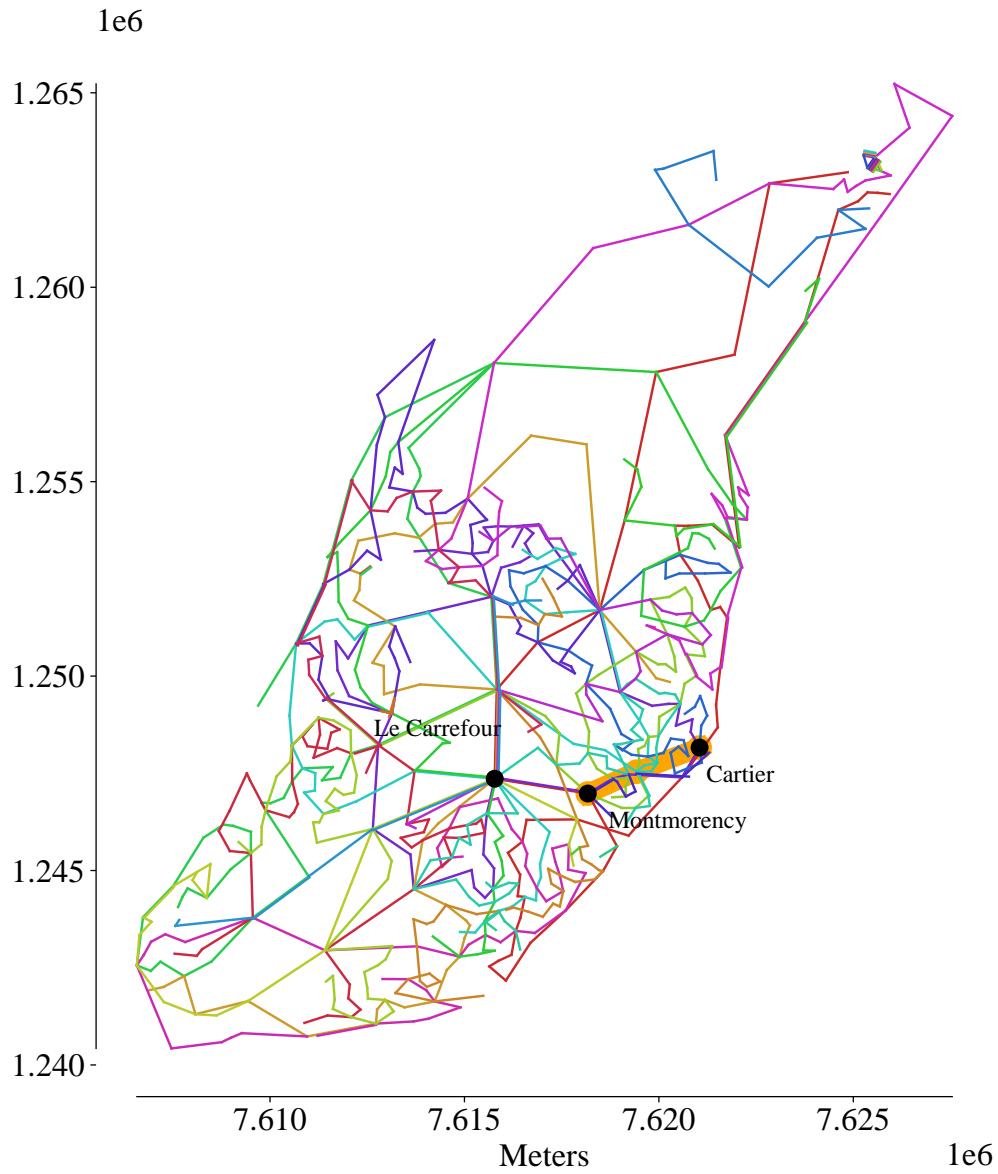


Figure 5.6: The routes of one of NEA's generated networks at $\alpha = 0.5$. The heavy orange line and its circles represent the orange line metro and its stops, while the black dots represent existing bus terminals.

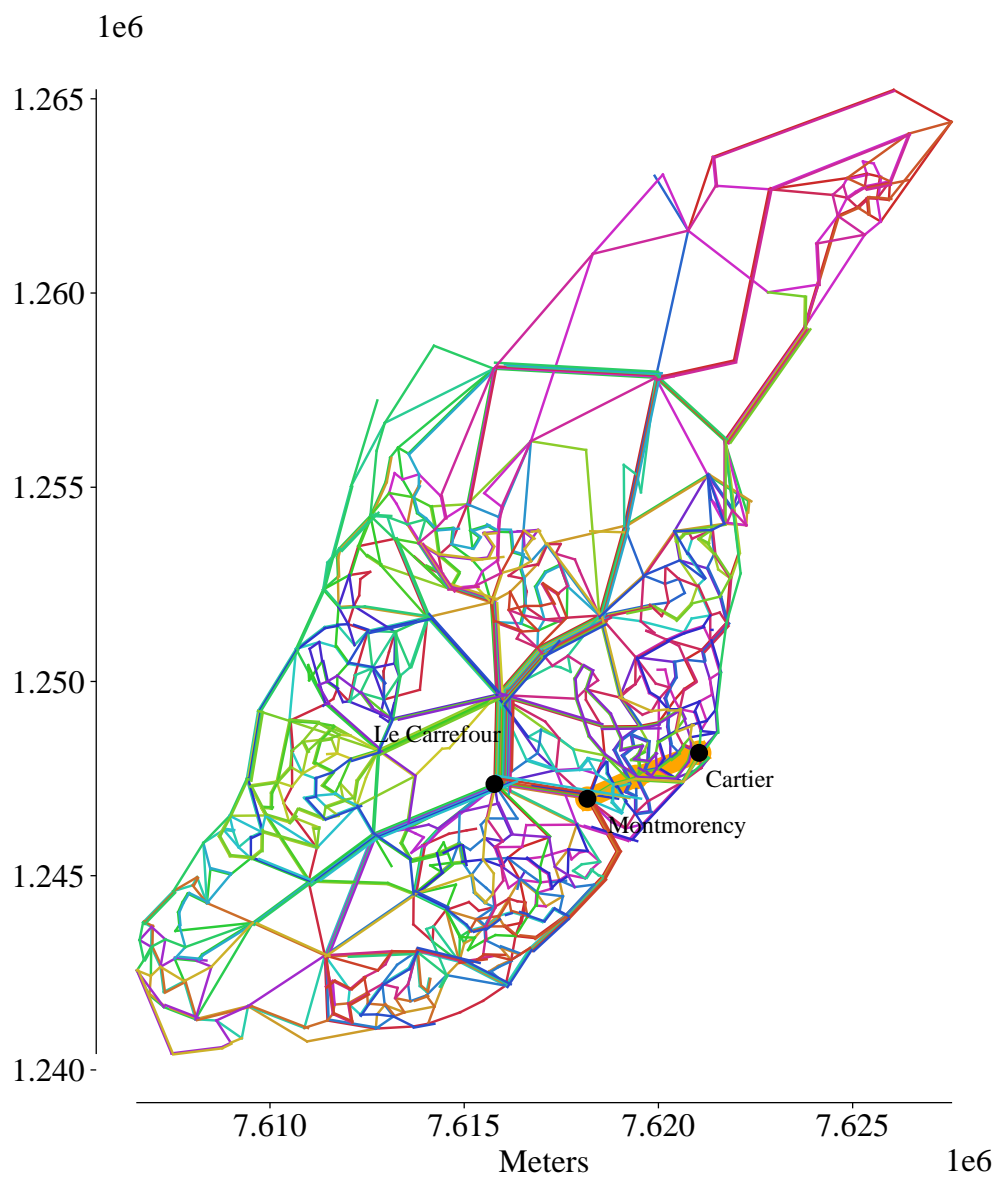


Figure 5.7: The routes of one of NEA's generated networks at $\alpha = 1.0$. The heavy orange line and its circles represent the orange line metro and its stops, while the black dots represent existing bus terminals.

confirm this, we found the number of routes that stop at each terminal node for STL and NEA each α value, averaged over the ten random seeds. We present these in Table 5.3. As the maps suggest, at $\alpha = 0.0$ and $\alpha = 0.5$, the number of routes that reach the terminals is very small compared to the STL network. At $\alpha = 1.0$, there are many more than at $\alpha = 0.0$ and $\alpha = 0.5$, but there are still less than half as many stops at bus terminals as in the STL network. This may suggest that a “hub and spoke” network where a few large terminals are served by many routes is less efficient than a more “distributed” network where routes provide direct trips between more diverse pairs of nodes. The fact that the number of transfers in NEA’s $\alpha = 0.0$ and $\alpha = 0.5$ networks is lower than in the STL network indicates that a distributed network need not require more transfers overall. The fact that the number of connections to these terminals increases with α is what we would expect: at low α , we want routes to be as short as possible. Connecting more nodes via transfers becomes more attractive as this allows routes to be shorter.

It is also interesting to note that the ordering of terminals by the number of routes that visit is reversed between the STL network and NEA’s networks: in STL, Cartier is the most-visited and Le Carrefour the least, while the reverse is true in the NEA networks on average. This means that NEA de-emphasizes direct connections to the orange line metro. We do note, however, that in each of the NEA maps, there is at least one direct line connecting Le Carrefour to Montmorency (the first orange line stop), with no bus stops in between - something that the STL network lacks. It appears that NEA uses Le Carrefour as a

major point of connection for Laval, perhaps due to its relative centrality compared with Montmorency and Cartier, and then uses a route from Le Carrefour to connect people to the orange line. This may partly explain why NEA's networks have higher numbers of one-transfer trips (d_1) and lower numbers of direct trips (d_0) compared with the STL network.

Inspecting Figure 5.5, we note that at $\alpha = 0.0$, there are twelve very short, two-node routes that appear along the same short edge. This is visible as a small multi-coloured block at about $7.6125e6$ on the x-axis and $1.2525e6$ on the y-axis. An inspection of the other $\alpha = 0.0$ networks from NEA reveals similar blocks in most of them, though not always in the same place. Figure 5.6 shows a similar cluster near the upper-right tip of Laval.

This is most likely the response of NEA to the need to plan a fixed number of routes ($S = 43$ for Laval), when it has already found some number $s < S$ of routes that adequately connect the city. The best way to minimize C_o is then to make the remaining $S - s$ routes as short as possible. Since we have set the minimum number of stops $m_{\min} = 2$, this is best done by placing all remaining routes along the shortest edge in the graph. Supporting this is as the likely cause is that in Figure 5.7, where $\alpha = 1.0$, we notice no obvious two-node routes, nor any "blocks" of these along a single edge - in this case, the lengths of routes doesn't matter, so it is never beneficial to make these very short routes.

We inspected the initial network, produced by LC-100, that we used for the NEA run that produced the network in Figure 5.5 (shown in Figure 5.8). We found that the same edge had six two-node routes along it in the LC-100 network. The other six were placed

there by NEA. We also performed a run of plain EA with the same initial network, α , and parameters that we used for NEA on Laval elsewhere; this run ended with ten two-node routes along this edge. So the neural mutator was not the main cause of these routes being added during the improvement method’s run. We thus conclude that this strategy of filling up the “quota” S of required routes with parallel very short routes was both learned by the neural policy π_θ and stumbled upon by the un-learned evolutionary algorithm, and both components contributed equally to this outcome.

In a real situation where we were only concerned with C_o , the appropriate thing to do when applying this plan to the real world would simply be to discard such routes, and treat this as a suggestion from the algorithm that S is set too high and ought to be $S - s$ instead.

The eastern end of the island of Laval (the upper-right quadrant of each map) is sparsely-populated compared to the rest of the city, as Figure 5.2 reveals by the relatively small number and large size of the census dissemination areas there. Directing our attention to this region of Figure 5.3, we see that the STL network has several routes that together wrap around the outside of this part of Laval, as well as others that pass through the more densely-populated areas near Laval’s eastern tip, and which are especially dense in a neighbourhood on the south side of that tip. Meanwhile, NEA’s routes are more uniformly distributed throughout this area. At no setting of α do these routes wrap fully around the outside of the island’s eastern tip; instead, NEA sends its routes through the middle of this region, connecting nodes at the periphery of the graph directly to nodes in the interior. The

routes in this region grow more dense as α increases, as we would expect, but remain more evenly distributed throughout this area than the tightly-clustered routes of the STL network. Apparently, this more uniform coverage is more efficient than the STL network's.

This seems to characterize the difference in other parts of Laval as well; the STL's routes are straight and run in parallel more often than NEA's, and NEA's routes are more meandering and tightly-wound upon themselves. At $\alpha = 1.0$, these paths together overlap cross often enough to create the appearance of a triangular mesh over large parts of the city. These meandering routes seem to stem from the learned policy: Figure 5.8 shows the initial networks used for NEA to get the networks shown in Figure 5.5, Figure 5.6, and Figure 5.7, and these networks exhibit the same qualitative "wiggleness" as the routes produced by NEA.

5.4 Practical takeaways

The likely aim of Laval's transit agency is to reduce costs while improving service quality (or at least not harming it too much). The "balanced" case, where $\alpha = 0.5$, is more relevant to that aim than the $\alpha = 0.0$ or $\alpha = 1.0$ cases. In this balanced case, we find that NEA proposes networks that reduce total route time by 17% versus the existing STL transit network. Some simple calculations can help understand the savings this represents.

The approximate cost of operating a Laval city bus is 200 Canadian dollars (CAD) per hour. Suppose that each route has the same headway (time between bus arrivals) H . Then, the number of buses N_r required by route r is the ceiling of the route's driving time τ_r

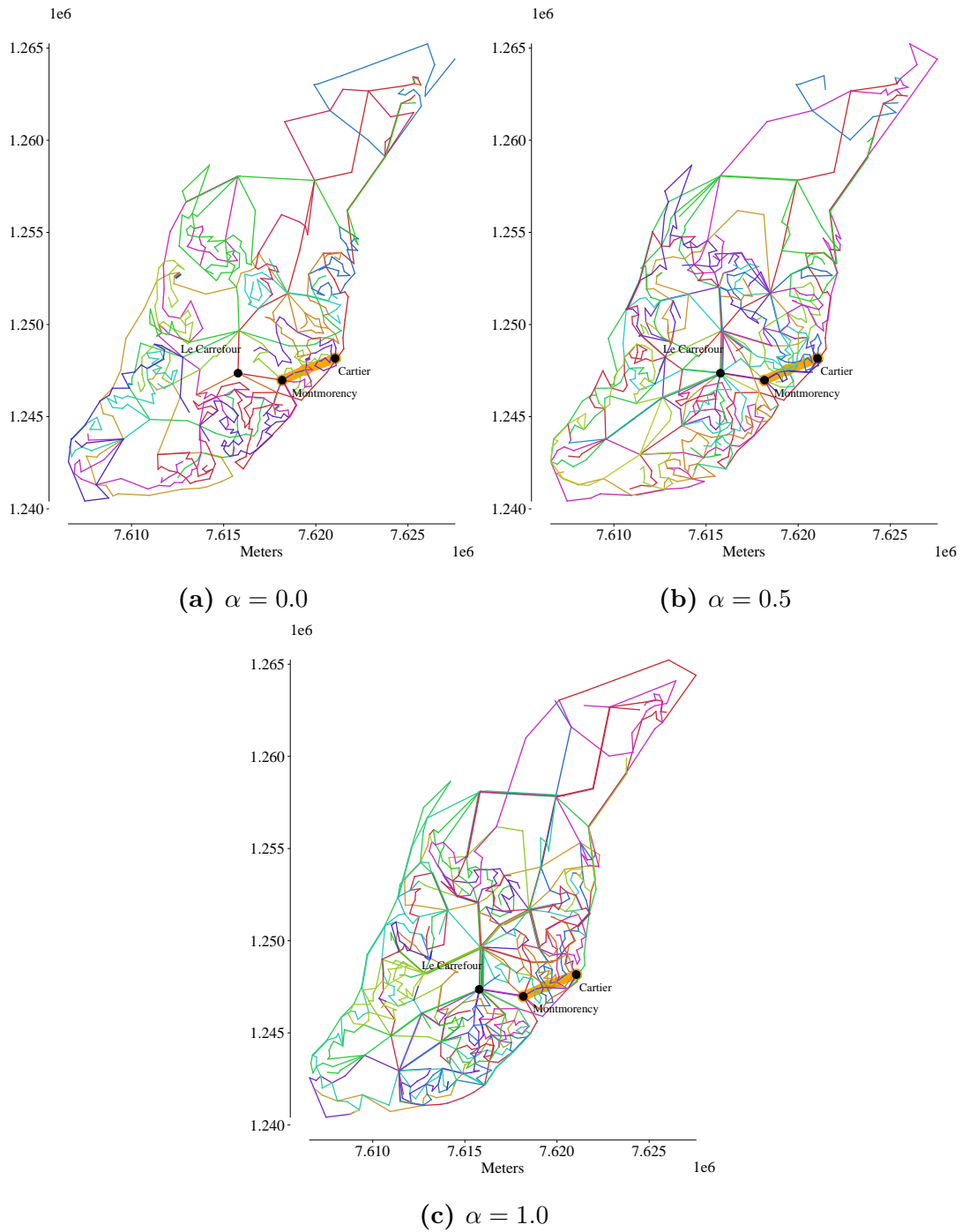


Figure 5.8: LC-100 initial networks for the three NEA runs shown in Figures 5.5, 5.6, and 5.7.

divided by the headway, $\lceil \frac{\tau_r}{H} \rceil$. The total number of buses $N_{\mathcal{R}}$ required for a transit network \mathcal{R} is then:

$$N_{\mathcal{R}} = \sum_{r \in \mathcal{R}} N_r \approx \frac{1}{H} \sum_{r \in \mathcal{R}} \tau_r = \frac{C_o}{H}$$

The total operating cost of the system is $N_{\mathcal{R}} * 200$ CAD. Assuming a headway of 15 minutes on all routes, that gives a per-hour operating cost of 319,387 CAD for the STL network, while the average operating cost of networks from NEA with $\alpha = 0.5$ is 266,373 CAD. So, under these simplifying assumptions, NEA could save the Laval transit agency on the order of 53,000 CAD per hour, or about 17% of operating costs. This is only a rough estimate: in practice, headways differ between routes, and there may be additional costs involved in altering the routes from the current system, such as from moving or building bus stops. But it shows that NEA, and neural heuristics more broadly, may offer practical savings to transit agencies.

In addition, NEA's balanced-case networks reduce the average passenger trip time by 33% versus the STL network, and reduce the number of transfers that passengers have to make, especially reducing the percentage of trips that require three or more transfers from 41.83% to 37.08%. Trips requiring three or more transfers are widely regarded as being so unattractive that riders will not make them (but note that these trips are still included in the calculation of C_p). So NEA's networks may even increase overall transit ridership. This not only makes the system more useful to the city's residents, but also increases the agency's revenue from fares.

We also note that at $\alpha = 1.0$, RC-EA achieves only 3% lower C_p than NEA. This supports our conclusions in subsection 4.2.3 and section 4.3 that the learned heuristics of the neural net policies π_θ are the main driver of NEA’s performance across α , rather than simply the heuristic of assembling routes from shortest paths.

In these experiments, the nodes of the graph represent Census Dissemination Area instead of existing bus stops. In order to be used in reality, the proposed routes would need to be fitted to the existing locations of bus stops in the CDAs, likely making multiple stops within each CDAs. To minimize the cost of the network redesign, it would be necessary to keep stops at most or all stop locations that have shelters, as constructing or moving these may cost tens of thousands of dollars, while stops with only a signpost at their locations can be moved at the cost of only a few thousand dollars. An algorithm for translating our census-level routes to real-stop-level routes, in a way that minimizes cost, is an important next step if the methods developed here are to be applied in real cities. We leave this for future work.

5.5 Summary

We have shown that our learned graph net policies are useful for transit planning in large, realistic cities. The learned policies can construct transit networks that outperform a model of the city’s existing transit, in terms of both estimated operating costs and passenger travel times. In combination with an evolutionary algorithm as described in Chapter 4, the resulting transit network can be further improved - in the case of the city of Laval, the neural-

evolutionary algorithm reduces operating costs by 17% and passenger travel times by 33% versus the existing transit network.

Our learned policies are trained on small synthetic cities of only twenty nodes, but our results show that they generalize well even to Laval’s graph of more than six hundred nodes. This shows that there exist good heuristics for the TNDP which are simple enough to be evident in very small graphs but which generalize to much larger graphs. It is likely that there are more heuristics which could be learned only from experience on larger graphs, and that policies trained on a range of graph sizes could outperform those considered here.

These results also demonstrate that our method is capable of incorporating fixed, pre-existing routes in its planning, in this case the Orange Line subway in Laval. This is an important capability for solving real instances of the TNDP, as rail and underground transit routes are common in real cities and must be integrated with more flexible forms of transit like buses.

A number of challenges must still be overcome to make these methods for the TNDP directly applicable to the design of transit networks for real cities, such as vehicle scheduling and accounting for time-varying demand. But finding good solutions to the TNDP is the first major challenge, and the results of this chapter show that our learning-based methods can capably address it.

Chapter 6

Conclusion

In this thesis, we explored various ways of using reinforcement learning (RL) with Graph Attention Nets to solve the Transit Network Design Problem. In Chapter 2, we develop a neural policy architecture and an reinforcement learning (RL) algorithm to train these policies to construct transit networks. In Chapter 3 we showed that such a policy can generate the initial transit networks for metaheuristic improvement methods to then optimize, and that this improves the quality of the final networks found by those methods, in comparison with the heuristic algorithms typically used to find initial solutions. And in Chapter 4, we integrated the policy more tightly with an improvement method - specifically, an evolutionary algorithm - by using it to propose neighbourhood moves at each step of improvement, finding that this improved the quality of networks found versus improvement methods that used unlearned heuristics to select neighbourhood moves. We refer to this hybrid method as a

Neural-Evolutionary Algorithm (NEA). Finally, in Chapter 5, we applied our combination of neural policy and evolutionary algorithm to a large real-world problem instance, and showed that it was able to improve on the existing transit on multiple metrics.

6.1 Future Work

In conducting this research, many more directions presented themselves to us than we were able to pursue. We present some of these here, in the hopes that we will inspire some of our readers to pursue them in our stead.

6.1.1 Learned Heuristics in Other Metaheuristic Algorithms

The evolutionary algorithm in which we use our learned heuristic was chosen for its speed and simplicity, which aided in implementation and rapid experimentation. But state-of-the-art algorithms, like NSGA-II, which are more computationally costly but more powerful, may allow still better performance to be gained from learned heuristics. Future work should attempt to use learned policies as low-level heuristics in a wider variety of metaheuristic algorithms.

It would also be interesting to use multiple different learned policies, perhaps trained under different conditions such as over certain limited ranges of α , on different values of n or S , or on training data generated by different processes, as different low-level heuristics within the same metaheuristic algorithm. This would coordinate a diverse set of policies

with potentially diverse heuristics for the TNDP to solve a given problem instance, in a way similar to ensemble methods, which are common in applications of machine learning.

6.1.2 Training Policies Differently, and Training Different Policies

Our method for learning policies has several limitations. One is that the construction MDP on which our neural policies are trained differs from the evolutionary algorithm - an improvement process - in which they is deployed. Another is that it learns just one type of policy, that for constructing a route from shortest paths. Natural next steps would be to learn a policies for a more diverse space of actions, perhaps including route-lengthening and -shortening operators, and to train our neural net policies directly in the context of an improvement process, which may yield learned heuristics that are better-suited to that process.

Another promising idea is to learn hyper-heuristics for a metaheuristic algorithm. A typical hyper-heuristic, as used by Ahmed et al. [2019] and Hüsselmann et al. [2023], dynamically adapts the probability of using each low-level heuristic based on its performance over the search so far. A neural net policy could be trained to act as a hyper-heuristic to select among low-level heuristics, given details about the scenario and previous steps taken during the algorithm. This could complement the neural policies we have here used as low-level heuristics.

6.1.3 Interactions with Mobility-On-Demand

As discussed in subsection 1.1.1, mobility-on-demand services and self-driving automobiles on their own are more likely to worsen urban mobility than to improve it. But they may still be beneficial if used as one component of a mass-transit-centric system for urban transport. A fully-autonomous urban transit system will need to make use of both point-to-point autonomous ride-sharing and fixed autonomous mass transit routes to be as useful and efficient as possible [Alonso-González et al., 2018, Leich and Bischoff, 2019]. There is an existing literature on the planning of such Autonomous Mobility on Demand (AMoD) systems, in which the main problem is planning where empty autonomous taxis should be sent to anticipate demand as it arises over the course of the day [Pavone et al., 2012, Spieser et al., 2014, Bischoff et al., 2017, Vakayil et al., 2017, Ruch et al., 2018, Enders et al., 2023].

The methods developed in this thesis could serve as part of an algorithm for planning such a combined autonomous transit system. Future work could explore how our NEA could be combined with techniques from the literature on autonomous mobility-on-demand planning to minimize travel times, operating costs, and congestion.

6.1.4 Going From Simulation to Reality

As discussed in section 5.3, in order to apply in a real-world city like Laval, many additional problems need to be solved. The routes our NEA proposes are at the level of Census

Dissemination Areas, of which there are less than seven hundred, while the actual number of transit stops in Laval is more than two thousand. To make use of our NEA in reality, one would either have to derive real-stop-level networks from the CDA-level networks it presently produces, or attempt to apply our NEA directly at the level of real transit stops. Either of these would be an interesting challenge: the former would require a sensible algorithm be developed, while the latter would require us to extend our NEA to the asymmetric TNDP, since one-way streets are part of the real street network of Laval.

Another problem that would have to be addressed is developing a schedule for the routes on the network. When applied to a given transit network, the Frequency-Setting Problem (FSP) is relatively simple, and many techniques for it have been proposed [Guihaire and Hao, 2008, Ceder, 2016]. But most of these rely on the chunking of time into fixed increments, usually of an hour, with demand assumed to be static within each chunk. Treating demand as a continuous function of time could allow for better results, as could solving the Frequency-Setting Problem (FSP) in tandem with the TNDP. Darwish et al. [2020] and Yoo et al. [2023] both apply RL to solve the TNDP and FSP jointly, though only for the very small Mandl city. It would be worthwhile to explore ways that our NEA could be extended to do the same.

6.2 Concluding Statement

Public transit is essential service to the health of modern cities, and one that has been too much neglected. But there is a tension at its heart. As one researcher put it to me, public transit must take you from where you aren't to where you don't want to go. To mitigate this drawback enough that city-dwellers will still find transit appealing, sound design of transit networks is needed.

The motivation for this thesis came from seeing that the methods of machine learning with deep neural nets, which in the past decade have underlain dramatic progress in many fields, had been neglected in the study of this complex design problem. The work we present here clearly shows the potential of these methods to improve the transit networks that tie together the world's cities. We hope that the community of researchers studying the Transit Network Design Problem will be inspired by it to further develop data-driven learning methods in this area, and that some day, practitioners may put them to use in reality, to tie the cities of the future more closely together.

Bibliography

Rusul Abduljabbar, Hussein Dia, Sohani Liyanage, and Saeed Asadi Bagloee. Applications of artificial intelligence in transport: An overview. *Sustainability*, 11(1):189, 2019.

Agence métropolitaine de transport. Enquête origine-destination 2013, 2013. Montreal, QC.

Leena Ahmed, Christine Mumford, and Ahmed Kheiri. Solving urban transit route design problem using selection hyper-heuristics. *European Journal of Operational Research*, 274(2):545–559, 2019.

Guanqun Ai, Xingquan Zuo, Gang Chen, and Binglin Wu. Deep reinforcement learning based dynamic optimization of bus timetable. *Applied Soft Computing*, 131:109752, 2022.

Takuya Akiba, Shotaro Sano, Toshihiko Yanase, Takeru Ohta, and Masanori Koyama. Optuna: A next-generation hyperparameter optimization framework. In *Proceedings of the 25rd ACM SIGKDD International Conference on Knowledge Discovery and Data Mining*, 2019.

María J Alonso-González, Theo Liu, Oded Cats, Niels Van Oort, and Serge Hoogendoorn.

The potential of demand-responsive transport as a complement to public transport: An assessment framework and an empirical evaluation. *Transportation Research Record*, 2672 (8):879–889, 2018.

David Applegate, Robert E. Bixby, Vašek Chvátal, and William J. Cook. Concorde tsp solver, 2001. URL <https://www.math.uwaterloo.ca/tsp/concorde/index.html>.

Peter W Battaglia, Jessica B Hamrick, Victor Bapst, Alvaro Sanchez-Gonzalez, Vinicius Zambaldi, Mateusz Malinowski, Andrea Tacchetti, David Raposo, Adam Santoro, Ryan Faulkner, et al. Relational inductive biases, deep learning, and graph networks. *arXiv preprint arXiv:1806.01261*, 2018.

Ryan Beene. A Florida monorail makes way for the robot bus of tomorrow. *Bloomberg*, 2018.

Richard Bellman. Dynamic programming and stochastic control processes. *Information and control*, 1(3):228–239, 1958.

Yoshua Bengio, Andrea Lodi, and Antoine Prouvost. Machine learning for combinatorial optimization: a methodological tour d’horizon. *European Journal of Operational Research*, 290(2):405–421, 2021.

James Bergstra, Daniel Yamins, and David Cox. Making a science of model search:

- Hyperparameter optimization in hundreds of dimensions for vision architectures. In *International conference on machine learning*, pages 115–123. PMLR, 2013.
- Joschka Bischoff, Ihab Kaddoura, Michal Maciejewski, and Kai Nagel. Re-defining the role of public transport in a world of shared autonomous vehicles. In *Symposium of the European Association for Research in Transportation (hEART)*, 2017.
- Shaked Brody, Uri Alon, and Eran Yahav. How attentive are graph attention networks?, 2021. URL <https://arxiv.org/abs/2105.14491>.
- Joan Bruna, Wojciech Zaremba, Arthur Szlam, and Yann LeCun. Spectral networks and locally connected networks on graphs. *arXiv preprint arXiv:1312.6203*, 2013.
- Robert A. Caro. *The Power Broker*. Random House, New York, 1974.
- Avishai Ceder. *Public Transit Planning and Operation: Modeling, Practice and Behaviour*. CRC Press, 2016.
- Sandip Chakrabarti. How can public transit get people out of their cars? An analysis of transit mode choice for commute trips in los angeles. *Transport Policy*, 54(October 2016):80–89, 2017. ISSN 1879310X. doi: 10.1016/j.tranpol.2016.11.005. URL <http://dx.doi.org/10.1016/j.tranpol.2016.11.005>.
- Xinyun Chen and Yuandong Tian. Learning to perform local rewriting for combinatorial optimization. *Advances in Neural Information Processing Systems*, 32, 2019.

- Steven I-Jy Chien, Yuqing Ding, and Chienhung Wei. Dynamic bus arrival time prediction with artificial neural networks. *Journal of transportation engineering*, 128(5):429–438, 2002.
- Jinho Choo, Yeong-Dae Kwon, Jihoon Kim, Jeongwoo Jae, André Hottung, Kevin Tierney, and Youngjune Gwon. Simulation-guided beam search for neural combinatorial optimization. *Advances in Neural Information Processing Systems*, 35:8760–8772, 2022.
- N Christophides. Worst-case analysis of a new heuristic for the traveling salesman problem. In *Proc. Symposium on New Directions and Recent Results in Algorithms and Complexity*, 1976.
- Paulo da Costa, Jason Rhuggenaath, Yingqian Zhang, and Alp Akcay. Learning 2-opt heuristics for the traveling salesman problem via deep reinforcement learning. In *Asian conference on machine learning*, pages 465–480. PMLR, 2020.
- Hanjun Dai, Elias B Khalil, Yuyu Zhang, Bistra Dilkina, and Le Song. Learning combinatorial optimization algorithms over graphs. *arXiv preprint arXiv:1704.01665*, 2017.
- Ahmed Darwish, Momen Khalil, and Karim Badawi. Optimising public bus transit networks using deep reinforcement learning. In *2020 IEEE 23rd International Conference on Intelligent Transportation Systems (ITSC)*, pages 1–7. IEEE, 2020.

- Katherine DeClerq. Drivers in toronto lose 142 hours on the roads during rush hour, report finds. <https://toronto.ctvnews.ca/drivers-in-toronto-lose-142-hours-on-the-roads-during-rush-hour-report-finds-1.4790478>, 1 2020. Accessed: 2024-09-27.
- Michaël Defferrard, Xavier Bresson, and Pierre Vandergheynst. Convolutional neural networks on graphs with fast localized spectral filtering. *CoRR*, abs/1606.09375, 2016. URL <http://arxiv.org/abs/1606.09375>.
- Javier Durán-Micco and Pieter Vansteenwegen. A survey on the transit network design and frequency setting problem. *Public Transport*, 14(1):155–190, 2022.
- Gilles Duranton and Matthew A Turner. The fundamental law of road congestion: Evidence from us cities. *American Economic Review*, 101(6):2616–52, 2011.
- David K Duvenaud, Dougal Maclaurin, Jorge Iparraguirre, Rafael Bombarell, Timothy Hirzel, Alán Aspuru-Guzik, and Ryan P Adams. Convolutional networks on graphs for learning molecular fingerprints. *Advances in neural information processing systems*, 28, 2015.
- Tobias Enders, James Harrison, Marco Pavone, and Maximilian Schiffer. Hybrid multi-agent deep reinforcement learning for autonomous mobility on demand systems. In *Learning for Dynamics and Control Conference*, pages 1284–1296. PMLR, 2023.

Lang Fan and Christine L Mumford. A metaheuristic approach to the urban transit routing problem. *Journal of Heuristics*, 16:353–372, 2010.

Steven Fortune. Voronoi diagrams and delaunay triangulations. *Computing in Euclidean geometry*, pages 225–265, 1995.

Agence France-Presse. Driverless electric bus hits the road in Spanish city of Málaga. <https://www.theguardian.com/world/2021/feb/25/driverless-electric-bus-hits-the-road-in-spanish-city-of-malaga>, 2 2021. Accessed: 2021-03-09.

B Alex Frank. How self-driving cars will reduce traffic congestion. <https://medium.com/swlh/how-self-driving-cars-will-reduce-traffic-congestion-8bad5594c5d0>, 1 2020. Accessed: 2021-03-26.

Lance Freeman. The effects of sprawl on neighborhood social ties: An explanatory analysis. *Journal of the American Planning Association*, 67(1):69–77, 2001.

Zhang-Hua Fu, Kai-Bin Qiu, and Hongyuan Zha. Generalize a small pre-trained model to arbitrarily large tsp instances. In *Proceedings of the AAAI conference on artificial intelligence*, volume 35, pages 7474–7482, 2021.

Kunihiko Fukushima. Visual feature extraction by a multilayered network of analog threshold elements. *IEEE Transactions on Systems Science and Cybernetics*, 5(4):322–333, 1969.

- Justin Gilmer, Samuel S. Schoenholz, Patrick F. Riley, Oriol Vinyals, and George E. Dahl. Neural message passing for quantum chemistry. In Doina Precup and Yee Whye Teh, editors, *Proceedings of the 34th International Conference on Machine Learning*, volume 70 of *Proceedings of Machine Learning Research*, pages 1263–1272. PMLR, 06–11 Aug 2017. URL <https://proceedings.mlr.press/v70/gilmer17a.html>.
- Ian Goodfellow, Yoshua Bengio, and Aaron Courville. *Deep Learning*. MIT Press, 2016. <http://www.deeplearningbook.org>.
- Google. Laval, quebec. <https://www.google.com/maps/place/Laval,+QC/@45.6100977,-73.8063121,11.61z>, 2024. Online; accessed 12 April 2024.
- J.F. Guan, Hai Yang, and S.C. Wirasinghe. Simultaneous optimization of transit line configuration and passenger line assignment. *Transportation Research Part B: Methodological*, 40:885–902, 12 2006. doi: 10.1016/j.trb.2005.12.003.
- Valérie Guihaire and Jin-Kao Hao. Transit network design and scheduling: A global review. *Transportation Research Part A: Policy and Practice*, 42(10):1251–1273, 2008.
- Mustapha Harb, Yu Xiao, Giovanni Circella, Patricia L Mokhtarian, and Joan L Walker. Projecting travelers into a world of self-driving vehicles: estimating travel behavior implications via a naturalistic experiment. *Transportation*, 45(6):1671–1685, 2018.

Dan Hendrycks and Kevin Gimpel. Gaussian error linear units (gelus). *arXiv preprint arXiv:1606.08415*, 2016.

Andrew Holliday and Gregory Dudek. Augmenting transit network design algorithms with deep learning. In *2023 26th IEEE International Conference on Intelligent Transportation Systems (ITSC)*. IEEE, 2023.

Andrew Holliday and Gregory Dudek. A neural-evolutionary algorithm for autonomous transit network design. In *presented at 2024 IEEE International Conference on Robotics and Automation (ICRA)*. IEEE, 2024.

André Hottung and Kevin Tierney. Neural large neighborhood search for the capacitated vehicle routing problem. *arXiv preprint arXiv:1911.09539*, 2019.

Günther Hüsselmann, Jan Harm van Vuuren, and Simen Johann Andersen. An improved solution methodology for the urban transit routing problem. *Computers & Operations Research*, page 106481, 2023.

Kazi Ashik Islam, Ibraheem Muhammad Moosa, Jaiaid Mobin, Muhammad Ali Nayeem, and M Sohel Rahman. A heuristic aided stochastic beam search algorithm for solving the transit network design problem. *Swarm and Evolutionary Computation*, 46:154–170, 2019.

Ranhee Jeong and R Rilett. Bus arrival time prediction using artificial neural network

model. In *Proceedings. The 7th international IEEE conference on intelligent transportation systems (IEEE Cat. No. 04TH8749)*, pages 988–993. IEEE, 2004.

Zhibin Jiang, Wei Fan, Wei Liu, Bingqin Zhu, and Jinjing Gu. Reinforcement learning approach for coordinated passenger inflow control of urban rail transit in peak hours. *Transportation Research Part C: Emerging Technologies*, 88:1–16, 2018. ISSN 0968-090X. doi: <https://doi.org/10.1016/j.trc.2018.01.008>. URL <https://www.sciencedirect.com/science/article/pii/S0968090X18300111>.

Matthew P John. *Metaheuristics for designing efficient routes & schedules for urban transportation networks*. PhD thesis, Cardiff University, 2016.

Matthew P. John, Christine L. Mumford, and Rhyd Lewis. An improved multi-objective algorithm for the urban transit routing problem. In Christian Blum and Gabriela Ochoa, editors, *Evolutionary Computation in Combinatorial Optimisation*, pages 49–60, Berlin, Heidelberg, 2014. Springer Berlin Heidelberg. ISBN 978-3-662-44320-0.

Armita Kar, Andre L Carrel, Harvey J Miller, and Huyen TK Le. Public transit cuts during covid-19 compound social vulnerability in 22 us cities. *Transportation Research Part D: Transport and Environment*, 110:103435, 2022.

Henry A Kautz, Bart Selman, et al. Planning as satisfiability. In *ECAI*, volume 92, pages 359–363. Citeseer, 1992.

- Konstantinos Kepaptsoglou and Matthew Karlaftis. Transit route network design problem: Review. *Journal of Transportation Engineering*, 135(8):491–505, 2009. doi: 10.1061/(ASCE)0733-947X(2009)135:8(491).
- Minsu Kim, Jinkyoo Park, et al. Learning collaborative policies to solve np-hard routing problems. *Advances in Neural Information Processing Systems*, 34:10418–10430, 2021.
- Diederik P. Kingma and Jimmy Ba. Adam: A method for stochastic optimization. In *ICLR*, 2015.
- Thomas N Kipf and Max Welling. Semi-supervised classification with graph convolutional networks. *arXiv preprint arXiv:1609.02907*, 2016.
- W. Kool, H. V. Hoof, and M. Welling. Attention, learn to solve routing problems! In *ICLR*, 2019.
- Fatih Kılıç and Mustafa Gök. A demand based route generation algorithm for public transit network design. *Computers & Operations Research*, 51:21–29, 2014. ISSN 0305-0548. doi: <https://doi.org/10.1016/j.cor.2014.05.001>. URL <https://www.sciencedirect.com/science/article/pii/S0305054814001300>.
- Le Corbusier. *The City of Tomorrow and Its Planning*. Dover Publications, 1929. English translation published 1987.

- Gregor Leich and Joschka Bischoff. Should autonomous shared taxis replace buses? a simulation study. *Transportation Research Procedia*, 41:450–460, 2019.
- Kevin M Leyden. Social capital and the built environment: the importance of walkable neighborhoods. *American journal of public health*, 93(9):1546–1551, 2003.
- Can Li, Lei Bai, Wei Liu, Lina Yao, and S Travis Waller. Graph neural network for robust public transit demand prediction. *IEEE Transactions on Intelligent Transportation Systems*, 2020.
- Haifeng Lin and Chengpei Tang. Analysis and optimization of urban public transport lines based on multiobjective adaptive particle swarm optimization. *IEEE Transactions on Intelligent Transportation Systems*, 23(9):16786–16798, 2022. doi: 10.1109/TITS.2021.3086808.
- Todd Litman. *Evaluating public transportation health benefits*. Victoria Transport Policy Institute, 2012.
- Luyu Liu, Harvey J Miller, and Jonathan Scheff. The impacts of covid-19 pandemic on public transit demand in the united states. *Plos one*, 15(11):e0242476, 2020.
- Yining Ma, Jingwen Li, Zhiguang Cao, Wen Song, Le Zhang, Zhenghua Chen, and Jing Tang. Learning to iteratively solve routing problems with dual-aspect collaborative transformer. *Advances in Neural Information Processing Systems*, 34:11096–11107, 2021.

Jenifer Joy Madden. Self-driving vehicles will improve our cities, if they don't ruin them. <https://ggwash.org/view/63147/self-driving-vehicles-will-improve-our-cities-if-they-dont-ruin-them>, 5 2017.

Christoph E Mandl. Evaluation and optimization of urban public transportation networks. *European Journal of Operational Research*, 5(6):396–404, 1980.

Azalia Mirhoseini, Anna Goldie, Mustafa Yazgan, Joe Wenjie Jiang, Ebrahim Songhori, Shen Wang, Young-Joon Lee, Eric Johnson, Omkar Pathak, Azade Nazi, et al. A graph placement methodology for fast chip design. *Nature*, 594(7862):207–212, 2021.

Charles Montgomery. *Happy City*. Doubleday Canada, New York, 2013.

Christine L Mumford. Simple population replacement strategies for a steady-state multi-objective evolutionary algorithm. In *Genetic and Evolutionary Computation Conference*, pages 1389–1400. Springer, 2004.

Christine L Mumford. Supplementary material for: New heuristic and evolutionary operators for the multi-objective urban transit routing problem, cec 2013. <https://users.cs.cf.ac.uk/C.L.Mumford/Research%20Topics/UTRP/CEC2013Supp.zip>, 2013a. Accessed: 2023-03-24.

Christine L Mumford. New heuristic and evolutionary operators for the multi-objective urban

- transit routing problem. In *2013 IEEE congress on evolutionary computation*, pages 939–946. IEEE, 2013b.
- T Nathan Mundhenk, Mikel Landajuena, Ruben Glatt, Claudio P Santiago, Daniel M Faissol, and Brenden K Petersen. Symbolic regression via neural-guided genetic programming population seeding. *arXiv preprint arXiv:2111.00053*, 2021.
- Miloš Nikolić and Dušan Teodorović. Transit network design by bee colony optimization. *Expert Systems with Applications*, 40(15):5945–5955, 2013.
- Simon Oh, Ravi Seshadri, Diem-Trinh Le, P Christopher Zegras, and Moshe E Ben-Akiva. Evaluating automated demand responsive transit using microsimulation. *IEEE Access*, 8: 82551–82561, 2020.
- Marco Pavone, Stephen L Smith, Emilio Frazzoli, and Daniela Rus. Robotic load balancing for mobility-on-demand systems. *The International Journal of Robotics Research*, 31(7): 839–854, 2012.
- Jason Plautz. Autonomous shuttles launch in Detroit. <https://www.smartcitiesdive.com/news/autonomous-shuttles-launch-in-detroit/526999/>, 7 2018. Accessed: 2019-11-27.
- Jeppe Rich, Ravi Seshadri, Ali Jamal Jomeh, and Sofus Rasmus Clausen. Fixed routing or

- demand-responsive? agent-based modelling of autonomous first and last mile services in light-rail systems. *Transportation Research Part A: Policy and Practice*, 173:103676, 2023.
- Jean-Paul Rodrigue. Parallel modelling and neural networks: An overview for transportation/land use systems. *Transportation Research Part C: Emerging Technologies*, 5(5):259–271, 1997. ISSN 0968-090X. doi: [https://doi.org/10.1016/S0968-090X\(97\)00014-4](https://doi.org/10.1016/S0968-090X(97)00014-4). URL <https://www.sciencedirect.com/science/article/pii/S0968090X97000144>.
- Tim Roughgarden and Éva Tardos. How bad is selfish routing? *Journal of the ACM (JACM)*, 49(2):236–259, 2002.
- Claudio Ruch, Sebastian Hörl, and Emilio Frazzoli. Amodeus, a simulation-based testbed for autonomous mobility-on-demand systems. In *2018 21st International Conference on Intelligent Transportation Systems (ITSC)*, pages 3639–3644. IEEE, 2018.
- Erika Sandow. *On the road: Social aspects of commuting long distances to work*. PhD thesis, Kulturgeografiska institutionen, Umeå universitet, 2011.
- Schaller Consulting. The new automobility: Lyft, Uber and the future of American cities. *Journal of Urban Economics*, 2018. URL www.schallerconsult.com/rideservices/automobility.pdf
<http://www.schallerconsult.com/rideservices/automobility.htm>.

- John Schulman, Filip Wolski, Prafulla Dhariwal, Alec Radford, and Oleg Klimov. Proximal policy optimization algorithms. *arXiv preprint arXiv:1707.06347*, 2017.
- Aditi Shrikant. The best and worst cities in america for public transportation, according to an urban planner. <https://www.vox.com/the-goods/2018/12/7/18131132/public-transportation-bus-subway-america-us>, 2018. Accessed: 2024-09-25.
- Société de Transport de Laval. GTFS data for the Société de Transport de Laval bus network. URL <https://transitfeeds.com/p/societe-de-transport-de-laval/38/1383528159>. Retrieved 2020.
- Kenneth Sörensen. Metaheuristics—the metaphor exposed. *International Transactions in Operational Research*, 22(1):3–18, 2015.
- Kenneth Sörensen, Marc Sevaux, and Fred Glover. A history of metaheuristics. In *Handbook of heuristics*, pages 791–808. Springer, 2018.
- Kevin Spieser, Kyle Treleaven, Rick Zhang, Emilio Frazzoli, Daniel Morton, and Marco Pavone. Toward a systematic approach to the design and evaluation of automated mobility-on-demand systems: A case study in singapore. In *Road vehicle automation*, pages 229–245. Springer, 2014.

- Statistics Canada. Census dissemination area boundary files, 2021. URL <https://www150.statcan.gc.ca/n1/en/catalogue/92-169-X>. Accessed: 2023-07-01.
- Statistics Canada. Census profile, 2021 census of population, 2023. URL <https://www12.statcan.gc.ca/census-recensement/2021/dp-pd/prof/details/page.cfm>. Accessed: 2023-10-25.
- C.M. Stieglitz. Robert Moses with Battery Bridge model, 1939. URL <http://hdl.loc.gov/loc.pnp/cph.3c36079>.
- Richard S Sutton and Andrew G Barto. *Reinforcement learning: An introduction*. MIT press, 2018.
- Quinlan Sykora, Mengye Ren, and Raquel Urtasun. Multi-agent routing value iteration network. In *International Conference on Machine Learning*, pages 9300–9310. PMLR, 2020.
- Akhil Vakayil, Wolfgang Gruel, and Samitha Samaranayake. Integrating shared-vehicle mobility-on-demand systems with public transit. Technical report, 2017.
- Christine L Valenzuela. A simple evolutionary algorithm for multi-objective optimization (seamo). In *Proceedings of the 2002 Congress on Evolutionary Computation. CEC'02 (Cat. No. 02TH8600)*, volume 1, pages 717–722. IEEE, 2002.

- Joop van Bilsen. Le Corbusier, 1964. URL <http://proxy.handle.net/10648/aa7b03b0-d0b4-102d-bcf8-003048976d84>.
- Rob van Nes. Multiuser-class urban transit network design. *Transportation Research Record*, 1835(1):25–33, 2003. doi: 10.3141/1835-04. URL <https://doi.org/10.3141/1835-04>.
- Ashish Vaswani, Noam Shazeer, Niki Parmar, Jakob Uszkoreit, Llion Jones, Aidan N Gomez, Lukasz Kaiser, and Illia Polosukhin. Attention is all you need. In *Advances in neural information processing systems*, pages 5998–6008, 2017.
- Petar Veličković, Guillem Cucurull, Arantxa Casanova, Adriana Romero, Pietro Liò, and Yoshua Bengio. Graph attention networks, 2018. URL <https://arxiv.org/abs/1710.10903>.
- Oriol Vinyals, Meire Fortunato, and Navdeep Jaitly. Pointer networks. *arXiv preprint arXiv:1506.03134*, 2015.
- Tao Wang, Zhipeng Zhu, Jing Zhang, Junfang Tian, and Wenyi Zhang. A large-scale traffic signal control algorithm based on multi-layer graph deep reinforcement learning. *Transportation Research Part C: Emerging Technologies*, 162:104582, 2024. ISSN 0968-090X. doi: <https://doi.org/10.1016/j.trc.2024.104582>. URL <https://www.sciencedirect.com/science/article/pii/S0968090X24001037>.

- Ronald J Williams. Simple statistical gradient-following algorithms for connectionist reinforcement learning. *Machine learning*, 8(3):229–256, 1992.
- Yaoxin Wu, Wen Song, Zhiguang Cao, Jie Zhang, and Andrew Lim. Learning improvement heuristics for solving routing problems. *IEEE transactions on neural networks and learning systems*, 33(9):5057–5069, 2021.
- Yihua Xiong and Jerry B Schneider. Transportation network design using a cumulative genetic algorithm and neural network. *Transportation Research Record*, 1364, 1992.
- Haoyang Yan, Zhiyong Cui, Xinqiang Chen, and Xiaolei Ma. Distributed multiagent deep reinforcement learning for multiline dynamic bus timetable optimization. *IEEE Transactions on Industrial Informatics*, 19:469–479, 2023.
- Jie Yang and Yangsheng Jiang. Application of modified nsga-ii to the transit network design problem. *Journal of Advanced Transportation*, 2020:1–24, 2020.
- Haoran Ye, Jiarui Wang, Zhiguang Cao, Helan Liang, and Yong Li. Deepaco: neural-enhanced ant systems for combinatorial optimization. *Advances in Neural Information Processing Systems*, 36, 2024.
- Jin Y Yen. An algorithm for finding shortest routes from all source nodes to a given destination in general networks. *Quarterly of applied mathematics*, 27(4):526–530, 1970.
- Rex Ying, Ruining He, Kaifeng Chen, Pong Eksombatchai, William L. Hamilton, and

- Jure Leskovec. Graph convolutional neural networks for web-scale recommender systems. *CoRR*, abs/1806.01973, 2018. URL <http://arxiv.org/abs/1806.01973>.
- Sunhyung Yoo, Jinwoo Brian Lee, and Hoon Han. A reinforcement learning approach for bus network design and frequency setting optimisation. *Public Transport*, pages 1–32, 2023.
- Liang Zou, Jian-min Xu, and Ling-xiang Zhu. Light rail intelligent dispatching system based on reinforcement learning. In *2006 International Conference on Machine Learning and Cybernetics*, pages 2493–2496, 2006. doi: 10.1109/ICMLC.2006.258785.
- Muhammed Yasin Çodur and Ahmet Tortum. An artificial intelligent approach to traffic accident estimation: Model development and application. *Transport*, 24(2):135–142, 2009. doi: 10.3846/1648-4142.2009.24.135-142.